Dissecting the roles of toxin bivalency, membrane affinity, and stoichiometry in DkTx-activation of TRPV1

A thesis

submitted in partial fulfillment of the requirements

for the degree of

Doctor of Philosophy

by

Yashaswi Singh

20142006

INDIAN INSTITUTE OF SCIENCE EDUCATION AND RESEARCH, PUNE

2023

Dedicated to maa who is always with me

Certificate

Certified that the work incorporated in the thesis entitled "**Dissecting the roles of toxin bivalency, membrane affinity, and stoichiometry in DkTx-activation of TRPV1**" submitted by **Yashaswi Singh** was carried out by the candidate under my supervision. The work presented here or any part of it has not been included in any other thesis submitted previously for the award of any degree or diploma from any other University or institution.

Date: 07.10.2023

Dr. Jeet Kalia

Thesis advisor

Declaration

I declare that this written submission represents my ideas in my own words and where other's ideas have been included, I have adequately cited and referenced the original sources. I also declare that I have adhered to all principles of academic honesty and integrity and have not misrepresented or fabricated or falsified any idea/data/fact/source in my submission. I understand that violation of the above will be cause for disciplinary action by the Institute and can also evoke penal action from the sources which have thus not been properly cited or from whom proper permission has not been taken when needed.

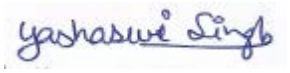

Date: 07.10.2023 Yashaswi Singh

Registration No. 20142006

Acknowledgements

I express my deepest gratitude to my Ph.D. thesis guide, Dr. Jeet Kalia, for being an incredible mentor throughout my doctoral studies. I feel incredibly privileged to have the opportunity to learn from Jeet, who has been an invaluable guide throughout my doctoral journey. Since I joined his lab, he has consistently inspired me to work hard, persevere through challenges, and be passionate about science.

I have been fortunate to receive unparalleled guidance, training, and support throughout my time in his lab. He has been a constant source of inspiration, pushing me to think critically, ask important questions, and approach scientific problems systematically and rigorously. More than that, Jeet has helped me develop the scientific attitudes essential for success in academia. He has shown me that scientific research is not only about getting results and being meticulous, thorough, and persistent in pursuing knowledge. His commitment to excellence, integrity, and intellectual rigor has been truly inspiring and helped me develop a deep appreciation for the values underpinning scientific research.

He has provided more than just expert technical guidance. He has also helped me improve my reading skills, allowing me to comprehend scientific literature better and incorporate it into my work. In addition, he has helped me to develop my scientific reporting skills, working with me to refine my writing style and ensuring that my reports are clear, concise, and effective. He has also helped me to hone my presentation skills, giving me constructive feedback on my talks and helping me to deliver engaging, informative presentations. Perhaps most importantly, he has helped me to develop my communication skills, emphasizing the importance of effective communication in all aspects of scientific research. He has taught me the value of clear, concise, and accurate communication, whether in writing, presentations, or discussions with colleagues.

I am deeply grateful for his guidance and mentorship, which helped shape me into who I am today. I know the lessons I have learned in his lab will stay with me for the rest of my career, and I feel fortunate to have had him as my mentor.

While in the program, I faced personal family hardships that made me question whether I could continue my studies. However, Jeet was there for me every step of the way, providing academic and emotional support. He went above and beyond, working with me to create a plan that allowed

me to take the necessary time to address my situation while still making progress toward my degree.

I am genuinely grateful for Jeet's unwavering confidence in me. His guidance and support have made all the difference in my academic and personal life. Thank you, Sir, for everything you have done for me.

I express my gratitude to my research advisory committee, Dr. Saikrishnan Kayarat from IISER Pune and Dr. Durba Sengupta from NCL Pune, for providing me with valuable feedback and assessments throughout my research progress.

I express my gratitude to the senior Ph.D. lab members of the Kalia lab, specifically Debayan Sarkar and Aditi Dixit, for the invaluable lessons I have learned while working with them. They have not only made work enjoyable, but they have also taught me essential skills such as maintaining lab decorum and fostering a positive work environment. Under their guidance, I have also learned how to mentor and support junior members of the lab. They showed me the importance of providing proper training and discussing research projects with junior members, helping them become independent. I would also like to express my appreciation to the present members of my lab - Manas, Satyajit, Saswati, Sucheta, Shreya, and Dr. Tanveer Alam Khan, for fostering a supportive and delightful environment in the lab.

I want to express my gratitude towards the administration of IISER Pune for their efforts in providing and maintaining excellent facilities for researchers such as myself. Additionally, I would like to thank the welcoming administration at IISER Bhopal. As relocating to a new institute posed challenges for our lab, I am immensely grateful to the administration of IISER Bhopal for their hospitality and generous provision of unrestricted access to all research facilities.

I am immensely grateful to my fellow Integrated Ph.D. batchmates for their camaraderie, which has made my journey unforgettable. Their constant support and shared memories will always remain close to my heart. In particular, Mayur, Deepak, and Saurav have been exceptional friends, giving me unwavering emotional or financial support whenever needed.

I want to extend my heartfelt gratitude to my younger sister Yakshi, whose unwavering support and encouragement have been instrumental in my life. Despite the age difference, she has always been a reliable confidant and a source of motivation during challenging times. Her unwavering

faith in my abilities and her constant encouragement has helped me to push through difficult situations. I am truly blessed to have her in my life.

Synopsis

Dissecting the roles of toxin bivalency, membrane affinity, and stoichiometry in DkTx-activation of TRPV1

Submitted by: Yashaswi Singh

Thesis Advisor: Dr. Jeet Kalia

Indian Institute of Science Education and Research, Pune

Dr. Homi Bhabha Road, Pashan, Pune-411008

Maharashtra, India

Ligand-mediated ion channel modulation is a complex biological process that plays a critical role in cellular signaling and cellular physiology. The protein-lipid interface is a critical component of this process and is formed not just by the interactions between ion channel proteins and membrane lipids, but also those between channel-targeting ligands and the membrane. These protein-lipid interactions play critical roles in channel activation, and understanding the molecular determinants of their roles in channel activation is critical for understanding the mechanisms underlying channel gating. Moreover, considering the crucial roles of ion channels in diverse physiological functions including pain and heat sensation, and their association with a variety of diseases, unraveling the roles of protein-lipid interfaces in channel is critical for the development of new therapeutic approaches targeting ion channels. Overall, this is a fascinating area of research that has the potential to uncover new insights into cellular signaling and the mechanisms of ion channel modulation.

In **chapter 1** of this thesis, I have provided a broad overview of the different ligands targeting ion channels. I have reviewed the diverse range of animal toxins that target ion channels and discussed their mode of action. I have also discussed the roles of membrane lipids in the mechanisms underlying the modulation of ion channels by these ligands, their mode of action and the implications of these mechanisms in drug development.

In **chapter 2**, I have described my analysis of the structure of the TRPV1 ion channel complexed with its potent inhibitory cysteine-knot (ICK) toxin agonist, double-knot toxin (DkTx), with the goal of using it as a model system to explore the impact of toxin-lipid interfaces on channel activation. This analysis yielded a list of lipid and channel-interacting residues of DkTx and served as the basis of my studies focused on unraveling the contributions of these residues in the membrane-partitioning propensity of DkTx that involved performing tryptophan fluorescence-based membrane partitioning experiments on site-directed variants of the toxin. In addition to describing the results of experiments, I have discussed their important implications on understanding the molecular basis of the sustained TRPV1-activation properties of DkTx, by correlating the membrane partitioning propensity of these variants with their TRPV1-potency and wash-off kinetics obtained as result of electrophysiological experiments performed by other students in my laboratory. I also describe our fascinating observation that the membrane interfaces formed by one of the knots of the toxin are responsible for its low channel dissociation rates, whereas those formed by other knots primarily contribute to its potency. The findings establish that protein-lipid interfaces have nuanced yet profound effects on the function of protein-protein complexes within membranes.

Our findings suggest that the membrane's contribution to the slow wash-off rates of DkTx is significant, challenging the conventional notion that the bivalency of the toxin is solely responsible for this effect. In **chapter 3** of my thesis, I outline my experiments designed to dissect the contributions of membrane partitioning and bivalency of DkTx to its channel activation properties. In order to achieve this goal, I created various DkTx-based toxin variants and analyzed their membrane affinity and TRPV1 activation properties to investigate the contribution of the toxin's membrane affinity and valence to its sustained mode of TRPV1 activation. The findings of this study provide clear evidence that the toxin's high membrane affinity is crucial in endowing it with its persistent TRPV1 activation property. One compelling piece of evidence supporting this conclusion is the slower wash-off rates of the single-knots of DkTx when attached to the Kv2.1 channel-targeting membrane partitioning toxin, SGTx. We used K1-SGTx and SGTx-K2 bifunctional chimeric double-knots to separate the effects of valence and membrane affinity. These monovalent double-knots possessed higher membrane affinities than the single-knots and served as powerful tools to analyze the importance of membrane affinity in TRPV1 activation. Furthermore, I observed that our tetra-knot variants, $(DkTx)_2$ and DkTx-$(SGTx)_2$, with hyper-

membrane affinities, washed off slower than wild-type DkTx, further emphasizing the significance of membrane affinity in TRPV1 activation.

DkTx's slow wash-off kinetics can be attributed not only to its bivalency and membrane affinity but also to its channel occupancy. The DkTx-TRPV1 complex's structure reveals that DkTx has a channel occupancy of two. In **chapter 4**, I describe my experiments aimed investigating the role of the channel-binding stoichiometry of DkTx in its channel activating properties by characterizing concatemeric TRPV1 variants designed to disrupt the binding of one of the two DkTx molecules to the channel. My results suggest demonstrate that a single DkTx molecule can bind to the TRPV1 channel and activate it, and that DkTx occupancy does not significantly contribute to its sustained TRPV1 channel activation property. In **chapter 5**, I discussed the future directions of the projects I have undertaken during my Ph.D. and tried to develop a hypothesis to quantitatively determine the role of membrane lipids in DkTx-mediated TRPV1 channel activation.

Taken together, my research on the DkTx-TRPV1 system suggests that the membrane is a key determinant of the TRPV1-activation properties of DkTx. Specifically, my results indicate that the extremely slow wash-off rates of DkTx post TRPV1-activation is primarily due to its high membrane affinity. Overall, these findings highlight the importance of the membrane in the functions of membrane-embedded protein-protein complexes.

In the **appendix** section of my thesis, I have described my studies on the plant cyclic nucleotide-gated channel (CNGC)-13 (in collaboration with Dr. Jyothilakshmi Vadassery's group at NIPGR, New Delhi). This work entailed two-electrode voltage clamp electrophysiology experiments on *Arabidopsis thaliana* CNGC13 expressed in *Xenopus laevis* oocytes, and revealed that CNGC13 is a Ca^{2+}-permeable ion channel.

Contents

List of Figures

List of Tables

Chapter 1:

Roles of protein-lipid interfaces in ligand mediated ion channel modulation

1.1 Introduction

Ion channels are membrane-embedded proteins that form pores and are controlled by gates.[1–4] They are responsible for regulating the influx and efflux of different ions across cellular membranes. This regulation is achieved in response to ligand binding or voltage changes. Ion channels serve as the basic units of various tissues including nerves, muscles, and glands.[2,5] The opening of ion channels results in the exchange of ions between the inside and outside of cells/organelles, triggering the generation of electrical signals.[2] These signals play a crucial role in numerous cellular and physiological processes[1,6] including nerve and muscle relaxation, cognition, sensory transduction, regulation of blood pressure, and cell proliferation.[7,8] Malfunction of ion channels has been linked to various diseases, including cardiac disorders, neurological indications, kidney failure, pain perception, and blindness.[9] Over 60 "channelopathies" have been identified as human diseases resulting from mutations in ion channels.[9–11] Moreover, various neurological disorders and cardiac arrhythmias, insomnia, epilepsy, schizophrenia, Parkinson's disease, Alzheimer's disease, long/short QT syndromes, have been associated with ion channel malfunction.[12,13] Ion channels are the second most significant group of membrane protein targets for FDA-approved drugs, after G protein-coupled receptors (GPCRs).[14,15]

Recent advances in high-resolution ion channel structure determination have greatly enhanced our comprehension of ion channel function.[16–19] These structures have furnished crucial insights into the three-dimensional structure of ion channels and the mechanisms underlying ion selectivity.[20,21] Over the past few decades, ion channels have gained tremendous prominence in biomedical research with respect to being targeted for drug discovery.[4,22] Due to their high potency and selectivity towards ion channels, diverse natural toxins and venom peptides have emerged as indispensable instruments for drug development and discovery.[23,24]

In this chapter, a comprehensive summary of the various ligands that target ion channels is presented. Additionally, a review of the various animal toxins that target ion channels is provided, along with a detailed discussion of their mechanisms of action. Furthermore, the involvement of membrane lipids in the modulation of ion channels by these toxins and their mechanisms of action is examined, and the implications of these mechanisms in the development of new drugs is discussed.

1.2 Functioning of ion channels

Simply put, ion channels are a group of protein domains that allow ions to pass through a cell membrane when triggered by chemical, temperature, or mechanical stimuli.[25] The domains that form the pore vary significantly in their sequence and structure, but they generally consist of four or five helices that come together to create a cylindrical shape. These helices are composed of repeating subunits from single or multiple subunits. To filter ions selectively, most ion channels also have a region called the ion selectivity filter that controls which ions can pass through the pore.

All ion channels have a gating mechanism that regulates the opening and closing of the pore by altering the structure of the channel protein. It also has a sensor mechanism that identifies and reacts to various stimuli. The intracellular and extracellular modules of the channel provide sites where ligands and accessory proteins can bind, which makes the system more complex.[25] The ion channel can quickly transition between open and closed states, and modulation of its function by a ligand or external stimulus stabilizes the channel structure in a specific state.

When the ion channel is open, the movement of ions through the pore is exceptionally rapid and occurs due to an electrochemical gradient. This process can be so fast that up to 10^8 ions can pass through the channel every second,[1] with only nanoseconds available for the channel to interact with each ion. This speed is close to the theoretical limits described by Ohm's law and Fick's law. Despite this brief interaction time, ion channels specific to potassium ions can selectively allow potassium ions to pass through with a fidelity of approximately 10000:1 over smaller sodium ions.[1,26] This selectivity is achieved by the careful arrangement of carbonyl oxygen atoms within the selectivity filter, which can accommodate two potassium ions at a time in the pore.[27] These contacts compensate for the energy required to remove solvent molecules from ions as they enter the filter by providing favorable interactions with the ion. The amount of energetic compensation varies depending on the ion's identity relative to the energy required to de-solvate it, leading to energy-driven selectivity.[27]

The specific mechanisms of channel gating responsible for all the physiological effects regulated by ion channels have been extensively studied by both functional and structural approaches. Ion channels have been found in various species, and bacterial channels, in particular, have been valuable to structural biology research having yielded high-resolution *X*-ray structures contributing tremendously to understanding channel function.[16,21,28] More recently, there have been notable

advancements in elucidating mammalian ion channel structures, especially in the voltage-gated family of potassium channels[29–31] and ligand-gated family of TRPV channels,[32–35] through techniques such as crystallography, cryo-EM,[34,35] and nuclear magnetic resonance.[36]

Prior to 2014, all cryo-EM PDB coordinates deposited for membrane proteins were derived from electron crystallography. However, with the successful determination of the first atomic structure of a membrane protein using single particle cryo-EM in 2013,[34,37] the number of membrane protein structures being determined using this technique has skyrocketed. In 2014, cryo-EM (encompassing both single particle cryo-EM and electron crystallography) accounted for less than 5% of total membrane protein structures determined, but by 2017, this number had surged to about 27%, and by early 2018, it had exceeded 35%.[38] The contribution of single particle cryo-EM is particularly remarkable in certain families of integral membrane proteins, where most new structures are being determined at an unprecedented pace. A striking example is that of the TRP channel family[39,40] the members of which did not succumb to *X*-ray crystallography despite substantial global efforts by structural biologists that yielded structures of a few small domains and fragments, and not the full-length channel protein.[41,42] However, with the successful determination of the atomic structure of TRPV1 in 2013 using single particle cryo-EM,[37] structures of all seven TRP channel subfamilies have now been elucidated using this technique.[34,35,37,43,44]

TRPV1 is the most extensively studied among the TRP channels, and researchers have utilized its rich pharmacology to capture images of substates of nanodisc-reconstituted channels through single-particle cryo-EM.[35] These substates serve as crucial structural intermediates that allow direct visualization of the small and large permeating cations' status, the stepwise engagement of ligands with TRPV1, and the stoichiometry of ligand binding at key regulatory points. Additionally, these substates illustrate the transitions between channel conformations and reveal a two-step mechanism in which extracellular protons, a significant component of the inflammatory milieu, modify the upper restriction's structure, allowing for the opening of the lower gate. These discoveries provide a framework for understanding the dynamic behavior of this extensive family of excitatory ion channels.[35]

1.3 The role of the membrane in the mechanism of action of local anesthetics on ion channels

Local anesthetics possess a bipolar characteristic due to their structural properties, enabling them to bind to protein surfaces at patches that match their amphiphilic pattern. These hydrophobic

molecules have a propensity to partition effectively into the lipid bilayer, where they can be found either near the core of the bilayer or below the carbonyl region in the upper acyl chain region.[45] The inherent structural and chemical diversity found in local anesthetics poses a significant challenge when attempting to discern their potential mechanisms of action. Two primary hypotheses have been put forward to elucidate how local anesthetics work. The first hypothesis, known as the protein hypothesis, posits that the interaction between membrane proteins and local anesthetics plays a role in modifying protein function, thereby serving as the foundation for the anesthetic effect.[46–49] Conversely, the lipid hypothesis suggests that anesthesia arises from the interaction between anesthetics and cell membranes, which leads to alterations in the physical properties of the membrane.[49–51] It is plausible that a combination of effects involving both proteins and lipids contributes to the overall generation of local anesthesia, and distinguishing the individual contributions of these two factors is a non-trivial task.[49,52,53] By modulating the physical properties of the membrane, they can impact the equilibrium between different conformational states of the affected proteins, leading to discernable responses in protein kinetics.[54] When considering the affinity to patches of similar amphiphilic characteristics, the interaction of local anesthetics with ion channels may not follow the classic key-lock or hand-glove recognition mechanisms known for toxins.[55]

Based on the conventional understanding of local anesthetic (LA) activity, these molecules possess a degree of hydrophobicity that enables them to cross the membrane and reach the inner part of the ion channel from the cytosolic side. However, this leads to a question: is it necessary for LAs to traverse the membrane to reach their target, or could they instead target the lipid bilayer itself and exert their effects by acting laterally within the membrane?

Effects of Local Anesthetics on membrane: Local anesthetics (LAs) have been observed to cause a reduction in the thickness of the lipid bilayer[56] and induce increased fluidity within the hydrophobic core of the membrane while reducing fluidity in the headgroup region.[57] Solid-state ^{2}H-NMR studies have determined that LAs localize either in or just below the headgroup region of the bilayer by examining changes in the order parameter and mobility of individual lipid segments.[58,59] When present in the headgroup region, LAs require additional space, resulting in an increase in the lateral volume of the bilayer in that region. These alterations in the mechanical and

structural properties of the bilayer coincide with modifications in the electrostatic properties, as LAs have been found to affect the surface charge and electric dipole.[59,60]

Lipid rafts are specific regions within cell membranes that play a significant role in recruiting receptors and other proteins to form protein-rich patches, which are important for cellular functions.[61–63] These rafts are primarily composed of sphingolipids and cholesterol, which separate from the rest of the lipids. The sphingolipid/cholesterol mixture within rafts forms a more viscous phase called "liquid-ordered" that has distinct solubility properties compared to the surrounding lipid bilayer. Certain receptors such as the NMDA (N-methyl-D-aspartate) and GABA (gamma-aminobutyric acid) receptors,[64–66] as well as ion channels involved in nerve impulse propagation,[67,68] have been observed to accumulate within lipid rafts, suggesting their potential significance in regulating their activity.[64,65,67]

The interaction between LAs and these microdomains has been investigated by various studies.[69–71] LAs have the ability to disrupt and disperse these raft-like domains by reducing lipid order and increasing fluidity. The extent of this effect on the rafts seems to be related to how deeply the LA molecules are inserted into the membrane and their size. For instance, researchers have conducted experiments using small angle X-ray scattering and fluorescence anisotropy, and they discovered that dibucaine, tetracaine, and lidocaine, in that specific order, are capable of eliminating the segregation of lipid phases. This physical impact correlates with the ranking in which they decrease lipid order and penetrate the membrane more deeply.[71]

Membrane-mediated binding of LAs to ion channels' specific binding site: Considering the substantial experimental evidence available, it is evident that the specific binding of local anesthetics (LAs) to ion channels and their direct interaction with their amino acid residues cannot be disregarded when examining the anesthetic effects of LAs. However, these findings do not exclude the possibility that LAs can act through both mechanisms: 1) direct interaction with the ion channel and 2) a membrane-mediated mechanism. Notably, sodium channels contain two binding sites: one site near the fenestrations accessible from the lipidic environment, associated with tonic block of the channel, and another site located close to the activation gate accessible through the cytosolic channel entrance, associated with use-dependent block.[55,72–74]

1.4 Venoms, Toxins, and Biologics

Venomous creatures have utilized the complex biological makeup of their prey by developing toxins that target various systems, such as the nervous, musculoskeletal, or cardiovascular systems. This adaptation helps them capture prey or protect themselves from predators. For instance, some predatory venoms contain neurotoxins that quickly paralyze their prey by disrupting neuromuscular transmission.[75] As most venom molecules are highly specific and potent, they have become a valuable resource for investigating various molecular targets, especially ligand-activated[76–79] and voltage-gated ion channels.[23,80–82]

Since the 1960s, it has been established that the venom peptide α-bungarotoxin from the banded krait *Bungarus multicinctus* blocks acetylcholine's depolarizing effects, resulting in specific and virtually irreversible functional antagonism at the vertebrate neuromuscular junction.[83] The cholinergic receptor protein was thought to be the target of α-bungarotoxin. The impact of α-neurotoxins on various biological processes has demonstrated the significance of nicotinic acetylcholine receptors (nAChRs) in normal bodily functions and diseases.[84] Recently, nAChRs have gained attention as potential therapeutic targets for numerous human disorders.[85] For instance, some nAChR subtypes are believed to have vital roles in chronic pain and inflammation.[85] Several α-conotoxins have good selectivity for these subtypes and are being developed as lead drugs.[86]

1.4.1 Venom peptides targeting potassium channels.

Kv channels are crucial for tightly regulating the permeability of K^+ ions across membranes by detecting changes in voltage, thereby playing an essential role in controlling action potentials and propagating electrical signals in excitable cells.[87] In non-excitable cells, Kv channels modulate cellular metabolism and facilitate downstream signaling cascades, as demonstrated by the Kv1.3 channel in T lymphocytes.[88] Kv channels are made up of homo- or heterotetramers, and each subunit contains six TM helices. The voltage sensing domain (VSD) (S1-S4) is linked to the pore domain (S5-S6) via the S4-S5 intracellular loop, which controls pore opening and closing.[29]

Research into venom peptide modulators of Kv channels started in the 1980s, and to date, over 200 peptides with inhibitory effects on Kv channels have been identified.[89,90] These polypeptides usually bind to Kv channels through two different mechanisms. Pore blockers attach to the extracellular pore region's shallow vestibule, while gating modifiers bind to the VSD's "paddle motif," which is accessible from the extracellular side.

In the 1980s, the use of venom peptides as modulators of Kv channels began, and since then, over 200 peptides with inhibitory effects on Kv channels have been discovered.[89,90] One of the earliest

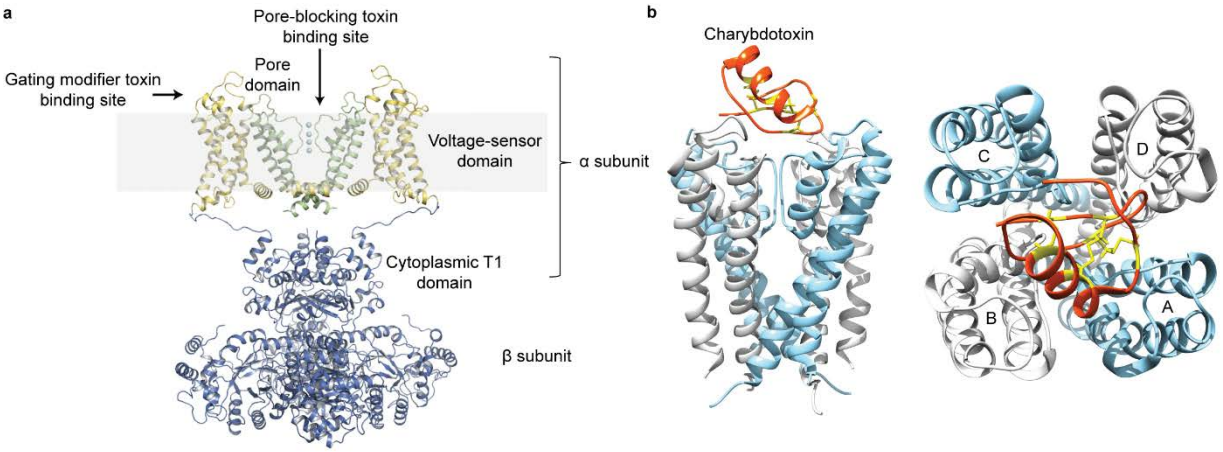

Figure 1.1: Structure of the Kv1.2-Kv2.1 paddle chimera channel and binding of ChTx to KcsA channel. (a) Side view showing two diagonal subunits of the paddle chimera channel in complex with the auxiliary ß-subunit shown in ribbon trace (PDB ID: 2R9R[18]. (b) The ribbon plots display the minimized structure of KcsA, represented by cyan and gray ribbons, along with charybdotoxin illustrated as an orange ribbon. Both side and top views of the channel, with the former on the left and the latter on the right. Additionally, disulphide linkages are depicted as yellow sticks. The four subunits of KcsA are identified as A-D.[92]

venom toxins used for research purposes was charybdotoxin (ChTx), a scorpion toxin, which helped to better understand Kv channel subunit stoichiometry,[91,92] auxiliary beta subunits,[93] and overall architecture.[20] On the other hand, sea anemone toxin ShK binds to all four subunits in the channel tetramer through two critical interactions in the external vestibule, blocking Kv channels with high potency (in the nanomolar to sub-nanomolar range).[94,95] Specifically, Lys22 occludes the channel pore like a "cork in a bottle," while Tyr23 and Lys22 form a "functional dyad" required

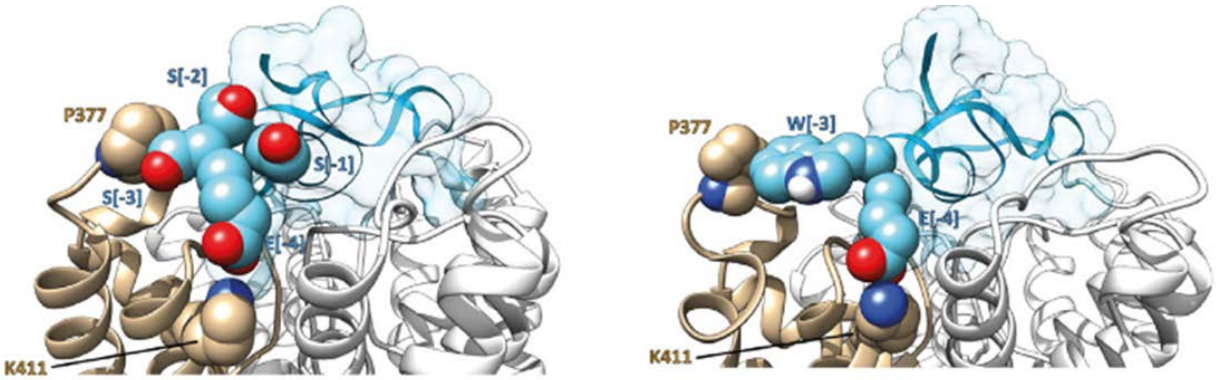

Figure 1.2: ShK in complex with Kv1.3. In the left panel, ShK is shown in complex with Kv1.3, with the side-chain atoms of Pro377 and Lys411 of the channel depicted as spheres in tan carbon coloring. The side-chain atoms of the ESSS four-residue extension are also displayed as spheres, represented by cyan carbon coloring. The right panel displays a homology model of ShK in complex with Kv1.3, with the side-chain atoms of Pro377 and Lys411 of the channel highlighted. The first two residues (EW) of the four-residue extension are also shown as spheres, represented by cyan carbon coloring.

for channel block. This blocking mechanism involving a lysine and an adjacent aromatic or aliphatic residue is shared by many K^+ channel-blocking peptides.[96]

Researchers spent almost a decade trying to modify the natural ShK peptide to create a highly specific Kv1.3 inhibitor. In 2006, they developed a stable analog known as ShK-186, by attaching L-phosphotyrosine via a aminoethyloxyethyloxyacetyl (Aeea) linker to the a-amino group of Arg1,[97] which binds specifically to Kv1.3 with a binding affinity of 69 pM and is 100 times more selective than other Kv channels.[98] Kineta is now developing ShK-186, which has passed phase I clinical trials and is the only venom-derived peptide that blocks K^+ channels being developed as a therapeutic.[99]

Inwardly rectifying potassium channels. Kir channels were first identified in frog skeletal muscles in 1949,[100] but it wasn't until 1993 that they were cloned and isolated.[101,102] These channels are called inwardly rectifying potassium channels because they allow inward current to flow more readily than outward current, enabling the influx of extracellular K^+ into cells. This unique molecular mechanism is due to the intracellular binding of Mg^{2+} and polyamines.[103] Kir channels are made up of homo- or hetero-tetramers formed from four Kir subunits containing two TM segments separated by a selectivity filter region.[104,105]

ChTx2 (α-KTx1.2), δ-dendrotoxin (δ-DTX), and Tertiapin (TPN) are venom peptides that have a strong affinity for Kir channels (with $IC_{50} < 0.5$ μM). These toxins contain high levels of cysteine and positively charged residues, which are common features among other venom peptides. Computational simulations and docking studies have suggested binding mechanisms for these toxins, which involve close contact between positively charged residues on the toxin and negatively charged residues on the channel pore region.[105] These interactions strengthen electrostatic forces between the two, while hydrophobic forces between aliphatic residues also contribute to binding affinity.

1.4.2 Venom peptides targeting voltage-gated sodium channels

Researchers have been able to gain a better understanding of ion selectivity, pore diameter, and the binding mechanism of sodium-channel acting local anesthetics and related drugs through various studies. Voltage-gated sodium (Nav) channels, found in most excitable cells, are crucial for the initiation and propagation of action potentials. The availability of ion channel toxins such as tetrodotoxin (TTX) and saxitoxin (STX) has aided researchers in elucidating the underlying mechanisms of Nav channels.[106–108] The Nav channel protein was isolated and purified by William Catterall and his team, who also utilized neuropeptides from scorpion toxin (ScTx) to advance their research, in addition to TTX and STX.[109–111]

The Nav channels, which are crucial for the initiation and propagation of action potentials in most excitable cells, are divided into nine subtypes, Nav1.1 to Nav1.9, based on their TTX binding, tissue expression, and sequence. These channels are composed of a 250 kDa α-subunit that is pseudo-tetrameric in nature. The α-subunit is made up of a single polypeptide chain, which folds into four homologous domains (DI to DIV) containing six transmembrane (TM) segments (S1 to S6) each. The voltage-sensing domain (VSD) is formed by the S1-S4 segments in each domain, while the central ion pore is formed by the S5-S6 segments of all four domains. A single channel is made up of one α-subunit that forms the core of the channel and may be accompanied by one or two β-subunits. The α-subunit is capable of functioning independently.[112]

Venom toxins from various animals can target Nav channels and impact the neuromuscular systems of both prey and adversaries. Typically, these toxins affect Nav channel function in two ways: obstructing the flow of Na^+ ions through the pore or modifying the gating mechanisms.

μ-conotoxin peptides from cone snail venom (genus Conus) are among the most extensively studied pore blockers for Na_V channels. These peptides are rich in disulfide bonds and are isolated from cone snail venom, which contains various peptide toxins targeting different ion channels and receptor proteins.[113,114] M-conotoxins have the strongest binding affinity for Nav1.4, the skeletal muscle isoform of Nav channels, they also exhibit variable binding affinity for other isoforms.[115]

The selectivity and affinity of each peptide for different Nav isoforms are crucial for distinguishing them. Toxin peptides interact with the voltage sensors of Nav channels, modifying their gating. Various classes of conotoxins interact with the voltage sensors of Nav channels, affecting their

gating properties. For example, Δ-conotoxins, which are present in different cone snail venoms, obstruct fast inactivation of the channel, whereas μ-conotoxins, which are gating modifiers, target the voltage sensors and prevent channel opening.[116–118]

Several spider toxins are being developed as Nav1.7 antagonists in pre-clinical studies, making Nav1.7 a promising target for non-opioid pain medication. One such toxin, Protoxin-II (ProTX-II), derived from the tarantula *Thrixopelma pruriens*, shifts the voltage dependence of Nav1.7 channel activation to positive potentials, inhibiting it. Using ProTX-II as a scaffold, a highly potent and selective Nav1.7 blocking peptide has been created, mimicking the Nav1.7-null phenotype.[119] Huwentoxin IV, a venom peptide from the Chinese bird-eating spider *Selenocosmia huwena*, selectively inhibits Nav1.7 by binding to one of the four VSDs of the channel.[120] This selectivity is an improvement over local anesthetics that bind the conserved channel pore. Through mutational studies, a triple mutant of huwentoxin IV (E1G, E4G, and Y33W) has been developed with high potency for Nav1.7 blocking.[121]

1.4.3 Venom peptides targeting transient receptor potential channels

TRP ion channels are a type of non-selective cation channel composed of four subunits and share a similar architecture with voltage-gated ion channels. Although some TRP channels exhibit slight voltage activation,[122,123] they are functionally distinct from voltage-gated ion channels. These channels were first discovered in a mutated strain of the fruit fly Drosophila[124] and there are currently 28 known TRP channels with shared structural similarities across different organisms.[125] Despite their similarities, each subfamily of TRP channels is unique and possesses distinct molecular sensing and regulatory functions. TRP channels have been identified as potential drug targets for a variety of diseases including neurological and psychiatric disorders, respiratory illnesses, diabetes, and cancer. Notably, the discovery of thermally sensitive TRP channels and pressure-sensing Piezo channels led to David Julius and Ardem Patapoutian receiving the Nobel Prize in Physiology or Medicine in 2021.[126] The use of animal toxins that target TRP channels as tools to study these channels has also been instrumental in understanding their functions. The interaction between animal toxins and TRP channels is an active area of research with implications for understanding the physiology and pathology of these channels, as well as the development of novel therapeutic approaches.

ProTx-I, an antagonist of voltage-gated sodium channels, was discovered from the venom of the Peruvian green velvet tarantula, *Thrixopelma pruriens*, in the specific search for TRPA1 ligands. Two-electrode voltage-clamp electrophysiology experiments on Nav1.2 and TRPA1 expressed in *Xenopus laevis* oocytes showed that ProTx-I had substantially higher affinity for voltage-gated sodium channels (IC_{50} of 30-90 nM) than for TRPA1 (IC_{50} 389 nM). Importantly, mutagenesis-based studies yielded a new ProTx-I(W5A) variant that was selective for TRPA1 and had the same activity on the channel as the wild-type ProTx-I.[127]

While mining spider venoms in search of polypeptide ligands for TRPV1, researchers discovered three closely related peptides called vanillotoxins (VaTx) in the venom of the tarantula *Psalmopoeus cambdridgei*. After conducting whole-cell patch-clamp analysis on TRPV1-transfected HEK-293 cells, they found that the currents induced by vanillotoxins exhibit pronounced outward rectification, similar to those observed with capsaicin and other TRPV1 agonists. The three peptides have varying effective concentrations for channel activation EC_{50} of 0.45 µM (VaTx3), 1.35 µM (VaTx2), and 9.9 µM (VaTx1), as well as different levels of selectivity for TRPV1 activation and Kv2.1 channel inhibition (VaTx2 = VaTx3 > VaTx1). Among the three, VaTx3 is the most potent agonist with the most excellent selectivity and activity toward TRPV1.[128]

Another TRPV1 agonist, known as double knot toxin (DkTx), was isolated from the venom of the Chinese bird spider *Ornithoctonus huwena*. DkTx has a molecular weight of 8522 Da and has a unique bivalent structure consisting of two tandemly repeated ICK motifs (three disulphide linkages in each motif) that share high homology (67% identity). This toxin selectively activates TRPV1 and due to its bivalent structure, forms a highly stable complex with TRPV1's outer pore region, resulting in persistent current conductance through the channel. In contrast, separated DkTx ICKs (knot 1, "K1"; knot 2, "K2") as well as the single knot vanillotoxins, VaTx1-3, bind and activate TRPV1 reversibly.[76]

The DkTx-TRPV1 complex structure has been determined using cryo-EM, and it has revealed that the ICK motifs of the two toxins bind two adjacent subunits in an anti-parallel orientation of the homo-tetrameric channel.[34,37,129] This means that two DkTx molecules can occupy a single TRPV1 channel completely by binding to its outer pore domain.[129,130] Upon DkTx binding to TRPV1, the toxin's seven amino acid linker takes a tense and constrained conformation, which may have evolved to match the distance between the two adjacent ICK binding sites.[129] The activation

stoichiometry of TRPV1 by different activators is not yet known, so Chapter 4 of the thesis aims to address this question. In each TRPV1 subunit, the different toxin knots bind equivalent binding sites located at the interface of two neighboring subunits.[129,130] Therefore, a single knot interacts with the pore helix of one subunit and the pore loop preceding S6 in an adjacent subunit.

DkTx's ICK motifs, although highly homologous and binding to the same site, exhibit different binding orientations, leading to greater potency in K2 than K1.[76,130] Results from alanine scanning experiments indicate that toxin residues that interact with lipids play a dominant role in sustained channel activation compared to toxin residues that interact with the channel itself.[131] A high-resolution cryo-EM structure of TRPV1 complexed with DkTx reveals that DkTx's hydrophobic fingers penetrate 9 Å into the membrane, causing local distortions in the lipid bilayer.[129] The structure also reveals that membrane lipids interact with both DkTx fingers and TRPV1 residues, forming a tripartite complex. For example, DkTx's W11 (K1) and W53 (K2) form hydrophobic interactions with aliphatic chains, while the chains' polar head groups bind to R534 (S4; rTRPV1) in TRPV1.[76,129] Additionally, membrane-affinity experiments such as tryptophan fluorescence experiments and toxin depletion assay indicate that DkTx partitions into the lipid membrane, predominantly driven by the lipid-interacting residues of the K1 knot (as described in chapter 2 of this thesis[131]).

RhTx is a peptide toxin (27 amino acids) that was identified in the venom of the Chinese red-headed centipede (*Scolopendra subspinipes mutilans*).[132] This aggressive arthropod, which populates parts of eastern Asia and Australasia, can cause extreme localized pain upon envenomation.[132] It is a selective TRPV1 activator with an EC_{50} of 521.5 nM[132,133] as it does not affect other TRPV channels (i.e., TRPV2-4). In addition, the voltage-gated potassium ion channel Kv2.1, which was previously shown to be inhibited by other peptide toxins targeting TRPV1 (i.e., VaTx1 and VaTx2), is neither inhibited nor activated by RhTx.[128] Similar to capsaicin-mediated

TRPV1 activation, RhTx displays very rapid kinetics, in both channel opening and washout. This is in contrast to the slow-developing, slow washing DkTx described above.[76]

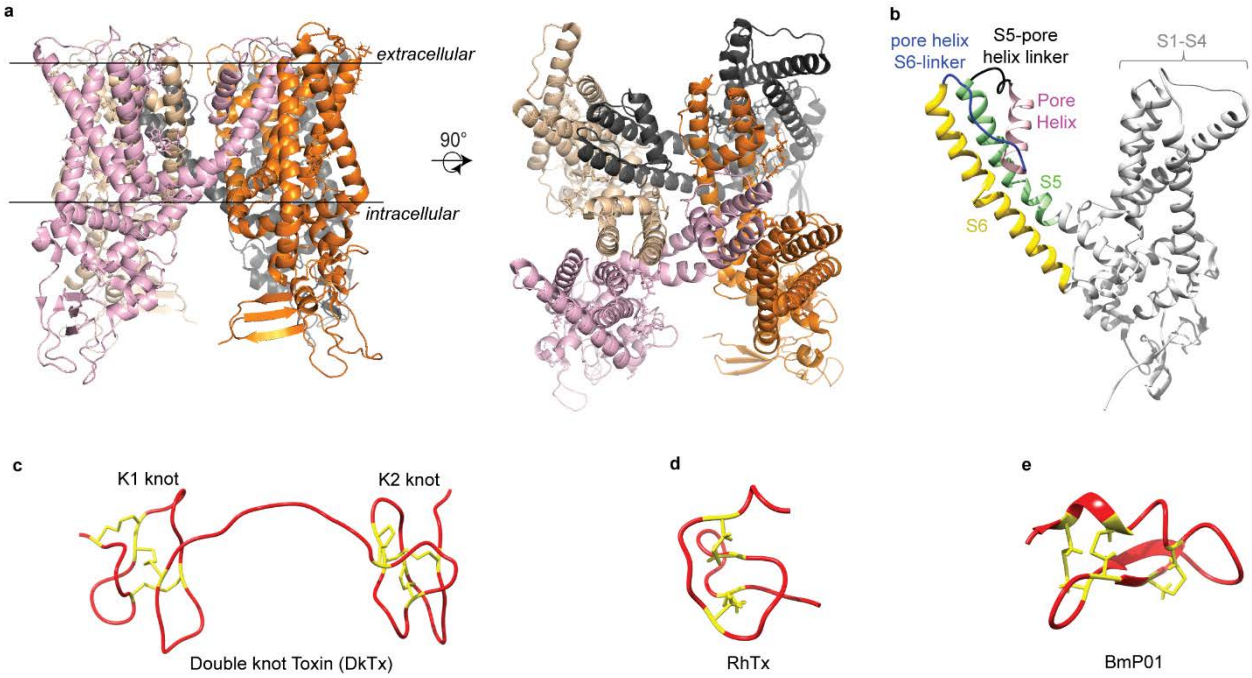

Figure 1.3: Structure of the TRPV1 tetramer and its peptide agonists (a) Top view of closed tetrameric TRPV1 channel showing transmembrane helices and emphasizing the intertwined subunits arranged around a central pore. Side view of the TRPV1 channel on the right panel. Each subunit is color-coded individually. PDB ID: 5IRZ. (b) The depiction shows a TRPV1 single subunit viewed from the side, with S5 (in green) connected to the pore helix (in pink) through its linker (in black). The outer pore linker (in blue), which contains the upper selectivity filter, connects the pore helix to S6 (in yellow). The lower selectivity filter is formed by S6, while S1-S4 are depicted in grey. (c) Peptide toxins targeting TRPV1 channel. *Left panel*: The amphipathic nature of the DkTx structure allows it to protrude the membrane bilayer. Individually visualized knots of DkTx, with the linker between the two knots. This amphipathic nature presumably enables DkTx to successfully protrude into the lipid environment of the cell membrane. Each knot has three disulfide linkages (indicated in yellow) indicating the typical ICK motif. *Middle panel*: The polar RhTx binds TRPV1 through its charged surface. Two cysteine bridges are highlighted in yellow. PDB ID: 2MVA. *Right panel*: BmP01 forms an electrostatic interaction with TRPV1 outer pore region. Structure of BmP01 indicating the typical ICK motif formed by three disulfide bonds (indicated in yellow).

RhTx has a compact structure with a flexible N-terminal tail (Figure 1.3, PDB ID: 2MVA). It has numerous charged residues situated in the C-terminus and charged side chain, which are exposed, thus rendering it a polarized molecule. Functional and structural investigation revealed that RhTx's charged C-terminus can directly interact with mTRPV1's charge-rich outer pore. mTRPV1 residues D602 in the turret, Y632 and T634 in the pore helix, and L461 are critical for RhTx-

induced channel activation.[132] In addition, the outer pore is a recognized hot spot, influencing the actions of several chemical activators, including H^+,[134] divalent cations,[135] and spider toxin DkTx.[76]

Upon systematic functional examination, it was discovered that RhTx has a significant impact on the heat activation process by lowering the activation threshold temperature. Through an allosteric mechanism, RhTx activates TRPV1 and facilitates its opening by preferentially binding to the activated state. However, RhTx is ineffective when the channel is held closed through cooling, indicating that it does not bind to the closed state of TRPV1. A modified version of RhTx called s-RhTx (which has the first three amino acids deleted at the N-terminus) has been developed as a positive allosteric modulator (PAM), showing potential as a promising starting point for the development of analgesic drugs targeting the TRPV1 channel.[136]

BmP01 is a protein consisting of 29 amino acids (3178.6 Da) and it is the first scorpion toxin known to activate TRPV1.[137] The toxin is present in the venom of *Mesobuthus martensii* and has a typical inhibitory cysteine knot (ICK) motif structure with three disulfide bonds that stabilize a compact and rigid protein fold.[138] Concentration-response relationship experiments showed that BmP01 activates the TRPV1 channel in a dose-dependent manner with a similar efficacy to capsaicin.[139] The kinetics of BmP01 activity and washout in electrophysiological recordings from TRPV1 expressing cells are also similar to capsaicin. In addition to TRPV1, BmP01 was found to modulate the activity of voltage-gated potassium channels by strongly inhibiting mKv1.3, hKv1.3, and rKv1.1, but not mKv1.1, showing species specificity. This bi-functionality of BmP01 could lead to an enhanced nociceptive response, as activating TRPV1 and inhibiting Kv channels would result in hyperexcitable nociceptors.[140]

1.5 Toxins, ion channels and plasma membrane

Some toxins just bind to the receptor and not the membrane. The ternary complex we see in TRPV1-DkTx and paddle toxins such as SGTx are very special. Other peptides, such as snake venom cytotoxins, gating-modifier toxins like VsTx, and spider toxins like DkTx, are known for their ability to interact with membranes.

1.5.1 Tripartite complexes. The majority of gating-modifier toxins (GMTs), feature an inhibitory cysteine knot (ICK) motif that is characterized by two to three anti-parallel β-sheets stabilized by

three disulfide bridges, connected by Cys1-Cys4, Cys2-Cys5, and Cys3-Cys6, as demonstrated in Figure 1.4 with examples such as ProTx-II, SgTx-1, Vstx-1, and HwTx-IV. It's worth noting that not all GMTs have anti-parallel beta sheets in their secondary structures, as seen in ProTx-II and HwTx-IV (Figure 1.4a), due to variations in the size of the interconnecting loops. Morever, the conserved cysteine knot connectivity provides stability to these peptides.[141] GMTs exhibit a conserved structural feature in which they fold to create an amphipathic surface profile that comprises a hydrophobic patch surrounded by a charged ring of amino acid residues (as depicted in Figure 1.4b).[142–145] The hydrophobic patch and charged ring are composed of specific amino acid residues, including Trp, Tyr, and Lys, which are frequently involved in peptide-lipid bilayer binding (refer to Figure 1.4c for the sequences).[146] Hence, the conserved hydrophobic patch and charged ring may give GMTs the ability to bind to lipid membranes, in addition to their interactions with voltage-gated ion channels.

The interactions between gating modifier toxins and voltage-gated ion channels can be stabilized by the lipid membrane, as observed in the case of VsTx-1.

The interaction of certain GMTs with lipid bilayers was initially established through studies on VsTx-1.[147] Their research revealed that VsTx-1 had a weaker affinity for the bacterial potassium channel KvAP when the channel was extracted from the membrane using detergent compared to when it was embedded in the membrane.[147] Furthermore, in a spin-down assay, when VsTx-1 was incubated with model lipid membranes, it was found to co-precipitate with the model membranes composed of 1-palmitoyl-2-oleoyl-sn-glycero-3-phosphoethanolamine (POPE): 1-palmitoyl-2-oleoyl-sn-glycero-3-phospho-(1’-rac-glycerol) (POPG) in 3:1 molar ratio.

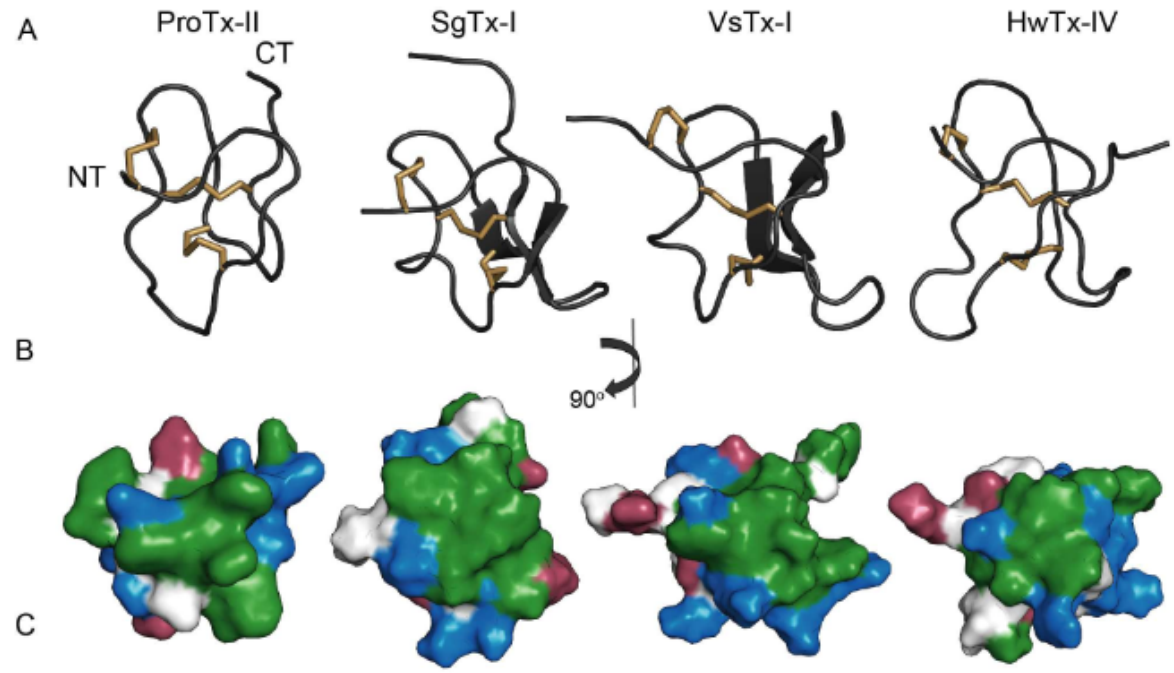

Peptide	Spider species	Sequence
ProTx-II	*Thrixopelma pruriens*	YCQKWMWTCDSERK-CCEGMV--CRL---WCKKKLW--
ProTx-I	*Thrixopelma pruriens*	ECRYWLGGCSAGQT-CCKHLV--CSRRHGWCVWDGTFS
SgTx-I	*Stromatopelma calceatum*	TCRYLFGGCKTTAD-CCKHLA--CRSDGKYCAWDGTF-
HwTx-IV	*Haplopelma schmidti*	ECLEIFKACNPSNDQCCKSSKLVCSRKTRWCKYQI*---
HnTx-IV	*Haplopelma hainanum*	ECLGFGKGCNPSNDQCCKSSNLVCSRKHRWCKYEI*---
VsTx-I	*Grammostola rosea*	ECGKFMWKCKNSND-CCKDLV--CSSRWKWCVLASPF-
HaTx-I	*Grammostola rosea*	ECRYLFGGCKTTSD-CCKHSG--CKFRDKYCAWDFTFS
Hd1a	*Haplopelma doriae*	ACLGFGKSCNPSNDQCCKSLSLACSTKHKWCKYEL---
		1 5 10 15 20 25 30 35

Figure 1.4: Conserved structural characteristics of ProTx-II (PDB ID: 2N9T), SgTx-1 (PDB ID: 1LA4), VsTx-1 (PDB ID: 2NLN), and HwTx-IV (PDB ID: 2M4X). (a) Ribbon representations are displayed in a way that demonstrates the ICK motif, which consists of three disulfide bridges (yellow) and two or three anti-parallel beta sheets in SgTx-1 and VsTx-1, respectively. ProTx-II and HwTx-IV are GMTs that possess the ICK motif but do not have anti-parallel beta sheets. The N-terminal (NT) and C-terminal (CT) are also labeled. (b) The GMTs are shown in surface representations that exhibit the conserved hydrophobic patch and charged ring, which are colored by residue type: hydrophobic in green, positively charged in blue, negatively charged in red, and polar uncharged in white. (c) A sequence alignment of GMTs mentioned in the review is presented, with sequences aligned based on cysteine residues. Trp, Tyr, and Lys residues are identified as crucial for lipid membrane interactions and are colored green (Trp and Tyr) and blue (Lys). The sequence numbers of residues are indicated according to HwTx-IV, HnTx-IV, and Hd1a, along with the spider species from which the peptides were obtained.[141]

The fluorescence emission spectrum of peptides' Trp residues is affected by the local environment, either surrounded by lipid or aqueous, resulting in a change in the quantum yield and a shift towards shorter wavelengths (blue shift). Therefore, the insertion of Trp residues into model membranes is expected to change the fluorescence emission spectrum of the peptide.[147–149]

In studies that investigated the tryptophan fluorescence emission of Trp in VsTx-1 upon titration with POPE/POPG model membranes, it was found that the fluorescence quantum yield increased and the fluorescence emission spectra shifted towards shorter wavelengths (blue shift), indicating that the Tryptophan residues of VsTx-1 are inserted into the lipid membranes. Similar results were obtained when VsTx-1 was studied in model membranes composed of 1-palmitoyl-2-oleoyl-sn-glycero-3-phosphocholine (POPC): POPG in a 1:1 molar ratio. These findings suggested that the difference in VsTx-1-KvAP binding observed with and without membranes was due to the excess free energy of partitioning provided by the lipid membranes. Moreover, the study proposed a stepwise mechanism of GMTs action in which the toxin initially binds to the membrane and then, by being concentrated there, can increase the frequency and apparent affinity of interaction with the paddle motif. A recent study has also suggested that the ability of VsTx-1 to interact with lipid membranes further enhances its affinity for the KvAP VSD.[150]

The electrostatic interactions between gating modifier toxins and the lipid membrane are promoted by the amphipathic structure of SGTx-1.

SGTx-1 is a gating modifier toxin that was first identified as a blocker of the rat potassium channel, Kv2.1.[151,152] It has been observed that certain amino acid residues of SGTx-1 are involved in binding to both the channel and the lipid membrane.[152,153] Specifically, residues Arg3, Tyr4, Leu5, Phe6, Arg22 and Trp30 were found to be important for interactions with Kv2.1 as well as with model membranes.[152,153] These findings suggest that there may be an overlapping binding mode where the same residues of SGTx-1 interact with both the membrane and the channel simultaneously. However, an alternative theory suggests that some GMTs may have a distinct binding face for the membrane and the channel, respectively.[141,154]

Quenchers like acrylamide, bromine, 5- and 16-doxy stearic acid can be used to determine the depth at which peptides insert into model membranes by quenching peptide Trp fluorescence. They can be located at different positions within the lipid bilayer or covalently linked to varying positions on the acyl chains of the phospholipid forming lipid bilayers.[148,149,155,156] To determine

the depth of interaction between the Trp30 residue of SGTx-1 and the membrane, model membranes composed of POPC/POPG (1:1 molar ratio) were prepared using phospholipids containing bromine at different lengths along the acyl chains of the lipids. The fluorescence emission from Trp30 on SGTx-1 was quenched when the bromine was located at a depth of around 9 Å from the center of the model membranes, suggesting a shallow location in the membrane. A similar location has been observed for VsTx-1 and HaTx-1 in anionic lipid membranes.[153,157]

The interaction between SGTx-1 and lipid bilayers appears to be driven by electrostatic interactions between the phospholipid head-groups and the peptide. This is evidenced by the fact that SGTx-1 shows greater affinity for anionic model membranes compared to zwitterionic ones, and also binds more strongly to lipid bilayers prepared using low ionic strength buffers than those prepared with high ionic strength buffers.[153] If GMTs are to be used as pharmacological agents, it is important to investigate whether these electrostatic interactions can be leveraged to enhance the inhibitory potency of the peptides against voltage-gated ion channels.

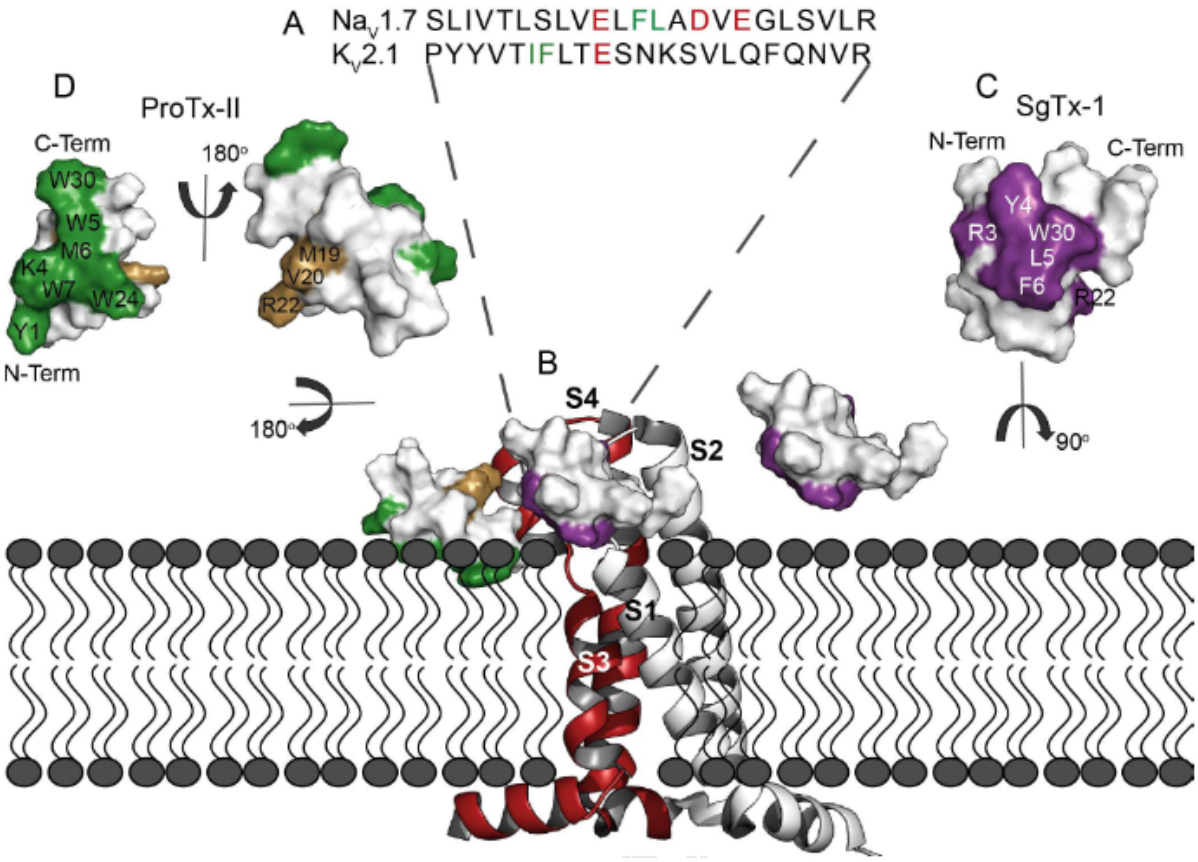

Figure 1.5: The tripartite complexes of SGTx-1 and ProTx-II. (a)The S3-S4 regions of $K_V2.1$ and $Na_V1.7$ are displayed, highlighting the hydrophobic and anionic residues targeted by GMTs in green and red, respectively. (b) Two possible modes of GMT-lipid membrane-ion channel binding are demonstrated using SGTx-1 (PDB ID: 1LA4) and ProTx-II (PDB ID: 2N9T) as examples. SgTx-1 represents a binding mode where the GMT is burrowed between the S1-S2 and S3-S4 loop, while ProTx-II illustrates a binding mode where the GMT interacts with the channel and membrane, mainly interacting with the S3-S4 loop. (c) The proposed overlapping region for channel and membrane binding of SGTx-1 is indicated in purple. (d) The residues proposed to be relevant for the membrane binding of ProTx-II are shown in green, forming a separate membrane binding region from the residues involved in channel binding, displayed in gold.[141]

The gating modifier toxins ProTx-I and ProTx-II increase their potency by taking advantage of electrostatic interactions. ProTx-I and ProTx-II exhibit a preference for interacting with anionic lipid bilayers through electrostatic interactions.[154] There has been also a correlation observed between the potency of ProTx-II at $Na_V1.7$ and its membrane interactions. To investigate the role of Trp and Lys residues in lipid membrane interactions, ProTx-II mutants were designed, and analogues with Tyr replacing Trp exhibited a decrease in both lipid affinity and potency on inhibition of $Na_V1.7$. On the other hand, [Glu17Lys]ProTx-II mutation showed a comparable potency to the wild-type ProTx-II sequence along with stronger affinity to lipid membranes. Membrane interactions have also been found to have a positive correlation with the inhibitory potency of ProTx-II on voltage-gated calcium channels[158] and gHwTx-IV's inhibition of $Na_V1.7$.[141] These findings suggest that enhancing the membrane binding of GMTs could be a potential strategy to increase their potency as inhibitors of voltage-gated ion channels.

1.6 Conclusion

Studies thus far indicate that the lipid membrane serves to anchor and orient toxins for optimal interactions with ion channels. This, in turn, can result in an increase in toxin concentration near the channel binding site.[141,147,150,154,157,159] Additionally, preliminary evidence suggests that regulating peptide-membrane interactions could be beneficial in enhancing the therapeutic effectiveness of GMTs.[121,141]

The idea of the tripartite complex is fascinating, and its existence and importance suggest a departure from the conventional lock-and-key model of drug design. This shift will enable drug

designers to take into account the role of the lipid membrane and consider it in the rational design of drugs.

1.7 References

1. Hille, B. Ion channels of excitable membranes (Sinauer, Sunderland, MA). (2001).

2. Chaffey, N. Alberts, B., Johnson, A., Lewis, J., Raff, M., Roberts, K. and Walter, P. Molecular biology of the cell. 4th edn. (2003).

3. Zhou, H.-X. & McCammon, J. A. The gates of ion channels and enzymes. *Trends in biochemical sciences* **35**, 179–185 (2010).

4. Catterall, W. A. & Swanson, T. M. Structural basis for pharmacology of voltage-gated sodium and calcium channels. *Molecular pharmacology* **88**, 141–150 (2015).

5. Ashcroft, F. M. From molecule to malady. *Nature* **440**, 440–447 (2006).

6. Minor, D. L. An overview of ion channel structure. *Functioning of Transmembrane Receptors in Cell Signaling* 351–358 (2011).

7. Drukarch, B. & Wilhelmus, M. M. Thinking about the action potential: the nerve signal as a window to the physical principles guiding neuronal excitability. *Frontiers in cellular neuroscience* **17**, (2023).

8. Stutzmann, G. E. & Mattson, M. P. Endoplasmic reticulum Ca2+ handling in excitable cells in health and disease. *Pharmacological reviews* **63**, 700–727 (2011).

9. Ashcroft, F. M. *Ion channels and disease*. (Academic press, 1999).

10. Kass, R. S. The channelopathies: novel insights into molecular and genetic mechanisms of human disease. *The Journal of clinical investigation* **115**, 1986–1989 (2005).

11. Staruschenko, A., Ma, R., Palygin, O. & Dryer, S. E. Ion channels and channelopathies in glomeruli. *Physiological Reviews* **103**, 787–854 (2023).

12. Kumar, P., Kumar, D., Jha, S. K., Jha, N. K. & Ambasta, R. K. Ion channels in neurological disorders. *Advances in protein chemistry and structural biology* **103**, 97–136 (2016).

13. Bernardi, J., Aromolaran, K. A. & Aromolaran, A. S. Neurological disorders and risk of arrhythmia. *International Journal of Molecular Sciences* **22**, 188 (2020).

14. Santos, R. *et al.* A comprehensive map of molecular drug targets. *Nature reviews Drug discovery* **16**, 19–34 (2017).

15. Hauser, A. S., Attwood, M. M., Rask-Andersen, M., Schiöth, H. B. & Gloriam, D. E. Trends in GPCR drug discovery: new agents, targets and indications. *Nature reviews Drug discovery* **16**, 829–842 (2017).

16. Payandeh, J., Scheuer, T., Zheng, N. & Catterall, W. A. The crystal structure of a voltage-gated sodium channel. *Nature* **475**, 353–358 (2011).

17. Tao, X., Lee, A., Limapichat, W., Dougherty, D. A. & MacKinnon, R. A Gating Charge Transfer Center in Voltage Sensors. *Science* **328**, 67–73 (2010).

18. Long, S. B., Tao, X., Campbell, E. B. & MacKinnon, R. Atomic structure of a voltage-dependent K+ channel in a lipid membrane-like environment. *Nature* **450**, 376–382 (2007).

19. Efremov, R. G., Gatsogiannis, C. & Raunser, S. Lipid nanodiscs as a tool for high-resolution structure determination of membrane proteins by single-particle cryo-EM. in *Methods in enzymology* vol. 594 1–30 (Elsevier, 2017).

20. Hidalgo, P. & MacKinnon, R. Revealing the Architecture of a K^+ Channel Pore Through Mutant Cycles with a Peptide Inhibitor. *Science* **268**, 307–310 (1995).

21. Doyle, D. A. *et al.* The Structure of the Potassium Channel: Molecular Basis of K^+ Conduction and Selectivity. *Science* **280**, 69–77 (1998).

22. Zhu, Z. *et al.* Simulation and Machine Learning Methods for Ion-Channel Structure Determination, Mechanistic Studies and Drug Design. *Frontiers in Pharmacology* **13**, 939555 (2022).

23. Kalia, J. *et al.* From foe to friend: using animal toxins to investigate ion channel function. *Journal of molecular biology* **427**, 158–175 (2015).

24. von Reumont, B. M. *et al.* Modern venomics—Current insights, novel methods, and future perspectives in biological and applied animal venom research. *GigaScience* **11**, (2022).

25. Hebert, S. C. General principles of the structure of ion channels. *The American journal of medicine* **104**, 87–98 (1998).

26. French, R. J. & Wells, J. B. Sodium ions as blocking agents and charge carriers in the potassium channel of the squid giant axon. *The Journal of general physiology* **70**, 707–724 (1977).

27. Gouaux, E. & MacKinnon, R. Principles of Selective Ion Transport in Channels and Pumps. *Science* **310**, 1461–1465 (2005).

28. Shaya, D. *et al.* Voltage-gated sodium channel (Na_V) protein dissection creates a set of functional pore-only proteins. *Proc. Natl. Acad. Sci. U.S.A.* **108**, 12313–12318 (2011).

29. Long, S. B., Campbell, E. B. & MacKinnon, R. Crystal Structure of a Mammalian Voltage-Dependent *Shaker* Family K^+ Channel. *Science* **309**, 897–903 (2005).

30. Brohawn, S. G., Del Mármol, J. & MacKinnon, R. Crystal Structure of the Human K2P TRAAK, a Lipid- and Mechano-Sensitive K^+ Ion Channel. *Science* **335**, 436–441 (2012).

31. Miller, A. N. & Long, S. B. Crystal Structure of the Human Two–Pore Domain Potassium Channel K2P1. *Science* **335**, 432–436 (2012).

32. Moiseenkova-Bell, V. Y., Stanciu, L. A., Serysheva, I. I., Tobe, B. J. & Wensel, T. G. Structure of TRPV1 channel revealed by electron cryomicroscopy. *Proc. Natl. Acad. Sci. U.S.A.* **105**, 7451–7455 (2008).

33. Moiseenkova-Bell, V. Y. & Wensel, T. G. Hot on the trail of TRP channel structure. *Journal of General Physiology* **133**, 239–244 (2009).

34. Cao, E., Liao, M., Cheng, Y. & Julius, D. TRPV1 structures in distinct conformations reveal activation mechanisms. *Nature* **504**, 113–118 (2013).

35. Zhang, K., Julius, D. & Cheng, Y. Structural snapshots of TRPV1 reveal mechanism of polymodal functionality. *Cell* **184**, 5138–5150 (2021).

36. Borcik, C. G. *et al.* A Cholesterol Dimer Stabilizes the Inactivated State of an Inward-Rectifier Potassium Channel. *Angew Chem Int Ed* **61**, e202112232 (2022).

37. Cheng, Y., Julius, D., Liao, M. & Cao, E. Structure of the TRPV1 ion channel determined by electron cryo-microscopy. (2013).

38. Cheng, Y. Single-particle cryo-EM—How did it get here and where will it go. *Science* **361**, 876–880 (2018).

39. Clapham, D. E. TRP channels as cellular sensors. *Nature* **426**, 517–524 (2003).

40. Julius, D. TRP Channels and Pain. *Annu. Rev. Cell Dev. Biol.* **29**, 355–384 (2013).

41. Lishko, P. V., Procko, E., Jin, X., Phelps, C. B. & Gaudet, R. The ankyrin repeats of TRPV1 bind multiple ligands and modulate channel sensitivity. *Neuron* **54**, 905–918 (2007).

42. Fujiwara, Y. & Minor Jr, D. L. X-ray crystal structure of a TRPM assembly domain reveals an antiparallel four-stranded coiled-coil. *Journal of molecular biology* **383**, 854–870 (2008).

43. Autzen, H. E. *et al.* Structure of the human TRPM4 ion channel in a lipid nanodisc. *Science* **359**, 228–232 (2018).

44. Schmiege, P., Fine, M. & Li, X. The regulatory mechanism of mammalian TRPML s revealed by cryo- EM. *The FEBS Journal* **285**, 2579–2585 (2018).

45. Fábián, B., Sega, M., Voloshin, V. P., Medvedev, N. N. & Jedlovszky, P. Lateral Pressure Profile and Free Volume Properties in Phospholipid Membranes Containing Anesthetics. *J. Phys. Chem. B* **121**, 2814–2824 (2017).

46. Arias, H. R. Role of local anesthetics on both cholinergic and serotonergic ionotropic receptors. *Neuroscience & Biobehavioral Reviews* **23**, 817–843 (1999).

47. Franks, N. P. & Honoré, E. The TREK K2P channels and their role in general anaesthesia and neuroprotection. *Trends in Pharmacological Sciences* **25**, 601–608 (2004).

48. Butterworth, J. F. & Strichartz, G. R. Molecular mechanisms of local anesthesia: a review. *Anesthesiology* **72**, 711–734 (1990).

49. Rao, B. D., Sarkar, P. & Chattopadhyay, A. Effect of tertiary amine local anesthetics on G protein-coupled receptor lateral diffusion and actin cytoskeletal reorganization. *Biochimica et Biophysica Acta (BBA)-Biomembranes* **1863**, 183547 (2021).

50. Papahadjopoulos, D. Studies on the mechanism of action of local anesthetics with phospholipid model membranes. *Biochimica et Biophysica Acta (BBA)-Reviews on Biomembranes* **265**, 169–186 (1972).

51. Urban, B. W., Duch, D. S., Frenkel, C., Rehberg, B. & Wartenberg, H. C. Do general anesthetics act on specific receptors? *Anasthesiologie, Intensivmedizin, Notfallmedizin, Schmerztherapie: AINS* **30**, 375–382 (1995).

52. De-Paula, E. & Schreier, S. Molecular and physicochemical aspects of local anesthetic-membrane interaction. *Brazilian Journal of Medical and Biological Research= Revista Brasileira de Pesquisas Medicas e Biologicas* **29**, 877–894 (1996).

53. Lirk, P., Hollmann, M. W. & Strichartz, G. The science of local anesthesia: basic research, clinical application, and future directions. *Anesthesia & Analgesia* **126**, 1381–1392 (2018).

54. Cantor, R. S. Breaking the Meyer-Overton rule: predicted effects of varying stiffness and interfacial activity on the intrinsic potency of anesthetics. *Biophysical journal* **80**, 2284–2297 (2001).

55. Martin, L. J. & Corry, B. Locating the route of entry and binding sites of benzocaine and phenytoin in a bacterial voltage gated sodium channel. *PLoS computational biology* **10**, e1003688 (2014).

56. Turner, G. L. & Oldfield, E. Effect of a local anaesthetic on hydrocarbon chain order in membranes. *Nature* **277**, 669–670 (1979).

57. Yun, I. *et al.* Amphiphilic effects of local anesthetics on rotational mobility in neuronal and model membranes. *Biochimica et Biophysica Acta (BBA)-Biomembranes* **1564**, 123–132 (2002).

58. Boulanger, Y., Schreier, S. & Smith, I. C. P. Molecular details of anesthetic-lipid interaction as seen by deuterium and phosphorus-31 nuclear magnetic resonance. *Biochemistry* **20**, 6824–6830 (1981).

59. Seelig, A., Allegrini, P. R. & Seelig, J. Partitioning of local anesthetics into membranes: surface charge effects monitored by the phospholipid head-group. *Biochimica et Biophysica Acta (BBA)-Biomembranes* **939**, 267–276 (1988).

60. Castro, V. *et al.* NMR investigations of interactions between anesthetics and lipid bilayers. *Biochimica et Biophysica Acta (BBA)-Biomembranes* **1778**, 2604–2611 (2008).

61. Hooper, N. M. Membrane biology: do glycolipid microdomains really exist? *Current Biology* **8**, R114–R116 (1998).

62. Simons, K. & Toomre, D. Lipid rafts and signal transduction. *Nature reviews Molecular cell biology* **1**, 31–39 (2000).

63. Lichtenberg, D., Goñi, F. M. & Heerklotz, H. Detergent-resistant membranes should not be identified with membrane rafts. *Trends in biochemical sciences* **30**, 430–436 (2005).

64. Besshoh, S., Bawa, D., Teves, L., Wallace, M. C. & Gurd, J. W. Increased phosphorylation and redistribution of NMDA receptors between synaptic lipid rafts and post-synaptic densities following transient global ischemia in the rat brain. *J Neurochem* **93**, 186–194 (2005).

65. Li, X., Serwanski, D. R., Miralles, C. P., Bahr, B. A. & De Blas, A. L. Two pools of Triton X-100-insoluble GABA $_{A}$ receptors are present in the brain, one associated to lipid rafts and another one to the post-synaptic GABAergic complex. *J Neurochem* **102**, 1329–1345 (2007).

66. Sierra-Valdez, F. J., Ruiz-Suárez, J. C. & Delint-Ramirez, I. Pentobarbital modifies the lipid raft-protein interaction: A first clue about the anesthesia mechanism on NMDA and GABAA receptors. *Biochimica et Biophysica Acta (BBA)-Biomembranes* **1858**, 2603–2610 (2016).

67. Maguy, A., Hebert, T. E. & Nattel, S. Involvement of lipid rafts and caveolae in cardiac ion channel function. *Cardiovascular research* **69**, 798–807 (2006).

68. Amsalem, M., Poilbout, C., Ferracci, G., Delmas, P. & Padilla, F. Membrane cholesterol depletion as a trigger of Nav1.9 channel-mediated inflammatory pain. *The EMBO Journal* **37**, e97349 (2018).

69. Bandeiras, C., Serro, A. P., Luzyanin, K., Fernandes, A. & Saramago, B. Anesthetics interacting with lipid rafts. *European Journal of Pharmaceutical Sciences* **48**, 153–165 (2013).

70. Yoshida, K., Takashima, A. & Nishio, I. Effect of dibucaine hydrochloride on raft-like lipid domains in model membrane systems. *MedChemComm* **6**, 1444–1451 (2015).

71. Kinoshita, M., Chitose, T. & Matsumori, N. Mechanism of local anesthetic-induced disruption of raft-like ordered membrane domains. *Biochimica Et Biophysica Acta (BBA)-General Subjects* **1863**, 1381–1389 (2019).

72. Boiteux, C. *et al.* Local anesthetic and antiepileptic drug access and binding to a bacterial voltage-gated sodium channel. *Proc. Natl. Acad. Sci. U.S.A.* **111**, 13057–13062 (2014).

73. Clairfeuille, T., Xu, H., Koth, C. M. & Payandeh, J. Voltage-gated sodium channels viewed through a structural biology lens. *Current opinion in structural biology* **45**, 74–84 (2017).

74. Buyan, A., Sun, D. & Corry, B. Protonation state of inhibitors determines interaction sites within voltage-gated sodium channels. *Proc. Natl. Acad. Sci. U.S.A.* **115**, (2018).

75. Fry, B. G. *et al.* The Toxicogenomic Multiverse: Convergent Recruitment of Proteins Into Animal Venoms. *Annu. Rev. Genom. Hum. Genet.* **10**, 483–511 (2009).

76. Bohlen, C. J. *et al.* A bivalent tarantula toxin activates the capsaicin receptor, TRPV1, by targeting the outer pore domain. *Cell* **141**, 834–845 (2010).

77. Baron, A. *et al.* Venom toxins in the exploration of molecular, physiological and pathophysiological functions of acid-sensing ion channels. *Toxicon* **75**, 187–204 (2013).

78. Lebbe, E. K., Peigneur, S., Wijesekara, I. & Tytgat, J. Conotoxins targeting nicotinic acetylcholine receptors: an overview. *Marine drugs* **12**, 2970–3004 (2014).

79. Dutertre, S., Nicke, A. & Tsetlin, V. I. Nicotinic acetylcholine receptor inhibitors derived from snake and snail venoms. *Neuropharmacology* **127**, 196–223 (2017).

80. Olivera, B. M., Miljanich, G. P., Ramachandran, J. & Adams, M. E. CALCIUM CHANNEL DIVERSITY AND NEUROTRANSMITTER RELEASE: The ω-Conotoxins and ω-Agatoxins. *Annu. Rev. Biochem.* **63**, 823–867 (1994).

81. King, G. F., Escoubas, P. & Nicholson, G. M. Peptide toxins that selectively target insect Na $_V$ and Ca $_V$ channels. *Channels* **2**, 100–116 (2008).

82. Osteen, J. D. *et al.* Selective spider toxins reveal a role for the Nav1. 1 channel in mechanical pain. *Nature* **534**, 494–499 (2016).

83. Cc, C. & CY, L. Isolation of neurotoxins from the venom of Bungarus multicinctus and their modes of neuromuscular blocking action. *Archives internationales de pharmacodynamie et de therapie* **144**, 241–257 (1963).

84. Dellisanti, C. D., Yao, Y., Stroud, J. C., Wang, Z.-Z. & Chen, L. Crystal structure of the extracellular domain of nAChR α1 bound to α-bungarotoxin at 1.94 Å resolution. *Nature neuroscience* **10**, 953–962 (2007).

85. Jami, S., Erickson, A., Brierley, S. M. & Vetter, I. Pain-causing venom peptides: insights into sensory neuron pharmacology. *Toxins* **10**, 15 (2017).

86. Lewis, R. J., Dutertre, S., Vetter, I. & Christie, M. J. Conus venom peptide pharmacology. *Pharmacological reviews* **64**, 259–298 (2012).

87. Yellen, G. The voltage-gated potassium channels and their relatives. *nature* **419**, 35–42 (2002).

88. Cahalan, M. D. & Chandy, K. G. The functional network of ion channels in T lymphocytes. *Immunological Reviews* **231**, 59–87 (2009).

89. Carbone, E., Wanke, E., Prestipino, G., Possani, L. D. & Maelicke, A. Selective blockage of voltage-dependent K+ channels by a novel scorpion toxin. *Nature* **296**, 90–91 (1982).

90. Kuzmenkov, A. I., Krylov, N. A., Chugunov, A. O., Grishin, E. V. & Vassilevski, A. A. Kalium: a database of potassium channel toxins from scorpion venom. *Database* **2016**, baw056 (2016).

91. Yellen, G., Jurman, M. E., Abramson, T. & MacKinnon, R. Mutations Affecting Internal TEA Blockade Identify the Probable Pore-Forming Region of a K $^+$ Channel. *Science* **251**, 939–942 (1991).

92. Yu, L. *et al.* Nuclear Magnetic Resonance Structural Studies of a Potassium Channel−Charybdotoxin Complex. *Biochemistry* **44**, 15834–15841 (2005).

93. Miller, C. The charybdotoxin family of K+ channel-blocking peptides. *Neuron* **15**, 5–10 (1995).

94. Castañeda, O. *et al.* Characterization of a potassium channel toxin from the Caribbean Sea anemone Stichodactyla helianthus. *Toxicon* **33**, 603–613 (1995).

95. Kalman, K. *et al.* Genomic Organization, Chromosomal Localization, Tissue Distribution, and Biophysical Characterization of a Novel MammalianShaker-related Voltage-gated Potassium Channel, Kv1. 7. *Journal of Biological Chemistry* **273**, 5851–5857 (1998).

96. Chang, S. C., Bajaj, S. & Chandy, Kg. ShK toxin: history, structure and therapeutic applications for autoimmune diseases. *WikiJournal of Science* **1**, 1–13 (2018).

97. Beeton, C. *et al.* Targeting effector memory T cells with a selective peptide inhibitor of Kv1. 3 channels for therapy of autoimmune diseases. *Molecular pharmacology* **67**, 1369–1381 (2005).

98. Chi, V. *et al.* Development of a sea anemone toxin as an immunomodulator for therapy of autoimmune diseases. *Toxicon* **59**, 529–546 (2012).

99. Tarcha, E. J. *et al.* Durable pharmacological responses from the peptide ShK-186, a specific Kv1. 3 channel inhibitor that suppresses T cell mediators of autoimmune disease. *Journal of Pharmacology and Experimental Therapeutics* **342**, 642–653 (2012).

100. Hodgkin, A. L. & Katz, B. The effect of sodium ions on the electrical activity of the giant axon of the squid. *The Journal of physiology* **108**, 37 (1949).

101. Ho, K. *et al.* Cloning and expression of an inwardly rectifying ATP-regulated potassium channel. *Nature* **362**, 31–38 (1993).

102. Kubo, Y., Baldwin, T. J., Nung Jan, Y. & Jan, L. Y. Primary structure and functional expression of a mouse inward rectifier potassium channel. *Nature* **362**, 127–133 (1993).

103. Lu, Y., Monsivais, P., Tempel, B. L. & Rubel, E. W. Activity-dependent regulation of the potassium channel subunits Kv1.1 and Kv3.1. *J. Comp. Neurol.* **470**, 93–106 (2004).

104. Whorton, M. R. & MacKinnon, R. Crystal structure of the mammalian GIRK2 K+ channel and gating regulation by G proteins, PIP2, and sodium. *Cell* **147**, 199–208 (2011).

105. Bajaj, S. & Han, J. Venom-derived peptide modulators of cation-selective channels: friend, foe or frenemy. *Frontiers in pharmacology* **10**, 58 (2019).

106. Hille, B. The permeability of the sodium channel to organic cations in myelinated nerve. *The Journal of general physiology* **58**, 599–619 (1971).

107. Model, A. F.-B. & Hille, B. Ionic Selectivity, Saturation, and Block in Sodium Channels. *The Journal of General Physiology* **66**, 535–56o (1975).

108. Hille, B. Local anesthetics: hydrophilic and hydrophobic pathways for the drug-receptor reaction. *The Journal of general physiology* **69**, 497–515 (1977).

109. Agnew, W. S., Levinson, S. R., Brabson, J. S. & Raftery, M. A. Purification of the tetrodotoxin-binding component associated with the voltage-sensitive sodium channel from Electrophorus electricus electroplax membranes. *Proc. Natl. Acad. Sci. U.S.A.* **75**, 2606–2610 (1978).

110. Beneski, D. A. & Catterall, W. A. Covalent labeling of protein components of the sodium channel with a photoactivable derivative of scorpion toxin. *Proc. Natl. Acad. Sci. U.S.A.* **77**, 639–643 (1980).

111. Hartshorne, R. P. & Catterall, W. A. Purification of the saxitoxin receptor of the sodium channel from rat brain. *Proc. Natl. Acad. Sci. U.S.A.* **78**, 4620–4624 (1981).

112. Xu, L. *et al.* Voltage-gated sodium channels: structures, functions, and molecular modeling. *Drug discovery today* **24**, 1389–1397 (2019).

113. Olivera, B. M. *et al.* Peptide Neurotoxins from Fish-Hunting Cone Snails. *Science* **230**, 1338–1343 (1985).

114. Olivera, B. M. *et al.* Diversity of *Conus* Neuropeptides. *Science* **249**, 257–263 (1990).

115. Zhang, M.-M. *et al.* Co-expression of $Na_V\beta$ subunits alters the kinetics of inhibition of voltage-gated sodium channels by pore-blocking μ-conotoxins: $Na_V\beta$ co-expression alters μ-conotoxin kinetics. *Br J Pharmacol* **168**, 1597–1610 (2013).

116. Daly, N. L. *et al.* Structures of μO-conotoxins from Conus marmoreus: Inhibitors of tetrodotoxin (TTX)-sensitive and TTX-resistant sodium channels in mammalian sensory neurons. *Journal of Biological Chemistry* **279**, 25774–25782 (2004).

117. Zorn, S. *et al.* The μO-conotoxin MrVIA inhibits voltage-gated sodium channels by associating with domain-3. *FEBS Letters* **580**, 1360–1364 (2006).

118. Leipold, E. *et al.* μO-Conotoxins Inhibit Na V Channels by Interfering with their Voltage Sensors in Domain-2. *Channels* **1**, 253–262 (2007).

119. Flinspach, M. *et al.* Insensitivity to pain induced by a potent selective closed-state Nav1. 7 inhibitor. *Scientific reports* **7**, 39662 (2017).

120. Peng, K., Shu, Q., Liu, Z. & Liang, S. Function and solution structure of huwentoxin-IV, a potent neuronal tetrodotoxin (TTX)-sensitive sodium channel antagonist from Chinese bird spider Selenocosmia huwena. *Journal of Biological Chemistry* **277**, 47564–47571 (2002).

121. Revell, J. D. *et al.* Potency optimization of Huwentoxin-IV on hNav1. 7: a neurotoxin TTX-S sodium-channel antagonist from the venom of the Chinese bird-eating spider Selenocosmia huwena. *Peptides* **44**, 40–46 (2013).

122. Nilius, B. *et al.* Gating of TRP channels: a voltage connection?: Voltage dependence of TRP channels. *The Journal of Physiology* **567**, 35–44 (2005).

123. Kalia, J. & Swartz, K. J. Exploring structure-function relationships between TRP and Kv channels. *Scientific reports* **3**, 1523 (2013).

124. Cosens, D. J. & Manning, A. Abnormal electroretinogram from a Drosophila mutant. *Nature* **224**, 285–287 (1969).

125. Islam, Md. S. TRP Channels of Islets. in *Transient Receptor Potential Channels* (ed. Islam, Md. S.) vol. 704 811–830 (Springer Netherlands, 2011).

126. Earley, S., Santana, L. F. & Lederer, W. J. The physiological sensor channels TRP and piezo: Nobel Prize in Physiology or Medicine 2021. *Physiological Reviews* **102**, 1153–1158 (2022).

127. Gui, J. *et al.* A tarantula-venom peptide antagonizes the TRPA1 nociceptor ion channel by binding to the S1–S4 gating domain. *Current Biology* **24**, 473–483 (2014).

128. Siemens, J. *et al.* Spider toxins activate the capsaicin receptor to produce inflammatory pain. *Nature* **444**, 208–212 (2006).

129. Julius, D., Gao, Y., Cao, E. & Cheng, Y. TRPV1 structures in nanodiscs reveal mechanisms of ligand and lipid action. (2016).

130. Bae, C. *et al.* Structural insights into the mechanism of activation of the TRPV1 channel by a membrane-bound tarantula toxin. *Elife* **5**, e11273 (2016).

131. Sarkar, D., Singh, Y. & Kalia, J. Protein–Lipid Interfaces Can Drive the Functions of Membrane-Embedded Protein–Protein Complexes. *ACS Chem. Biol.* **13**, 2689–2698 (2018).

132. Yang, S. *et al.* A pain-inducing centipede toxin targets the heat activation machinery of nociceptor TRPV1. *Nature communications* **6**, 8297 (2015).

133. Ombati, R., Luo, L., Yang, S. & Lai, R. Centipede envenomation: Clinical importance and the underlying molecular mechanisms. *Toxicon* **154**, 60–68 (2018).

134. Lee, B. H. & Zheng, J. Proton block of proton-activated TRPV1 current. *Journal of General Physiology* **146**, 147–159 (2015).

135. Yang, F., Ma, L., Cao, X., Wang, K. & Zheng, J. Divalent cations activate TRPV1 through promoting conformational change of the extracellular region. *Journal of General Physiology* **143**, 91–103 (2014).

136. Zhang, H. *et al.* Structure-guided peptide engineering of a positive allosteric modulator targeting the outer pore of TRPV1 for long-lasting analgesia. *Nature Communications* **14**, 4 (2023).

137. Smith, J. J. *et al.* Unique scorpion toxin with a putative ancestral fold provides insight into evolution of the inhibitor cystine knot motif. *Proc. Natl. Acad. Sci. U.S.A.* **108**, 10478–10483 (2011).

138. Wu, G. *et al.* Solution structure of BmP01 from the venom of scorpion Buthus martensii Karsch. *Biochemical and Biophysical Research Communications* **276**, 1148–1154 (2000).

139. Hakim, M. A. *et al.* Scorpion toxin, BmP01, induces pain by targeting TRPV1 channel. *Toxins* **7**, 3671–3687 (2015).

140. Yang, S. *et al.* A bimodal activation mechanism underlies scorpion toxin–induced pain. *Sci. Adv.* **3**, e1700810 (2017).

141. Agwa, A. J., Henriques, S. T. & Schroeder, C. I. Gating modifier toxin interactions with ion channels and lipid bilayers: Is the trimolecular complex real? *Neuropharmacology* **127**, 32–45 (2017).

142. Jung, H. J. *et al.* Solution Structure and Lipid Membrane Partitioning of VSTx1, an Inhibitor of the KvAP Potassium Channel ⁺. *Biochemistry* **44**, 6015–6023 (2005).

143. King, G. F., Tedford, H. W. & Maggio, F. STRUCTURE AND FUNCTION OF INSECTICIDAL NEUROTOXINS FROM AUSTRALIAN FUNNEL-WEB SPIDERS. *Journal of Toxicology: Toxin Reviews* **21**, 361–389 (2002).

144. Takahashi, H. *et al.* Solution structure of hanatoxin1, a gating modifier of voltage-dependent K+ channels: common surface features of gating modifier toxins. *Journal of molecular biology* **297**, 771–780 (2000).

145. Xiao, Y. *et al.* Tarantula huwentoxin-IV inhibits neuronal sodium channels by binding to receptor site 4 and trapping the domain ii voltage sensor in the closed configuration. *Journal of Biological Chemistry* **283**, 27300–27313 (2008).

146. Killian, J. A. & von Heijne, G. How proteins adapt to a membrane–water interface. *Trends in biochemical sciences* **25**, 429–434 (2000).

147. Lee, S.-Y. & MacKinnon, R. A membrane-access mechanism of ion channel inhibition by voltage sensor toxins from spider venom. *Nature* **430**, 232–235 (2004).

148. Instrumentation for Fluorescence Spectroscopy. in *Principles of Fluorescence Spectroscopy* (ed. Lakowicz, J. R.) 27–61 (Springer US, 2006). doi:10.1007/978-0-387-46312-4_2.

149. Ladokhin, A. S., Jayasinghe, S. & White, S. H. How to measure and analyze tryptophan fluorescence in membranes properly, and why bother? *Analytical biochemistry* **285**, 235–245 (2000).

150. Lau, C. H., King, G. F. & Mobli, M. Molecular basis of the interaction between gating modifier spider toxins and the voltage sensor of voltage-gated ion channels. *Scientific Reports* **6**, 34333 (2016).

151. Marvin, L. *et al.* Isolation, amino acid sequence and functional assays of SGTx1. The first toxin purified from the venom of the spider Scodra griseipes. *Eur J Biochem* **265**, 572–579 (1999).

152. Wang, J. M. *et al.* Molecular surface of tarantula toxins interacting with voltage sensors in Kv channels. *The Journal of general physiology* **123**, 455–467 (2004).

153. Milescu, M. *et al.* Tarantula toxins interact with voltage sensors within lipid membranes. *The Journal of general physiology* **130**, 497–511 (2007).

154. Deplazes, E. *et al.* Membrane-Binding Properties of Gating-Modifier and Pore Blocking Toxins: Membrane Interaction is not a Prerequisite for Modification of Channel Gating. *Biophysical Journal* **110**, 29a (2016).

155. Abrams, F. S. & London, E. Calibration of the parallax fluorescence quenching method for determination of membrane penetration depth: refinement and comparison of quenching by spin-labeled and brominated lipids. *Biochemistry* **31**, 5312–5322 (1992).

156. Ladokhin, A. S. Analysis of protein and peptide penetration into membranes by depth-dependent fluorescence quenching: theoretical considerations. *Biophysical journal* **76**, 946–955 (1999).

157. Revell Phillips, L. *et al.* Voltage-sensor activation with a tarantula toxin as cargo. *Nature* **436**, 857–860 (2005).

158. Salari, A., Vega, B. S., Milescu, L. S. & Milescu, M. Molecular interactions between tarantula toxins and low-voltage-activated calcium channels. *Scientific Reports* **6**, 23894 (2016).

159. Jung, H. H. *et al.* Structure and orientation of a voltage-sensor toxin in lipid membranes. *Biophysical journal* **99**, 638–646 (2010).

Chapter 2:

Structural analysis of the TRPV1-DkTx complex and investigating the intrinsic membrane-interaction properties of wild-type DkTx and its variants by tryptophan fluorescence-based membrane partitioning experiments

This chapter has been published:

Sarkar, D., Singh, Y. and Kalia, J.* (2018). Protein–Lipid Interfaces Can Drive the Functions of Membrane-Embedded Protein–Protein Complexes. *ACS Chemical Biology* **13**, 2689-2698.

2.1 Introduction

Membrane proteins are classified as peripheral or integral based on their interaction or integration with biological membranes, distinguishing them from soluble proteins. Among integral membrane proteins, G protein-coupled receptors (GPCRs), ion channels, and transporters are the most commonly targeted small-molecule drug targets.[1–3] Our understanding of the function, dynamics, and pharmacology of these proteins has expanded tremendously in the past decade due to an increase in published structures.[4–9] As more ligand-bound membrane protein structures are discovered, traditional notions of ligand activity based on ligand-protein interactions are being challenged. Many observed ligands bind to intramembrane sites at the protein-lipid interface and make only partial contact with the target protein, leaving large portions of the molecule exposed to the membrane phase.[10–12] Classic pharmacology studies support these emerging structural data, suggesting that ligand-membrane interactions are an overlooked component of ligand-mediated channel activity.

Recent structural research on the homo-tetrameric rat TRPV1 ion channel protein and the double-knot spider toxin (DkTx), its powerful agonist, provides an excellent view of protein-protein complexes in a natural membrane-like environment.[8] These studies have revealed that both lobes (K1 and K2 cystine knots) of the toxin interact with the channel by placing two of their loops (loops 2 and 4) into the membrane, producing a toxin-lipid-channel tripartite complex as shown in Figure 2.1. DkTx is an inhibitory cystine-knot (ICK) toxin that belongs to a family of toxins known to target several types of ion channels,[13–16] but is the only one with two ICK motifs (K1 and K2 separated by a seven-amino-acids-long linker). DkTx stands out among its ICK toxin family, that it is the sole pore-binding toxin documented to undergo membrane partitioning. Other toxins that also partition into the membrane, like Hanatoxin,[15,17,18] inhibit voltage-activated ion channels by targeting their voltage sensors, which are connected to the pore but located far away from it. Unfortunately, the toxin-channel complexes created by these voltage sensor-binding toxins lack structural data, making it impossible to examine the function of toxin-lipid interfaces in channel modulation at the molecular level, thereby obviating molecular-level investigations into the role of toxin-lipid interfaces in channel modulation.

DkTx has an interesting feature wherein it shows an extremely slow wash-off of the toxin after channel activation. This is a curious observation because the TRPV1-DkTx complex structures[7,8] not show any electrostatic, cation-pi, or pi-stacking interactions between the residues of the toxin and those of the channel, which are typically responsible for tight complex formation between proteins. Instead, the structures reveal two close protein-lipid interfaces, one formed by DkTx's K1 knot and the other by its K2 knot. This leads to the hypothesis that protein-lipid interfaces play a significant role in the toxin's binding and potency, despite the relatively sparse protein-protein interaction landscape.[19] Collectively, these structural and functional properties of the DkTx-TRPV1 complex make it an excellent model system for investigating the poorly understood roles of protein-lipid interfaces in the function of protein-protein complexes within membranes.

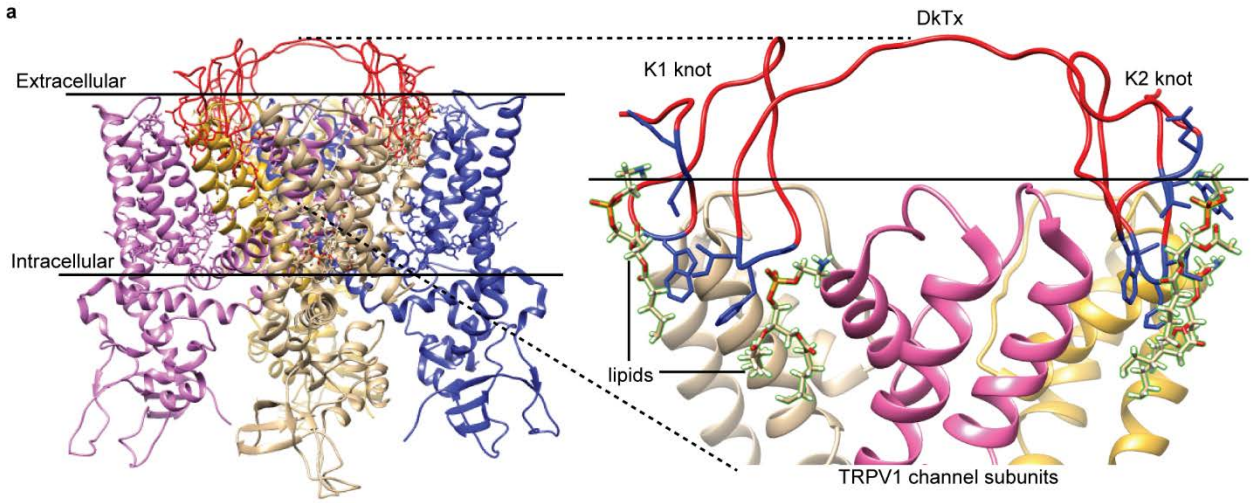

Figure 2.1: The DkTx-TRPV1 complex (PDB: 5irx[8]) viewed sideways from within the membrane, where two DkTx molecules are bound to the outer pore region of TRPV1 and the disulfide linkages present in DkTx molecules have been omitted for the sake of clarity. Solid horizontal lines represent the boundary of lipid membrane. The zoomed-in view of the complex showing the intricate interactions of toxin-lipid-channel subunits, forming a "Tripartite complex". Toxin residues (both K1 and K2 lobes) which are interacting with lipid ligands are depicted in blue.

2.2 Research design and background

DkTx-TRPV1 Structures Enable Generation of Protein-Lipid and Protein-Protein Interaction Maps. We conducted a study on the activation of TRPV1 by DkTx, focusing on the roles of protein-protein and protein-lipid interactions.[19] We used site-directed mutagenesis to create DkTx variants and tested their TRPV1 activation properties using electrophysiology. We selected specific toxin residues for substitution based on the cryo-EM structure of the rat TRPV1-DkTx complex in a lipidic environment,[8] and a molecular dynamics simulation study that predicted lipid-

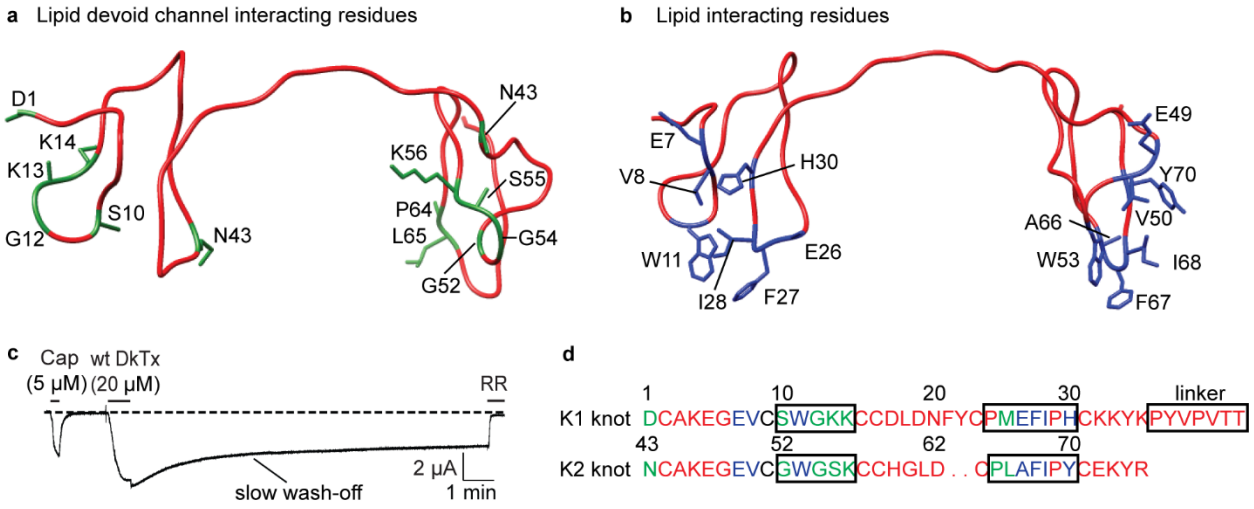

Figure 2.2: DkTx structure. (a) DkTx structure depicted in green color, residues that exclusively interact with TRPV1 channel residues (b) DkTx structure depicted in blue color, residues that interact with lipid ligands. The same color scheme has been used in sequence of K1 and K2 knots (d), the residues of loops 2 and 4 are boxed. (c) A two-electrode voltage clamp electrophysiology recording of TRPV1 expressing oocyte, activation by capsaicin (5 µM) and wash-off, then by DkTx (20 µM), followed by wash-off for ~8 min, complete channel block by ruthenium red (RR, 7 µM). The dotted line represents zero current.

binding sites on the toxin and reported a DkTx-TRPV1 complex structure model.[7] To identify interacting toxin residues, I classified residues lying within 4.4 Å of nearby channel residues or lipid molecules in either of these structures as "interacting" and created interaction maps of all contact points. I found 27 toxin residues that interact with the channel and/or lipids, with 13 exclusively interacting with the channel and 14 interacting with lipids shown in figure 2.2. Of the lipid-interacting residues, eight interacted only with lipids and not the channel, while six interacted with both lipids and channel residues. I have summarized these findings in Table 2.2.

After identifying channel or/and lipid ligand interacting DkTx residues, Debayan Sarkar, a fellow Ph.D. student in Dr. Jeet Kalia's laboratory, generated alanine variants of each of these residues, except for A66 which was substituted to serine. Wild-type DkTx and its variants were

recombinantly expressed in *E. coli* inclusion bodies, refolded and purified to homogeneity by HPLC (except E49A which did not refold under tested conditions). Debayan then determined the EC_{50} values of wild-type DkTx and its variants (depicted in figure 2.3) by performing two electrode voltage clamp (TEVC) experiments on exogenously expressed rat TRPV1 channel in *Xenopus laevis* oocytes.

EC_{50} values data clearly show that the variants of DkTx that interact with channel residues independent of lipid ligands have a moderate effect (2-4 fold change in EC_{50} value with respect to wild-type) on the potency of the toxin. In contrast, variants of several lipid interacting toxin residues caused a profound effect on toxin-potency. In particular, W11A and W53A mutants, where W11A yielded an 80-fold higher EC_{50} value with respect to wild-type and in case of W53A variant were found to be such a poor TRPV1 agonist that its dose response is incomplete due to lack of solubility of toxin at the extremely high concentrations required to achieve full channel activation. A similar pattern is observed in the case of V8A, V50A, F27A, and F67A where toxins variants have more than ~14 fold lower potency when compared to wild-type. Indeed, the residues that are found to be most important for toxin activity are either aliphatic hydrophobic (V8, I28, V50 and I68) or aromatic residues (W11, F27, W53 and F67). Interestingly, none of the toxin residues interacting exclusively with TRPV1 channel residues exhibits a huge impact on toxin potency in comparison with lipid-interacting toxin residues.

Another important observation from the electrophysiological experiments is the effect of substituting DkTx residues on the toxin's wash-off rates. For this analysis, I used electrophysiological recordings (done by Debayan Sarkar) to extract the wash off traces for 3 or 5 min in axon test file (.atf) format using the "Clampfit 10.5" software. The extracted traces were then subjected to data point extraction at every 7500^{th} point interval using the R3.4.1 package.

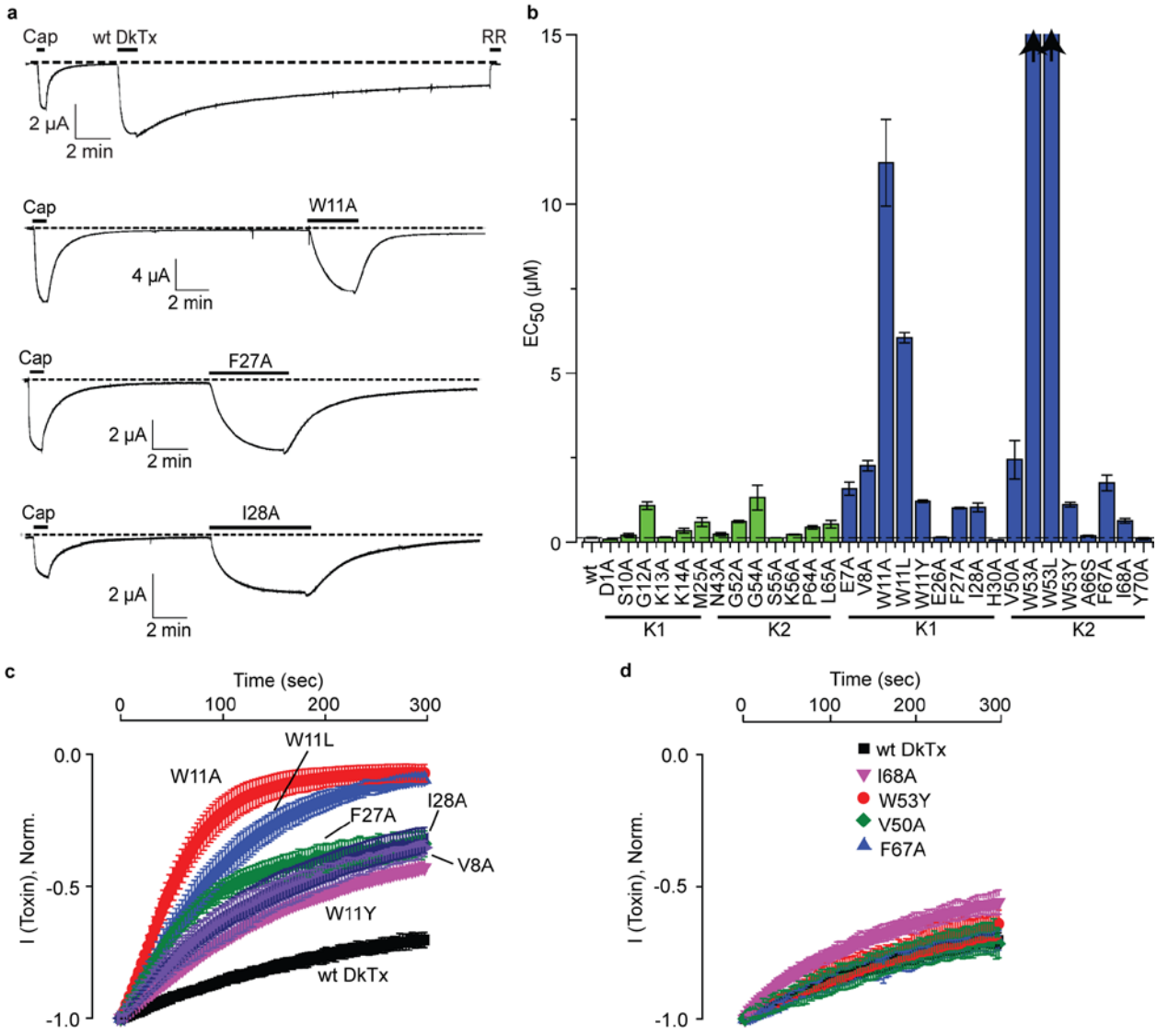

Figure 2.3: Electrophysiology results of DkTx variants. (a) TEVC recordings of wildtype DkTx, along with lipid interacting variants of K1 knot. (b) EC_{50} bar graph: Effect on the potency of DkTx by altering channel-toxin interfaces (green color) and toxin lipid interfaces (blue color). Dotted line depicts the potency level of the WT DkTx. (c) Normalized fast wash-off traces of lipid interacting K1 knot variants with respect to wild-type toxin and normalized slow wash-off of lipid interacting K2 knot variants (d). All data acquired by Debayan Sarkar.

The extracted points from 3-5 normalized traces were used to obtain averaged representative traces for wash-off kinetic plots along with their respective SEM values (error bars). Interestingly, all the DkTx variants demonstrating fast wash-off, W11, F27, I28, and V8, are all lipid interacting residues of K1 lobe, whereas variants of W53, F67, I68, and V50 of K2 lobe demonstrate a relatively similar wash-off pattern as that of the wild-type toxin (depicted in figure 2.3).

The slow washing-off property of DkTx has been previously attributed to its bivalency—the presence of two agonist channel-binding motifs (K1 and K2) within the DkTx molecule. This conclusion is supported by the observation that when the single knots of DkTx are individually used to activate TRPV1, the toxin wash-off rates are considerably faster. W11A and F27A mutants revealed that toxin variants containing both knots could also undergo fast wash-off suggesting that this assumption is probably too simplistic. Indeed, if bivalency were the sole reason for slow wash-off, substituting merely one residue at a time, as in the case of the W11A, F27A, and I28A variants, would not be expected to so drastically speed-up toxin wash-off (figure 2.3). To investigate the causation of the fast wash-off trend of the toxin variants of specially lipid interacting residues we assumed that these toxin variants could interact intimately with the bulk lipid. Thus to study the intrinsic membrane affinity of the variants, I have done tryptophan fluorescence based membrane partitioning experiments with DkTx and its variants.

2.3 Results

The substitution of lipid-interacting residues resulting in the generation of fast washing-off toxin variants suggests a link between wash-off kinetics and toxin-membrane lipid interactions. In order to compare the intrinsic membrane lipid-interacting properties of these toxin variants, we conducted tryptophan fluorescence-based membrane partitioning experiments on large unilamellar vesicles (LUVs) made of POPC-POPG (1:1) using similar approaches to those reported previously.[20,21] Our experiments with wild-type DkTx demonstrated that it partitions well into vesicles, with a robust increase in fluorescence emission and a blue shift of 13 nm and a modest increase in emission intensity in the presence of vesicles generated with the same concentration of lipids (red traces in Figure 2.4a). In contrast, the W11A variant demonstrated only a 3 nm blueshift and a modest increase in emission intensity under the same conditions. Consistent with these observations, normalized relative fluorescence versus lipid concentration plots (Figure 2.4b) revealed that in contrast to the wild-type toxin that partitions so well that the curve saturates at ~0.25 mM lipid concentration, the W11A variant partitions poorly, not saturating even at a 1.25 mM lipid concentration. Other fast washing-off K1 knot variants of DkTx, such as W11L and F27A, also demonstrated greatly reduced membrane partitioning compared to the wild-type toxin.

However, variants of analogous K2 knot residues of DkTx, such as W53A and F67A, demonstrated efficient membrane partitioning similar to the wild-type toxin.

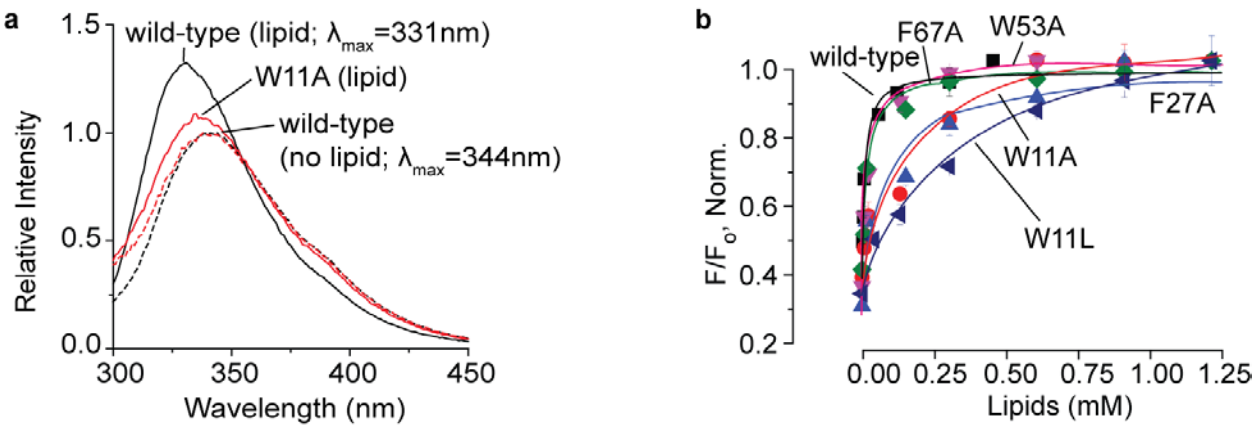

Figure 2.4: Lipid membrane-interaction studies with DkTx variants by tryptophan fluorescence. a) Tryptophan emission spectra of DkTx (black) and the W11A variant (red) in the presence of 1:1 POPC:POPG liposomes (total lipid concentration: 0.1 mM) have been depicted as solid curves, whereas the ones obtained in the absence of lipids are shown as dashed curves. Only the traces obtained in presence of lipids are labeled. b) Plots of normalized relative fluorescence intensity (F/F_o) at 320 nm for the wild-type toxin and the Ala variants of analogous Phe and Trp residues of the K1 and K2 knots as a function of the available lipid concentration.

I generated similar partitioning plots for other fast washing-off DkTx variants and their analogous K2 knot variants that yielded slow wash-off and obtained their Kx values (Figure 2.4 of for each variant's partitioning plots and fluorescence emission spectra, and Table 2.2 for their Kx values). Plotting the Kx values of the wild-type toxin and those of the K2 and fast washing-off K1 variants versus the percentage of wash-off yielded a plot that demonstrated a good correlation (Pearson's r = -0.90) for the fast washing-off K1 variants. The K2 variants of DkTx such as W53Y, I68A, and F67A that wash-off slowly demonstrated efficient membrane partitioning similar to the wild-type DkTx. These results suggest that the slow wash-off demonstrated by DkTx is a consequence of its high intrinsic affinity for the membrane, which is orchestrated by the protein-lipid interactions of the K1 knot and not the K2 knot.

To examine the interactions between DkTx and its variants with membranes that more closely resemble physiological conditions, Debayan Sarkar, a Ph.D. student in our lab has conducted experiments to determine their binding affinity to *Xenopus laevis* oocytes. These experiments followed established protocols developed by Swartz and colleagues[22] for investigating the membrane-interacting properties of toxins that target voltage-activated ion channels. Table 2.1

shows the results of these experiments, which indicate that the slow washing-off toxins (wild-type DkTx and variants of the K2 knot residues W53, F67, and I68) were significantly depleted, while the fast washing-off K1 variants (W11A, W11L, and F27A) showed lower depletion. A correlation analysis between the % wash-off and fractional depletion for the fast washing-off K1 variants yielded a good correlation (Pearson's r = -0.94), similar to the analysis shown in Figure 2.6a for LUVs.

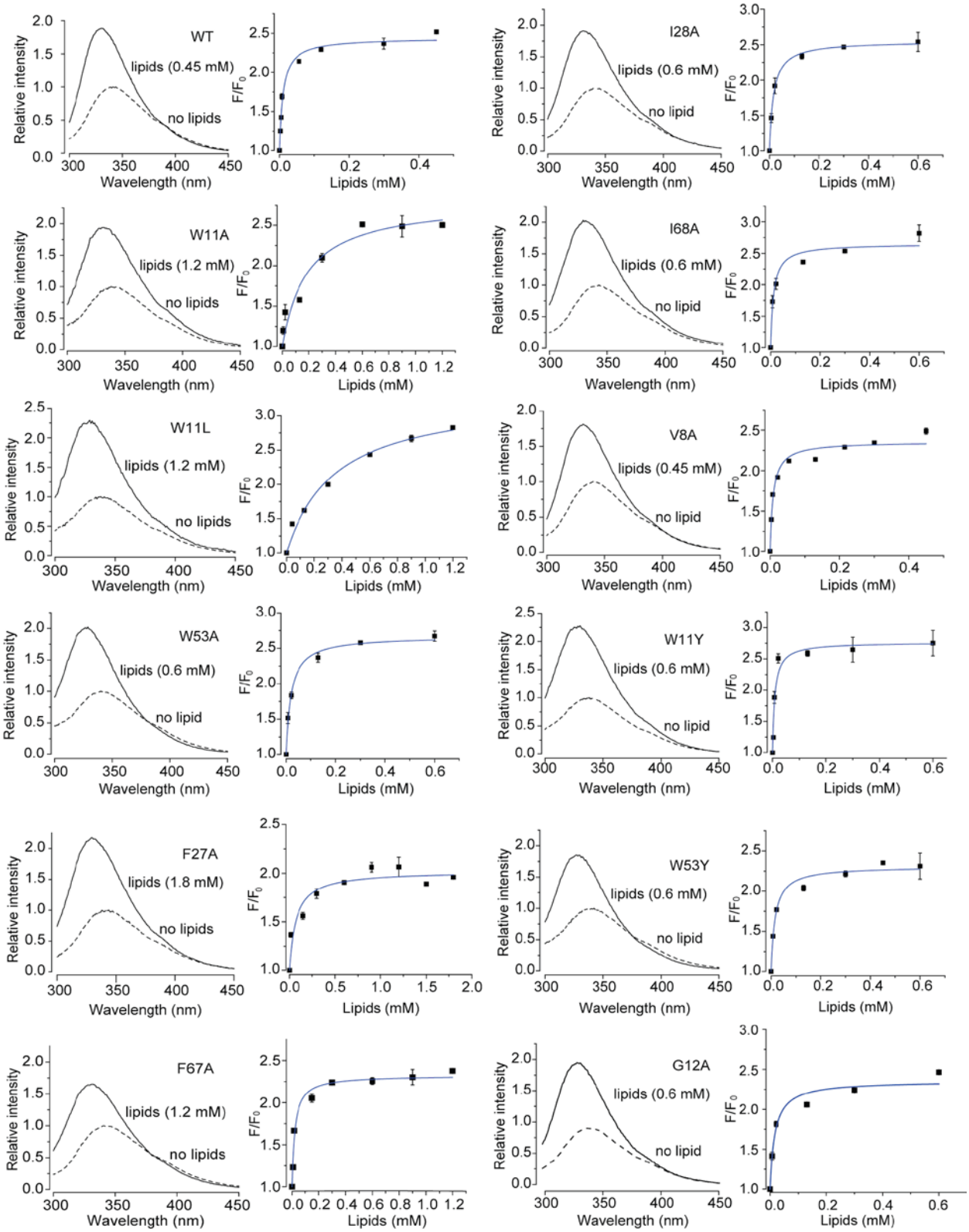
WT
lipids (0.45 mM)
no lipids
I28A
lipids (0.6 mM)
no lipid
W11A
lipids (1.2 mM)
no lipids
I68A
lipids (0.6 mM)
no lipid
W11L
lipids (1.2 mM)
no lipids
V8A
lipids (0.45 mM)
no lipid
W53A
lipids (0.6 mM)
no lipid
W11Y
lipids (0.6 mM)
no lipid
F27A
lipids (1.8 mM)
no lipids
W53Y
lipids (0.6 mM)
no lipid
F67A
lipids (1.2 mM)
no lipids
G12A
lipids (0.6 mM)
no lipid
Relative intensity
Wavelength (nm)
F/F0
Lipids (mM)

Figure 2.5: Interaction of wild-type DkTx and its variants with lipid membranes measured using tryptophan fluorescence. Tryptophan emission spectra of DkTx and its variants (left panel) in absence (dotted lines) and in presence (solid lines) of LUVs made from a 1:1 molar ratio of POPC: POPG. Relative fluorescence intensity (right panel) at 320 nm (F/F_0) as a function of the available lipid concentration (60% of total lipid concentration). All values of Kx of DkTx variants are provided in Table 6. Error bars correspond to SEM (n = 3 or 4).

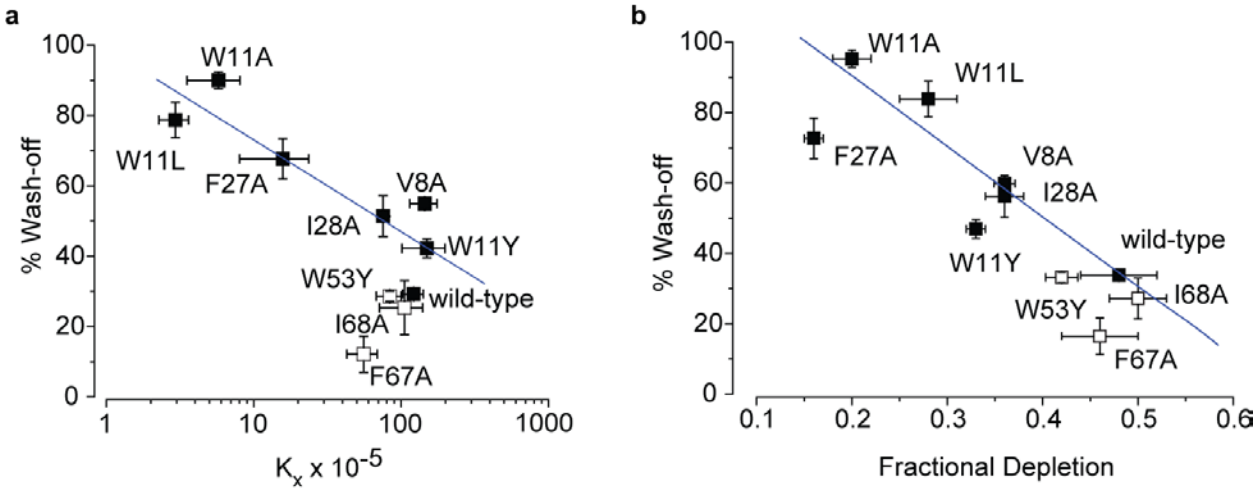

Figure 2.6: Correlation plot of percentage wash-off and membrane partitioning coefficient and the fractional depletion values for DkTx and its variants. Plot of percentage wash-off of wild-type DkTx and K1 variants (solid squares), and those of K2 variants (open squares) after 3 min of buffer perfusion post TRPV1 activation by saturation concentrations of the toxins (obtained from the electrophysiology experiments; done by Debayan Sarkar) versus mol. fraction partitioning coefficients (K_X) values (obtained from the tryptophan fluorescence experiments). The blue line shown was generated by fitting a linear equation to the data for the K1 variants. Plot of % wash-off of wild-type DkTx and K1 variants (solid squares) and K2 variants (open squares) after 3 min of buffer perfusion post TRPV1 activation by saturation concentrations of the toxins (obtained from the electrophysiology experiments; done by Debayan Sarkar) versus fractional depletion (obtained from HPLC peak areas; done by Debayan Sarkar). The blue line shown was generated by fitting a linear equation to the data for the K1 variants. Each data point is an average of three to five recordings/assays, and the error bars correspond to standard deviation values.

Table 2.1. Consolidated data summary for all DkTx variants.

S. No.	Knot	DkTx variant	EC_{50} (μM) Courtesy: Debayan Sarkar	Fold Change in EC_{50} Courtesy: Debayan Sarkar	Hill Coefficient (nH) Courtesy: Debayan Sarkar	% Wash-off after 3 min of buffer perfusion post channel activation by saturation concentration of toxin Courtesy: Debayan Sarkar	Mol. fraction partition coefficient (Kx)	Fractional depletion (oocytes) Courtesy: Debayan Sarkar
1		Wild-type	0.14 ± 0.02	1.0	1.32 ± 0.17	33.77 ± 1.26 (1.1 μM)	(9.03±1.38)E6	0.48 ± 0.04
2	K1	D1A	0.08 ± 0.00	0.6	1.84 ± 0.22	25.81 ± 3.29 (0.55 μM)	N.D	N.D
3		E7A	1.59 ± 0.19	11.4	1.32 ± 0.17	25.97 ± 4.17 (13.2 μM)	N.D.	N.D
4		V8A	2.26 ± 0.15	16.1	1.13 ± 0.06	59.81 ± 0.69 (13.2 μM)	(1.06±0.21)E7	0.36 ± 0.01
5		S10A	0.22 ± 0.05	1.6	1.67 ± 0.38	12.13 ± 1.50 (1.1 μM)	N.D	N.D
6		W11A	11.22 ± 1.3	80.1	1.68 ± 0.17	95.30 ± 2.45 (26.4 μM)	(4.99±1.86)E5	0.20 ± 0.02
7		W11L	6.04 ± 2.01	43.1	1.54 ± 0.43	83.87 ± 5.10 (19.8 μM)	(2.63±0.57)E5	0.28 ± 0.03
8		W11Y	1.21 ± 0.04	8.6	1.41 ± 0.07	46.92 ± 2.70 (6.6 μM)	(1.1±0.4)E7	0.33 ± 0.01
9		G12A	1.08 ± 0.11	7.7	1.21 ± 0.16	68.91 ± 3.58 (13.2 μM)	(5.55±1.62)E6	0.62 ± 0.03
10		K13A	0.15 ± 0.02	1.1	1.01 ± 0.11	32.35 ± 5.32 (2.2 μM)	N.D	N.D
11		K14A	0.35 ± 0.07	2.5	1.26 ± 0.22	21.44 ± 3.63 (2.2 μM)	N.D	N.D
12		M25A	0.60 ± 0.13	4.3	0.96 ± 0.14	30.56 ± 6.10 (6.6 μM)	N.D	N.D
13		E26A	0.15 ± 0.03	1.1	1.31 ± 0.39	20.78 ± 3.03 (0.55 μM)	N.D	N.D
14		F27A	1.01 ± 0.02	7.2	2.14 ± 0.09	72.67± 5.78 (6.6 μM)	(1.29±0.61)E6	0.16 ±0.01
15		I28A	1.03 ± 0.13	7.4	1.22 ± 0.20	56.18 ± 5.90 (13.2 μM)	(5.74±0.4)E6	0.36 ±0.02
16		H30A	0.07 ± 0.00	0.5	2.12 ± 0.42	22.05 ± 5.45 (1.1 μM)	N.D	N.D
17	K2	N43A	0.25 ± 0.05	1.8	1.47 ± 0.27	42.94 ± 3.39 (1.1 μM)	N.D	N.D
18		V50A	2.44 ± 0.57	17.4	1.13 ±0.20	29.99 ± 2.93 (19.8 μM)	N.D.	N.D
19		G52A	0.62 ± 0.22	4.4	1.14 ± 0.34	41.06 ± 9.56 (6.6 μM)	N.D	N.D
20		W53A	N.A.	>100	N.A.	N.A.	(4.6±0.65)E6	0.49 ± 0.04
21		W53L	N.A.	>100	N.A.	N.A.	N.D	N.D
22		W53Y	1.11 ± 0.07	7.4	1.92 ± 0.22	33.12 ± 1.48 (6.6 μM)	(6.34±1.16)E6	0.42 ± 0.02
23		G54A	1.32 ± 0.37	9.4	0.99 ± 0.16	24.80 ± 3.07 (6.6 μM)	N.D	N.D

24		S55A	0.14 ± 0.01	1.0	1.24 ± 0.07	29.48 ± 3.72 (1.1 µM)	N.D	N.D
25		K56A	0.24 ± 0.01	1.7	1.55 ± 0.07	20.02 ± 6.66 (2.2 µM)	N.D	N.D
26		P64A	0.45 ± 0.05	3.2	2.30 ± 0.63	32.37 ± 2.83 (1.1 µM)	N.D	N.D
27		L65A	0.54 ± 0.11	3.9	1.05 ± 0.18	18.67 ± 7.73 (2.2 µM)	N.D	N.D
28		A66S	0.20 ± 0.02	1.4	1.25 ± 0.14	30.20 ± 5.13 (1.1 µM)	N.D	N.D
29		F67A	1.76 ± 0.23	12.6	1.59 ± 0.28	16.43 ± 5.20 (13.2 µM)	(4.30±0.95)E6	0.46 ± 0.04
30		I68A	0.64 ± 0.07	4.6	2.93 ± 0.98	27.15 ± 5.80 (6.6 µM)	(7.88±2.44)E6	0.5 ± 0.03
31		Y70A	0.11 ± 0.04	0.8	1.61 ± 0.83	36.75 ± 7.34 (0.55 µM)	N.D	N.D

Table 2.2. Map of interactions between DkTx and TRPV1/lipids.

Lipids are numbered according to the scheme employed in Figure 2.2. The paper that reported the docking model[7] also reported MD simulations to predict lipid-interacting residues of DkTx—this information is also provided in the table below.

5irx structure[8]		Docking model[7]	
Toxin residue:Channel residue/Lipid	**Distance (Å)**	**Toxin residue:Channel residue**	**Distance (Å)**
1 ASP(CB):535 LYS(NZ)	4.374		
7 GLU(N):lipid 1 6O9(H011)	4.124	Predicted as lipid-interacting (MD simulations)	
7 GLU(CA):lipid 1 6O9(N01)	3.41		
7 GLU(CA):lipid 1 6O9(H012)	3.661		
7 GLU(CA):lipid 1 6O9(H011)	2.88		
7 GLU(C):lipid 1 6O9(N01)	3.741		
7 GLU(C):lipid 1 6O9(H012)	3.627		
7 GLU(C):lipid 1 6O9(H011)	3.298		
7 GLU(CB):lipid 1 6O9(N01)	3.4		
7 GLU(CB):lipid 1 6O9(H012)	3.696		
7 GLU(CB):lipid 1 6O9(H011)	3.221		
7 GLU(CG):lipid 1 6O9(N01)	3.733		
7 GLU(CG):lipid 1 6O9(H012)	4.3		
7 GLU(CG):lipid 1 6O9(H011)	3.594		
8 VAL(N):lipid 1 6O9(N01)	3.06	Predicted as lipid-interacting (MD simulations)	
8 VAL(N):lipid 1 6O9(H012)	2.674		
8 VAL(N):lipid 1 6O9(H011)	2.815		
8 VAL(N):lipid 1 6O9(H032)	4.218		
8 VAL(CA):lipid 1 6O9(N01)	4.09		
8 VAL(CA):lipid 1 6O9(H012)	3.468		
8 VAL(CA):lipid 1 6O9(H011)	3.947		
8 VAL(C):lipid 1 6O9(H012)	4.354		
8 VAL(O):lipid 1 6O9(H012)	4.229		
8 VAL(CB):lipid 1 6O9(N01)	3.948		
8 VAL(CB):lipid 1 6O9(H012)	3.168		
8 VAL(CB):lipid 1 6O9(H011)	3.958		
8 VAL(CB):lipid 1 6O9(H032)	3.655		
8 VAL(CB):lipid 1 6O9(H101)	3.827		
8 VAL(CG1):lipid 1 6O9(H101)	3.7		
8 VAL(CG1):lipid 1 6O9(H112)	4.222		
8 VAL(CG2):lipid 1 6O9(N01)	3.763		

5irx structure		Docking model	
Toxin residue:Channel residue/Lipid	**Distance (Å)**	**Toxin residue:Channel residue**	**Distance (Å)**
8 VAL(CG2):lipid 1 6O9(C03)	3.782		
8 VAL(CG2):lipid 1 6O9(C20)	4.395		
8 VAL(CG2):lipid 1 6O9(O22)	3.614		
8 VAL(CG2):lipid 1 6O9(H012)	3.157		
8 VAL(CG2):lipid 1 6O9(H011)	3.569		
8 VAL(CG2):lipid 1 6O9(H032)	2.903		
8 VAL(CG2):lipid 1 6O9(H031)	3.951		
8 VAL(CG2):lipid 1 6O9(H101)	3.673		
10 SER(N):653 TYR(O)	4.372	Predicted as lipid-interacting (MD simulations)	
10 SER(CA):653 TYR(O)	3.953		
10 SER(CA):655 PHE(N)	4.347		
10 SER(CA):656 LYS(N)	3.685		
10 SER(CA):656 LYS(CA)	4.242		
10 SER(CA):656 LYS(CB)	3.839		
10 SER(CA):657 ALA(N)	3.974		
10 SER(C):655 PHE(N)	3.803		
10 SER(C):655 PHE(CA)	3.89		
10 SER(C):655 PHE(C)	4.15		
10 SER(C):656 LYS(N)	3.513		
10 SER(C):656 LYS(CA)	4.377		
10 SER(C):657 ALA(N)	3.695		
10 SER(C):657 ALA(CB)	4.175		
10 SER(O):655 PHE(N)	3.604		
10 SER(O):655 PHE(CA)	3.242		
10 SER(O):655 PHE(C)	3.301		
10 SER(O):655 PHE(O)	4.309		
10 SER(O):656 LYS(N)	2.809		
10 SER(O):656 LYS(CA)	3.652		
10 SER(O):656 LYS(C)	3.616		
10 SER(O):656 LYS(CB)	4.137		
10 SER(O):657 ALA(N)	2.735		
10 SER(O):657 ALA(CA)	3.615		
10 SER(O):657 ALA(C)	4.301		
10 SER(O):657 ALA(CB)	3.488		
10 SER(O):658 VAL(N)	3.952		
10 SER(CB):656 LYS(N)	4.086		
10 SER(CB):656 LYS(CA)	4.145		
10 SER(CB):656 LYS(C)	4.141		

5irx structure		Docking model	
Toxin residue:Channel residue/Lipid	**Distance (Å)**	**Toxin residue:Channel esidue**	**Distancev (Å)**
10 SER(CB):656 LYS(CB)	3.575		
10 SER(CB):656 LYS(CG)	4.285		
10 SER(CB):657 ALA(N)	3.407		
10 SER(CB):657 ALA(CA)	4.149		
10 SER(CB):657 ALA(CB)	3.78		
11 TRP(N):655 PHE(N)	4.22	Predicted as lipid-interacting (MD simulations)	
11 TRP(CA):655 PHE(N)	4.292		
11 TRP(CA):655 PHE(CA)	4.347		
11 TRP(C):655 PHE(N)	4.043		
11 TRP(C):655 PHE(CA)	4.313		
11 TRP(C):655 PHE(CG)	4.352		
11 TRP(C):655 PHE(CD1)	4.064		
11 TRP(C):655 PHE(CE1)	4.079		
11 TRP(C):655 PHE(CZ)	4.347		
11 TRP(O):655 PHE(N)	3.4	11 TRP(CA):655 PHE(N)	3.953
11 TRP(O):655 PHE(CA)	3.627	11 TRP(CA):655 PHE(CA)	4.169
11 TRP(O):655 PHE(CB)	4	11 TRP(CA):655 PHE(CD2)	4.371
11 TRP(O): 655PHE(CG)	3.213	11 TRP(C):655 PHE(N)	3.576
11 TRP(O):655 PHE(CD1)	3.028	11 TRP(C):655 PHE(CA)	4.21
11 TRP(O):655 PHE(CD2)	3.401	11 TRP(C):655 PHE(CD2)	4.305
11 TRP(O):655 PHE(CE1)	3.069	11 TRP(O):655 PHE(N)	2.94
11 TRP(O):655 PHE(CE2)	3.438	11 TRP(O):655 PHE(CA)	3.928
11 TRP(O):655 PHE(CZ)	3.256	11 TRP(O):655 PHE(CG)	4.5
11 TRP(CG):657 ALA(CB)	4.398	11 TRP(O):654 ASP(C)	3.69
11 TRP(CD1):657 ALA(CB)	3.935	11 TRP(O):654 ASP(CA)	3.488
11 TRP(CD2):657 ALA(CB)	4.217	11 TRP(O):654 ASP(CB)	3.868
11 TRP(CD2):658 VAL(CG2)	3.505	11 TRP(CG):655 PHE(CD2)	4.24
11 TRP(NE1):657 ALA(CB)	3.38	11 TRP(CD1):657 ALA(CB)	4.279
11 TRP(CE2):657 ALA(CB)	3.575	11 TRP(CD2):658 VAL(CG2)	3.941
11 TRP(CE3):657 ALA(CG2)	3.505	11 TRP(NE1):657 ALA(CB)	4.127
11 TRP(CZ2):657 ALA(CB)	3.895	11 TRP(CE3):657 ALA(CG2)	3.596
11 TRP(CZ3):658 VAL(CG2)	3.531	11 TRP(CE3):655 PHE(CD2)	4.018
11 TRP(CH2):658 VAL(CG2)	4.311	11 TRP(CE3):657 PHE(CE2)	4.252
11 TRP(CH2):661 ILE(CD2)	4.318	11 TRP(CZ3):658 VAL(CG2)	3.89
		11 TRP(CB):655 PHE(N)	4.108
		11 TRP(CB):655 PHE(CA)	3.838
		11 TRP(CB):655 PHE(CG)	4.017
		11 TRP(CB):655 PHE(CD2)	3.31

5irx structure		Docking model	
Toxin residue:Channel residue/Lipid	**Distance (Å)**	**Toxin residue:Channel residue**	**Distance (Å)**
11 TRP (CB): lipid 1 6O9 (H112)	3.682	11 TRP(CB):655 PHE(CE2)	3.71
11 TRP (CG):lipid 1 6O9 (O18)	4.233		
11 TRP (CG):lipid 1 6O9 (H112)	3.841		
11 TRP (CD1):lipid 1 6O9 (H112)	4.28		
11 TRP (CD2):lipid 1 6O9 (C13)	4.054		
11 TRP (CD2):lipid 1 6O9 (O18)	3.745		
11 TRP (CD2):lipid 1 6O9 (H112)	4.289		
11 TRP (CD2):lipid 1 6O9 (H142)	4.054		
11 TRP (CD2):lipid 1 6O9 (H151)	4.183		
11 TRP (NE1):lipid 1 6O9 (H142)	4.235		
11 TRP (CE2):lipid 1 6O9 (C13)	4.337		
11 TRP (CE2):lipid 1 6O9 (C14)	4.345		
11 TRP (CE2):lipid 1 6O9 (O18)	4.369		
11 TRP (CE2):lipid 1 6O9 (H142)	3.669		
11 TRP (CE2):lipid 1 6O9 (H151)	4.324		
11 TRP (CE2):lipid 1 6O9 (H162)	4.279		
11 TRP (CE3):lipid 2 6OE (H181)	4.255		
11 TRP (CE3):lipid 1 6O9 (C13)	4.076		
11 TRP (CE3):lipid 1 6O9 (C15)	4.345		
11 TRP (CE3):lipid 1 6O9 (O18)	3.463		
11 TRP (CE3):lipid 1 6O9 (H142)	4.238		
11 TRP (CE3):lipid 1 6O9 (H151)	3.535		
11 TRP (CZ2):lipid 1 6O9 (C14)	4.215		
11 TRP (CZ2):lipid 1 6O9 (C15)	4.291		
11 TRP (CZ2):lipid 1 6O9 (C16)	4.166		
11 TRP (CZ2):lipid 1 6O9 (H142)	3.496		
11 TRP (CZ2):lipid 1 6O9 (H151)	3.916		
11 TRP (CZ2):lipid 1 6O9 (H162)	3.308		
11 TRP (CZ3): lipid 2 6OE (H181)	4.043		
11 TRP (CZ3):lipid 1 6O9 (C13)	4.373		
11 TRP (CZ3):lipid 1 6O9 (C14)	4.287		
11 TRP (CZ3):lipid 1 6O9 (C15)	3.812		
11 TRP (CZ3):lipid 1 6O9 (C16)	4.147		
11 TRP (CZ3):lipid 1 6O9 (O18)	3.878		
11 TRP (CZ3):lipid 1 6O9 (H142)	4.061		
11 TRP (CZ3):lipid 1 6O9 (H151)	2.99		
11 TRP (CZ3):lipid 1 6O9 (H162)	3.604		
11 TRP (CZ3):lipid 1 6O9 (H172)	4.294		

5irx structure		Docking model	
Toxin residue:Channel residue/Lipid	**Distance (Å)**	**Toxin residue:Channel residue**	**Distance (Å)**
11 TRP (CH2):lipid 1 6O9 (C14)	4.176		
11 TRP CH2):lipid 1 6O9 (C15)	3.786		
11 TRP (CH2):lipid 1 6O9 (C16)	3.662		
11 TRP (CH2):lipid 1 6O9 (C17)	4.315		
11 TRP (CH2):lipid 1 6O9 (H142)	3.698		
11 TRP (CH2):lipid 1 6O9 (H151)	3.22		
11 TRP (CH2):lipid 1 6O9 (H162)	2.877		
11 TRP (CH2):lipid 1 6O9 (H172)	4.185		
12 GLY(C):535 LYS(CD)	4.24	12 GLY(O):535 LYS(CE)	4.374
12 GLY(C):654 ASP(CB)	4.333	12 GLY(O):535 LYS(NZ)	3.858
12 GLY(O):535 LYS(CG)	4.273	12 GLY(O):535 LYS(CD)	3.921
12 GLY(O):535 LYS(CD)	3.511	12 GLY(O):535 LYS(CE)	3.741
12 GLY(O):654 ASP(CA)	4.351	12 GLY(O):535 LYS(NZ)	2.894
12 GLY(O):654 ASP(CB)	3.545	12 GLY(O):654 ASP(CG)	4.02
12 GLY(O):655 PHE(CD2)	4.284	12 GLY(O):654 ASP(OD1)	4.078
12 GLY(O):655 PHE(CE2)	3.907	12 GLY(O):654 ASP(OD2)	4.156
		12 GLY(N):655 PHE(CE2)	4.312
		12 GLY(N):655 PHE(CZ)	4.382
		12 GLY(CA):535 LYS(CD)	3.84
		12 GLY(CA):535 LYS(CE)	4.085
		12 GLY(CA):535 LYS(NZ)	4.094
		12 GLY(CA):655 PHE(CZ)	4.319
13 LYS(CA):654 ASP(CB)	4.163	13 LYS(O):654 ASP(OD1)	4.219
13 LYS(C):654 ASP(CA)	4.393		
13 LYS(C):654 ASP(CB)	4.35		
14 LYS (N):654 ASP(N)	4.398	14 LYS(CD):654 ASP(OD1)	4.274
14 LYS (N):654 ASP(CA)	4.112	14 LYS(CE):654 ASP(CG)	4.244
14 LYS (N):654 ASP(CB)	4.072	14 LYS(CE):654 ASP(OD1)	3.818
14 LYS(CA):653 TYR(O)	4.36	14 LYS(CE):654 ASP(OD2)	3.823
14 LYS(CB):653 TYR(C)	3.944	14 LYS(NZ):654 ASP(CG)	3.386
14 LYS(CB):653 TYR(O)	4.015	14 LYS(NZ):652 ASP(OD1)	2.958
14 LYS (CB):654 ASP(N)	3.854	14 LYS(NZ):652 ASP(OD2)	3.129
14 LYS (CB):654 ASP(CA)	4.395	14 LYS(CG):652 ASP(OD1)	3.571
14 LYS(CE):652 ASN(C)	4.178		
14 LYS(CE):652 ASN(O)	3.653		

5irx structure		Docking model	
Toxin residue:Channel residue/Lipid	**Distance (Å)**	**Toxin residue:Channel residue**	**Distance (Å)**
14 LYS(CE):652 ASN(CB)	3.917		
14 LYS(NZ):652 ASN(C)	4.107		
14 LYS(NZ):652 ASN(O)	3.214		
14 LYS(NZ):652 ASN(CB)	4.222		
		23 CYS(CA):656 LYS(NZ)	4.201
		23 CYS(C):656 LYS(NZ)	3.847
		23 CYS(O):656 LYS(CE)	3.623
		23 CYS(O):656 LYS(NZ)	2.861
		23 CYS(CB):656 LYS(CE)	4.304
		23 CYS(CB):656 LYS(NZ)	3.523
		23 CYS(SG):656 LYS(CE)	3.91
		23 CYS(SG):656 LYS(NZ)	3.783
25 MET(C):631 TYR(CD2)	3.843	25 MET(C):629 SER(OG)	4.384
25 MET(C):631 TYR(CE2)	4.08	25 MET(SD):648 GLU(OE2)	3.909
25 MET(O):631 TYR(CG)	4.358	25 MET(SD):650 THR(CG2)	3.822
25 MET(O):631 TYR(CD2)	3.191	25 MET(CE):635 LEU(CD1)	3.934
25 MET(O):631 TYR(CE2)	3.099	25 MET(CE):650 THR(CG2)	4.226
25 MET(O):631 TYR(CZ)	4.215	25 MET(CE):660 ILE(CG1)	4.012
25 MET(CE):635 LEU(CD1)	3.732	25 MET(N):629 SER(OG)	4.296
25 MET(CE):649 PHE(CB)	4.066	25 MET(CB):629 SER(OG)	4.005
25 MET(CE):649 PHE(CD2)	4.165	25 MET(CG):635 LEU(CD1)	4.162
25 MET(CE):660 ILE(CD1)	4.374	25 MET(CG):648 GLU(OE1)	3.394
26 GLU(N):631 TYR(CD2)	4.194	26 GLU(CA):631 TYR(CB)	3.822
26 GLU(CA):631 TYR(CB)	3.983	26 GLU(CA):631 TYR(CG)	3.605
26 GLU(CA):631 TYR(CG)	4.022	26 GLU(CA):631 TYR(CD2)	3.577
26 GLU(CA):631 TYR(CD2)	3.61	26 GLU(CA):631 TYR(CE2)	4.153
26 GLU(CA):631 TYR(CE2)	4.367	26 GLU(CA):631 TYR(CD1)	4.205
26 GLU(C):631 TYR(CG)	4.211	26 GLU(N):629 SER(OG)	4.094
26 GLU(C):631 TYR(CD2)	3.949	26 GLU(N):631 TYR(CB)	3.775
26 GLU(CB):631 TYR(CB)	4.287	26 GLU(N):631 TYR(CG)	4.102
26 GLU(CB):629 SER(CB)	4.395	26 GLU(N):631 TYR(CD2)	4.191
26 GLU(CB):629 SER(OG)	3.882	26 GLU(O):631 TYR(CD2)	4.241
		26 GLU(CG):629 SER(CB)	4.345
		26 GLU(CG):629 SER(OG)	3.585
		26 GLU(CD):629 SER(CB)	4.353
		26 GLU(CD):629 SER(OG)	3.5

5irx structure		Docking model	
Toxin residue:Channel residue/Lipid	**Distance (Å)**	**Toxin residue:Channel residue**	**Distance (Å)**
		26 GLU(CD):630 LEU(N)	4.122
		26 GLU(CD):631 TYR(N)	3.938
		26 GLU(CD):631 TYR(CB)	4.164
		26 GLU(CD):631 TYR(CG)	3.969
		26 GLU(CD):631 TYR(CD1)	3.588
		26 GLU(CD):631 TYR(CE1)	4.165
		26 GLU(OE1):631 TYR(CG)	4.008
		26 GLU(OE1):631 TYR(CD1)	3.337
		26 GLU(OE1):631 TYR(CE1)	3.514
		26 GLU(OE1):631 TYR(CZ)	4.302
		26 GLU(OE2):629 SER(CA)	3.509
		26 GLU(OE2):629 SER(C)	3.467
		26 GLU(OE2):629 SER(OG)	4.383
		26 GLU(OE2):629 SER(CB)	3.514
		26 GLU(OE2):629 SER(OG)	2.652
		26 GLU(OE2):630 LEU(N)	2.993
		26 GLU(OE2):630 LEU(CA)	3.685
		26 GLU(OE2):630 LEU(C)	3.788
		26 GLU(OE2):630 LEU(CB)	3.874
		26 GLU(OE2):631 TYR(N)	2.973
		26 GLU(OE2):631 TYR(CA)	3.937
		26 GLU(OE2):631 TYR(CB)	3.738
		26 GLU(OE2):631 TYR(CG)	3.874
		26 GLU(OE2):631 TYR(CD1)	3.489
		26 GLU(OE2):631 TYR(CE1)	4.363
26 GLU (CA):lipid 3 6OE (O07)	3.224	Predicted as lipid-interacting (MD simulations)	
26 GLU (C):lipid 3 6OE (P05)	4.143		
26 GLU (C):lipid 3 6OE (O07)	2.638		
26 GLU (C):lipid 3 6OE (H092)	4.365		
26 GLU (O):lipid 3 6OE (O04)	4.354		
26 GLU (O):lipid 3 6OE (P05)	3.236		
26 GLU (O):lipid 3 6OE (O06)	3.752		
26 GLU (O):lipid 3 6OE (O07)	1.819		
26 GLU (O):lipid 3 6OE (O08)	4.04		
26 GLU (O):lipid 3 6OE (H092)	3.964		
26 GLU (CB):lipid 3 6OE (C03)	4.166		
26 GLU (CB):lipid 3 6OE (O04)	4.253		
26 GLU (CB):lipid 3 6OE (P05)	4.126		
26 GLU (CB):lipid 3 6OE (O07)	2.973		

5irx structure		Docking model	
Toxin residue:Channel residue/Lipid	**Distance (Å)**	**Toxin residue:Channel residue**	**Distance (Å)**
26 GLU (CB):lipid 3 6OE (H031)	3.342		
27 PHE(N):631 TYR(CG)	4.312	27 PHE(N):631 TYR(CD2)	3.948
27 PHE(N):631 TYR(CD2)	3.796	27 PHE(N):631 TYR(CE2)	3.745
27 PHE(N):631 TYR(CE2)	3.822	27 PHE(N):631 TYR(CZ)	4.284
27 PHE(N):631 TYR(CZ)	4.351	27 PHE(CA):631 TYR(CE2)	4.228
27 PHE(CA):631 TYR(CE2)	4.141	27 PHE(CB):631 TYR(CE2)	4.387
27 PHE(CA):631 TYR(CZ)	4.215		
27 PHE(O):657 ALA(CB)	4.14		
27 PHE(CB):631 TYR(CG)	4.044		
27 PHE(CB):631 TYR(CD1)	3.756		
27 PHE(CB):631 TYR(CD2)	4.079		
27 PHE(CB):631 TYR(CE1)	3.515		
27 PHE(CB):631 TYR(CE2)	3.856		
27 PHE(CB):631 TYR(CZ)	3.563		
27 PHE(CB):631 TYR(OH)	4.065		
27 PHE(CG):631 PHE(CE1)	4.03		
27 PHE(CG):631 TYR(CZ)	4.236		
27 PHE(CG):631 TYR(OH)	4.391		
27 PHE(CD1):631 TYR(CE1)	4.125		
27 PHE(CD1):631 TYR(CZ)	4.134		
27 PHE(CD1):631 TYR(OH)	3.855		
27 PHE(CE1):661 ILE(CD1)	3.792		
27 PHE (N):lipid 3 6OE (O07)	3.71	Predicted as lipid-interacting (MD simulations)	
27 PHE (CA):lipid 3 6OE (O07)	4.244		
27 PHE (CB):lipid 3 6OE (O07)	3.89		
27 PHE (CB):lipid 3 6OE (C09)	4.25		
27 PHE (CB):lipid 3 6OE (H092)	3.33		
27 PHE (CG):lipid 3 6OE (O20)	4.227		
27 PHE (CG):lipid 3 6OE (H092)	3.837		
27 PHE (CG):lipid 3 6OE (H232)	3.635		
27 PHE (CD1):lipid 3 6OE (H232)	3.612		
27 PHE (CD1):lipid 3 6OE (H252)	3.911		
27 PHE (CD1):lipid 3 6OE (H251)	4.309		
27 PHE (CD2):lipid 3 6OE (O20)	3.807		
27 PHE (CD2):lipid 3 6OE (C21)	4.336		
27 PHE (CD2):lipid 3 6OE (H092)	3.786		
27 PHE (CD2):lipid 3 6OE (H232)	3.669		
27 PHE (CE1):lipid 3 6OE (C25)	4.306		
27 PHE (CE1):lipid 3 6OE (H232)	3.624		

5irx structure		Docking model	
Toxin residue:Channel residue/Lipid	**Distance (Å)**	**Toxin residue:Channel residue**	**Distance (Å)**
27 PHE (CE1):lipid 3 6OE (H252)	3.517		
27 PHE (CE1):lipid 3 6OE (H251)	4.383		
27 PHE (CE2):lipid 3 6OE (O20)	4.271		
27 PHE (CE2):lipid 3 6OE (C21)	4.361		
27 PHE (CE2):lipid 3 6OE (H221)	3.949		
27 PHE (CE2):lipid 3 6OE (H232)	3.681		
27 PHE (CZ):lipid 3 6OE (H162)	4.019		
27 PHE (CZ):lipid 3 6OE (H221)	4.097		
27 PHE (CZ):lipid 3 6OE (H232)	3.66		
27 PHE (CZ):lipid 3 6OE (H252)	4.124		
28 ILE (N):lipid 3 6OE (O07)	4.21	Predicted as lipid-interacting (MD simulations)	
28 ILE (CD1):lipid 1 6O9 (O12)	4.395		
28 ILE (CD1):lipid 1 6O9 (C14)	3.91		
28 ILE (CD1):lipid 1 6O9 (H141)	3.968		
28 ILE (CD1):lipid 1 6O9 (H142)	3.078		
30 HIS		Predicted as lipid-interacting (MD simulations)	
43 ASN(O):535 LYS(NZ)	4.322	43 ASN(OD1):535 LYS(NZ)	4.343
43 ASN(CB):535 LYS(NZ)	3.708	43 ASN(ND2):654 ASP(CG)	3.832
		43 ASN(ND2):654 ASP(OD1)	4.275
		43 ASN(ND2):654 ASP(OD2)	3.228
49 GLU (CA):lipid 4 6O9 (N01)	3.756	Predicted as lipid-interacting (MD simulations)	
49 GLU (CA):lipid 4 6O9 (H012)	4.192		
49 GLU (CA):lipid 4 6O9 (H011)	3.126		
49 GLU (C):lipid 4 6O9 (N01)	3.955		
49 GLU (C):lipid 4 6O9 (H012)	4.074		
49 GLU (C):lipid 4 6O9 (H011)	3.359		
49 GLU (CB):lipid 4 6O9 (N01)	3.792		
49 GLU (CB):lipid 4 6O9 (H012)	4.266		
49 GLU (CB):lipid 4 6O9 (H011)	3.473		
49 GLU (CG):lipid 4 6O9 (N01)	4.167		
49 GLU (CG):lipid 4 6O9 (H011)	3.936		
50 VAL (N):lipid 4 6O9 (N01)	3.15	Predicted as lipid-interacting (MD simulations)	
50 VAL (N):lipid 4 6O9 (H012)	3.03		
50 VAL (N):lipid 4 6O9 (H011)	2.705		

5irx structure		Docking model	
Toxin residue:Channel residue/Lipid	**Distance (Å)**	**Toxin residue:Channel residue**	**Distance (Å)**
50 VAL (CA):lipid 4 6O9 (N01)	4.093		
50 VAL (CA):lipid 4 6O9 (H012)	3.683		
50 VAL (CA):lipid 4 6O9 (H011)	3.771		
50 VAL (CB):lipid 4 6O9 (N01)	3.84		
50 VAL (CB):lipid 4 6O9 (O06)	4.338		
50 VAL (CB):lipid 4 6O9 (H012)	3.179		
50 VAL (CB):lipid 4 6O9 (H011)	3.71		
50 VAL (CB):lipid 4 6O9 (H032)	3.986		
50 VAL (CB):lipid 4 6O9 (H101)	3.744		
50 VAL (CG1):lipid 4 6O9 (H101)	3.719		
50 VAL (CG1):lipid 4 6O9 (H112)	4.041		
50 VAL (CG2):lipid 4 6O9 (N01)	3.66		
50 VAL (CG2):lipid 4 6O9 (C03)	4.017		
50 VAL (CG2):lipid 4 6O9 (O06)	4.276		
50 VAL (CG2):lipid 4 6O9 (C10)	4.326		
50 VAL (CG2):lipid 4 6O9 (C20)	4.259		
50 VAL (CG2):lipid 4 6O9 (O22)	3.538		
50 VAL (CG2):lipid 4 6O9 (H012)	3.113		
50 VAL (CG2):lipid 4 6O9 (H011)	3.369		
50 VAL (CG2):lipid 4 6O9 (H032)	3.094		
50 VAL (CG2):lipid 4 6O9 (H031)	4.37		
50 VAL (CG2):lipid 4 6O9 (H101)	3.372		
		51 CYS(SG):656 LYS(CE)	4.227
52 GLY(N):653 TYR(O)	4.348	52 GLY(C):655 PHE(N)	3.692
52 GLY(CA):653 TYR(O)	3.965	52 GLY(C):655 PHE(CA)	4.042
52 GLY(CA):656 LYS(N)	3.767	52 GLY(C):654 ASP(OD1)	4.221
52 GLY(CA):656 LYS(CA)	4.307	52 GLY(O):655 PHE(CA)	3.398
52 GLY(CA):656 LYS(CB)	3.872	52 GLY(O):655 PHE(C)	4.291
52 GLY(CA):657 ALA(N)	4.045	52 GLY(O):656 LYS(N)	4.137
52 GLY(C):655 PHE(N)	3.846	52 GLY(O):654 ASP(CA)	3.973
52 GLY(C):655 PHE(CA)	3.945	52 GLY(O):654 ASP(C)	3.797
52 GLY(C):655 PHE(C)	4.177	52 GLY(O):654 ASP(CG)	4.139
52 GLY(C):656 LYS(N)	3.509	52 GLY(O):654 ASP(OD1)	3.034
52 GLY(C):656 LYS(CA)	4.349	52 GLY(O):654 ASP(N)	2.753
52 GLY(C):657 ALA(N)	3.676		
52 GLY(C):657 ALA(CB)	4.163		
52 GLY(O):655 PHE(N)	3.596		

5irx structure		Docking model	
Toxin residue:Channel residue/Lipid	Distance (Å)	Toxin residue:Channel residue	Distance (Å)
52 GLY(O):655 PHE(CA)	3.261		
52 GLY(O):655 PHE(C)	3.275		
52 GLY(O):655 PHE(O)	4.291		
52 GLY(O):656 LYS(N)	2.73		
52 GLY(O):656 LYS(CA)	3.552		
52 GLY(O):656 LYS(C)	3.54		
52 GLY(O):656 LYS(CB)	4.007		
52 GLY(O):657 ALA(N)	2.677		
52 GLY(O):657 ALA(CA)	3.594		
52 GLY(O):657 ALA(C)	4.319		
52 GLY(O):657 ALA(CB)	3.49		
52 GLY(O):658 VAL(N)	3.995		
53 TRP(N):655 PHE(N)	4.28	53 TRP(CA):655 PHE(CD2)	4.174
53 TRP(CA):655 PHE(N)	4.329	53 TRP(C):655 PHE(CD2)	3.717
53 TRP(CA):655 PHE(CA)	4.27	53 TRP(C):655 PHE(CE2)	3.72
53 TRP(C):655 PHE(N)	4.032	53 TRP(O):655 PHE(CD1)	3.523
53 TRP(C):655 PHE(CA)	4.272	53 TRP(O):655 PHE(CE2)	3.2
53 TRP(C):655 PHE(CG)	4.364	53 TRP(O):655 PHE(CZ)	4.182
53 TRP(C):655 PHE(CD1)	4.065	53 TRP(O):636 GLU(CG)	4.113
53 TRP(C):655 PHE(CE1)	4.112	53 TRP(CD1):657 ALA(CB)	4.117
53 TRP(O):655 PHE(N)	3.373	53 TRP(CD2):657 ALA(CB)	4.02
53 TRP(O):655 PHE(CA)	3.56	53 TRP(CD2):658 VAL(CG2)	
53 TRP(O):655 PHE(CB)	3.961	53 TRP(NE1):657 ALA(CB)	3.472
53 TRP(O):655 PHE(CG)	3.209	53 TRP(CE2):657 ALA(CB)	3.396
53 TRP(O):655 PHE(CB)	3.004	53 TRP(CE3):658 VAL(CG2)	3.646
53 TRP(O):655 PHE(CD1)	3.454	53 TRP(CZ2):657 ALA(CB)	3.538
53 TRP(O):655 PHE(CD2)	3.089	53 TRP(CZ3):658 VAL(CG2)	3.495
53 TRP(O):655 PHE(CE2)	3.528	53 TRP(CH2):658 VAL(CG2)	4.305
53 TRP(O):655 PHE(CZ)	3.332	53 TRP(CH2):661 ILE(CD1)	3.982
53 TRP(CG):657 ALA(CB)	4.328	53 TRP(CH2):657 ALA(CB)	4.256
53 TRP(CD1):657 ALA(CB)	3.895		
53 TRP(CD2):657 ALA(CB)	4.166		
53 TRP(CD2):658 VAL(CG2)	4.305		
53 TRP(NE1):657 ALA(CB)	3.39		
53 TRP(CE2):657 ALA(CB)	3.576		
53 TRP(CE3):658 VAL(CG2)	3.52		
53 TRP(CZ2):657 ALA(CB)	3.931		
53 TRP(CZ3):658 VAL(CG2)	3.568		
53 TRP(CH2):658 VAL(CG2)	4.382		

5irx structure		Docking model	
Toxin residue:Channel residue/Lipid	**Distance (Å)**	**Toxin residue:Channel residue**	**Distance (Å)**
53 TRP(CH2):661 ILE(CD1)	4.28		
53 TRP (CB):lipid 4 6O9 (H112)	3.837	Predicted as lipid-interacting (MD simulations)	
53 TRP (CG):lipid 4 6O9 (O18)	4.372		
53 TRP (CG):lipid 4 6O9 (H112)	3.959		
53 TRP (CD1):lipid 4 6O9 (H112)	4.371		
53 TRP (CD2):lipid 4 6O9 (C13)	4.206		
53 TRP (CD2):lipid 4 6O9 (O18)	3.863		
53 TRP (CD2):lipid 4 6O9 (H112)	4.37		
53 TRP (CD2):lipid 4 6O9 (H142)	4.238		
53 TRP (CD2):lipid 4 6O9 (H151)	4.385		
53 TRP (NE1):lipid 4 6O9 (H142)	4.33		
53 TRP (CE2):lipid 4 6O9 (H142)	3.809		
53 TRP (CE2):lipid 4 6O9 (H162)	4.34		
53 TRP (CE3):lipid 4 6O9 (C13)	4.252		
53 TRP (CE3):lipid 4 6O9 (O18)	3.609		
53 TRP (CE3):lipid 4 6O9 (H151)	3.8		
53 TRP (CE3):lipid 5 6OE (H181)	4.36		
53 TRP (CZ2):lipid 4 6O9 (C14)	4.324		
53 TRP (CZ2):lipid 4 6O9 (C15)	4.395		
53 TRP (CZ2):lipid 4 6O9 (C16)	4.237		
53 TRP (CZ2):lipid 4 6O9 (H142)	3.623		
53 TRP (CZ2):lipid 4 6O9 (H151)	4.027		
53 TRP (CZ2):lipid 4 6O9 (H162)	3.369		
53 TRP (CZ3):lipid 4 6O9 (C15)	4.058		
53 TRP (CZ3):lipid 4 6O9 (C16)	4.356		
53 TRP (CZ3):lipid 4 6O9 (O18)	3.964		
53 TRP (CZ3):lipid 4 6O9 (H142)	4.268		
53 TRP (CZ3):lipid 4 6O9 (H151)	3.249		
53 TRP (CZ3):lipid 4 6O9 (H162)	3.764		
53 TRP (CZ3):lipid 4 6O9 (H181)	4.071		
53 TRP (CH2):lipid 4 6O9 (C14)	4.326		
53 TRP (CH2):lipid 4 6O9 (C15)	3.95		
53 TRP (CH2):lipid 4 6O9 (C16)	3.808		
53 TRP (CH2):lipid 4 6O9 (H142)	3.86		
53 TRP (CH2):lipid 4 6O9 (H151)	3.384		
53 TRP (CH2):lipid 4 6O9 (H162)	3.001		
53 TRP (CH2):lipid 4 6O9 (H172)	4.324		
54 GLY(C):654 ASP(CB)	4.365	54 GLY(C):654 ASP(CG)	4.043

5irx structure		Docking model	
Toxin residue:Channel residue/Lipid	Distance (Å)	Toxin residue:Channel residue	Distance (Å)
54 GLY(O):535 LYS(CD)	3.748	54 GLY(C):654 ASP(OD1)	3.313
54 GLY(O):654 ASP(CA)	4.381	54 GLY(C):654 ASP(OD2)	4.097
54 GLY(O):654 ASP(CB)	3.601	54 GLY(O):654 ASP(CG)	3.274
54 GLY(O):655 PHE(CD2)	4.202	54 GLY(O):654 ASP(OD1)	2.877
54 GLY(O):655 PHE(CE2)	3.813	54 GLY(O):654 ASP(OD2)	3.072
54 GLY(O):655 PHE(CZ)	4.307	54 GLY(N):654 ASP(OD2)	3.735
		54 GLY(N):655 PHE(CD2)	4.245
		54 GLY(N):655 PHE(CE2)	4.143
		54 GLY(CA):654 ASP(OD1)	3.683
		54 GLY(CA):655 PHE(CE2)	3.909
		54 GLY(CA):655 PHE(CZ)	4.109
55 SER(CA):654 ASP(CB)	4.147	55 SER(C):654 ASP(OD1)	4.257
55 SER(C):654 ASP(CA)	4.145	55 SER(O):654 ASP(CA)	4.258
55 SER(C):654 ASP(CB)	4.074	55 SER(O):654 ASP(CG)	3.897
		55 SER(O):654 ASP(OD1)	3.342
		55 SER(N):654 ASP(OD1)	4.082
56 LYS(N):654 LYS(N)	4.35		
56 LYS(N):654 LYS(CA)	4.043		
56 LYS(N):654 LYS(CB)	3.885		
56 LYS(CA):654 ASP(N)	4.344		
56 LYS(CG):653 TYR(C)	3.924		
56 LYS(CG):654 ASP(N)	3.414		
56 LYS(CG):654 ASP(CA)	4.126		
56 LYS(CG):654 ASP(CB)	4.115		
56 LYS(CE):652 ASN(O)	4.399		
56 LYS(CE):654 ASP(N)	4.283		
		63 CYS(CB):656 LYS(NZ)	4.339
		63 CYS(SG):656 LYS(CE)	3.937
		63 CYS(SG):656 LYS(NZ)	3.905
64 PRO(O):656 LYS(CE)	3.623	64 PRO(O):656 LYS(CE)	4.293
		64 PRO(O):656 LYS(CE)	4.06
65 LEU(O):632 SER(CB)	4.338	65 LEU(O):631 TYR(CD2)	3.642
65 LEU(CB):632 SER(CB)	4.383	65 LEU(O):631 TYR(CE2)	3.638
65 LEU(CG):632 SER(CA)	4.386	65 LEU(O):635 LEU(CD1)	4.074

5irx structure		Docking model	
Toxin residue:Channel residue/Lipid	**Distance (Å)**	**Toxin residue:Channel residue**	**Distance (Å)**
65 LEU(CG):632 SER(CB)	3.947	65 LEU(CB):650 THR(CG2)	4.38
65 LEU(CD1):635 LEU(CD1)	4.301	65 LEU(CG):635 LEU(CD1)	3.933
65 LEU(CD1):660 ILE(CD1)	3.747	65 LEU(CG):650 THR(CG2)	4.215
65 LEU(CD2):632 SER(CA)	4.163	65 LEU(CD1):650 THR(CG2)	3.803
65 LEU(CD2):632 SER(CB)	3.663	65 LEU(CD1):656 LYS(O)	4.395
		65 LEU(CD1):657 ALA(CA)	4.186
		65 LEU(CD1):660 ILE(CG1)	3.824
		65 LEU(CD2):635 LEU(CD1)	3.594
		65 LEU(CD2):648 GLU(CB)	4.017
		65 LEU(CD2):648 GLU(CG)	3.754
		65 LEU(CD2):648 GLU(CD)	4.045
		65 LEU(CD2):648 GLU(OE1)	3.419
		65 LEU(CD2):650 THR(CG2)	3.825
		65 LEU(CD2):660 ILE(CG1)	4.235
66 ALA (CA):lipid 6 6OE (O07)	3.781	66 ALA(CA):631 TYR(CD2)	3.785
66 ALA (C):lipid 6 6OE (O07)	3.886	66 ALA(CA):631 TYR(CE2)	4.135
66 ALA (CB):lipid 6 6OE (O07)	3.295	66 ALA(O):657 ALA(CB)	4.028
		66 ALA(CB):631 TYR(CD2)	3.803
		Predicted as lipid-interacting (MD simulations)	
67 PHE(N):631 TYR(CB)	4.371	67 PHE(CE1):631 TYR(CE2)	3.901
67 PHE(N):631 TYR(CG)	3.817	67 PHE(CE1):631 TYR(CZ)	3.688
67 PHE(N):631 TYR(CD1)	4.164	67 PHE(CE1):631 TYR(OH)	4.224
67 PHE(N):631 TYR(CD2)	3.661	67 PHE(CZ):631 TYR(CE1)	4.027
67 PHE(N):631 TYR(CE1)	4.362	67 PHE(CZ):631 TYR(CE2)	4.365
67 PHE(N):631 TYR(CE2)	3.879	67 PHE(CZ):631 TYR(CZ)	3.88
67 PHE(N):631 TYR(CZ)	4.219	67 PHE(CZ):631 TYR(OH)	3.95
67 PHE(CA):631 TYR(CD1)	4.382		
67 PHE(CA):631 TYR(CD2)	4.373		
67 PHE(CA):631 TYR(CE1)	4.216		
67 PHE(CA):631 TYR(CE2)	4.204		
67 PHE(CA):631 TYR(CZ)	4.117		
67 PHE(O):657 ALA(CB)	3.653		
67 PHE(CB):631 TYR(CD1)	4.069		
67 PHE(CB):631 TYR(CE1)	4.006		
67 PHE(CB):631 TYR(CZ)	4.384		
67 PHE(CD1):631 TYR(CE1)	4.04		
67 PHE(CD1):631 TYR(CZ)	4.348		

5irx structure		Docking model	
Toxin residue:Channel residue/Lipid	**Distance (Å)**	**Toxin residue:Channel residue**	**Distance (Å)**
67 PHE(CD1):631 TYR(OH)	4.24		
67 PHE(CE1):661 ILE(CD1)	3.922		
67 PHE (N):lipid 6 6OE (O07)	3.03	Predicted as lipid-interacting (MD simulations)	
67 PHE (N):lipid 6 6OE (H092)	3.986		
67 PHE (CA):lipid 6 6OE (O07)	3.961		
67 PHE (CA):lipid 6 6OE (H092)	4.227		
67 PHE (CB):lipid 6 6OE (O07)	3.83		
67 PHE (CB):lipid 6 6OE (O08)	4.159		
67 PHE (CB):lipid 6 6OE (C09)	4.05		
67 PHE (CB):lipid 6 6OE (O20)	4.037		
67 PHE (CB):lipid 6 6OE (H092)	3.241		
67 PHE (CB):lipid 6 6OE (H232)	4.035		
67 PHE (CG):lipid 6 6OE (O20)	4.277		
67 PHE (CG):lipid 6 6OE (H092)	4.262		
67 PHE (CG):lipid 6 6OE (H232)	3.584		
67 PHE (CD1):lipid 6 6OE (C23)	4.18		
67 PHE (CD1):lipid 6 6OE (C25)	4.223		
67 PHE (CD1):lipid 6 6OE (H232)	3.247		
67 PHE (CD1):lipid 6 6OE (H252)	3.575		
67 PHE (CD1):lipid 6 6OE (H251)	4.095		
67 PHE (CD2):lipid 6 6OE (H232)	4.217		
67 PHE (CE1):lipid 6 6OE (C24)	4.5		
67 PHE (CE1):lipid 6 6OE (C25)	4.143		
67 PHE (CE1):lipid 6 6OE (H232)	3.641		
67 PHE (CE1):lipid 6 6OE (H241)	4.246		
67 PHE (CE1):lipid 6 6OE (H252)	3.308		
67 PHE (CE1):lipid 6 6OE (H251)	4.32		
67 PHE (CE2):lipid 4 6O9 (C16)	4.063		
67 PHE (CE2):lipid 4 6O9 (H161)	3.713		
67 PHE (CE2):lipid 4 6O9 (H162)	3.502		
67 PHE (CZ):lipid 4 6O9 (C16)	4.106		
67 PHE (CZ):lipid 4 6O9 (H161)	4.025		
67 PHE (CZ):lipid 4 6O9 (H162)	3.416		
67 PHE (CZ):lipid 6 6OE (H232)	4.267		
67 PHE (CZ):lipid 6 6OE (H252)	4.28		
68 ILE (N):lipid 6 6OE (O07)	4.265	Predicted as lipid-interacting (MD simulations)	
68 ILE (CG1):lipid 4 6O9 (H142)	3.627		
68 ILE (CD1):lipid 4 6O9 (C14)	4.191		

5irx structure		Docking model	
Toxin residue:Channel residue/Lipid	**Distance (Å)**	**Toxin residue:Channel residue**	**Distance (Å)**
68 ILE (CD1):lipid 4 6O9 (H141)	3.864		
68 ILE (CD1):lipid 4 6O9 (H142)	3.606		
70 TYR (OH):lipid 4 6O9 (H212)	3.565	Predicted as lipid-interacting (MD simulations)	

2.4 Discussion

Based on the electrophysiological and membrane partitioning experiments, it is evident that the binding of DkTx to TRPV1 channel is not only derived from protein-protein interactions but, in fact, its binding is driven by toxin-lipid interactions. Cryo-EM structure provides the initial look at the intricate tripartite complex formed by toxin-lipid-channel, but it does not shed any light on functional manifestations of the structure. This work enables us to dissect the role of toxin-lipid interaction in TRPV1 channel modulation by DkTx and its variants.

Our findings offer a crucial understanding that interactions between proteins and lipids are not just

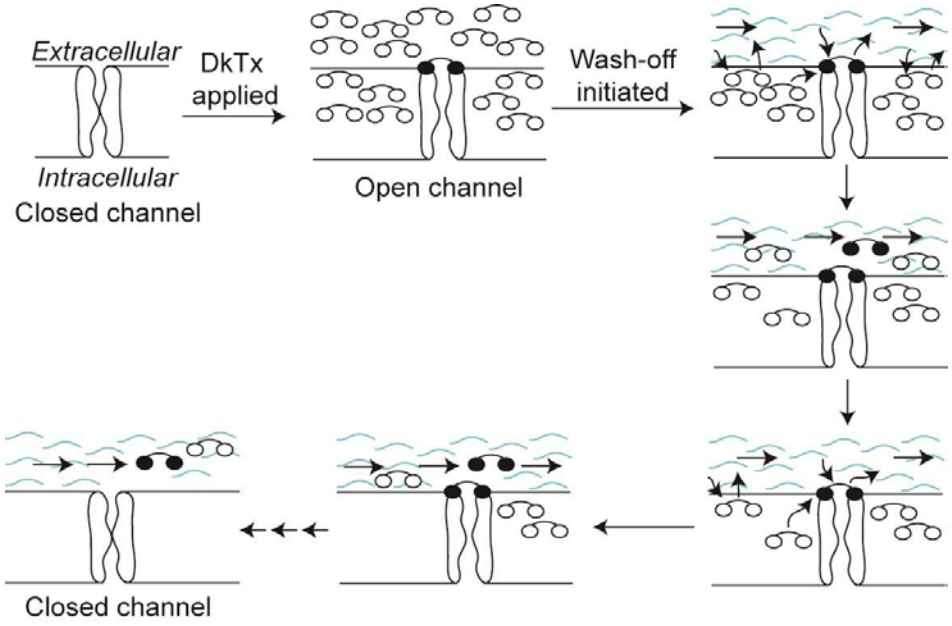

Figure 2.7: Toxin-relay hypothesis. Proposed "toxin relay" model that explains the slow wash-off feature of DkTx. DkTx is represented by a dumbbell-shaped object with its 2 ellipses denoting the 2 knots of the toxin. The knots of the toxin molecules that do not bind to the channel are depicted as empty ellipses, and those that bind to the channel as filled circles. The wavy blue curves depict buffer flow.[19]

minor adjustments, but rather, they can substantially influence protein function. One of the noteworthy findings from our study is the contrasting behavior between wild-type DkTx and

various variants of the K1 knot residue in terms of their wash-off rates (as shown in Table 2.1). Interestingly, these wash-off rates exhibit an inverse correlation with the membrane partitioning ability of these toxin variants, as demonstrated both in artificial lipid vesicles (Figure 2.6a) and on cells (Figure 2.6b). Notably, these partitioning experiments were conducted on lipid vesicles and cells that did not contain the TRPV1 channel. This observation suggests that the slow wash-off exhibited by the wild-type toxin can be attributed to its high intrinsic affinity for the membrane.

Taken together, these results (electrophysiology and partitioning experiments) are consistent with a "toxin relay mechanism" depicted in Figure 2.7. When the toxin is applied, it accumulates in the membrane at high concentrations owing to its highly efficient partitioning ability, and a few of these molecules bind to TRPV1 channels resulting in channel activation. Upon subsequent initiation of wash-off by buffer perfusion, the channel-bound toxin molecules (the knots of which are depicted as filled ellipses) begin to get dislodged and are rapidly replaced by the surrounding membrane partitioned toxin molecules that are present at a high concentration. Buffer perfusion also causes toxin molecules within the membrane that are not bound to TRPV1 (whose knots are depicted as open ellipses) to wash-off resulting in depletion of the toxin in the vicinity of the channels, thereby slowing down the relay process leading to an increase in the population of the toxin-free closed channels that manifests itself as a slowly decreasing TRPV1 current in the electrophysiology recording. This model convincingly explains the observation that the toxin variants that partition poorly wash-off rapidly (Figure 2.7) as the application of high concentrations of the toxin for channel activation will result in the accumulation of a large number of toxin molecules within the membrane that can participate in the relay mechanism, resulting in slowing down of wash-off. The high phenomena, is, therefore, not merely due to a tight bimolecular binding event but also due to the high concentration of neighbouring toxin molecules in the membrane that are available to replace channel-bound toxin molecules as they are lost due to buffer perfusion. In this way, the characteristically slow wash-off of the toxin is a cumulative effect of this relay mechanism and its enhanced residence time on the channel owing to its bivalent binding.

2.5 Materials and methods

Detailed protocol for generating the interaction map of the DkTx–lipids–TRPV1 complex

The distances between the atoms of the amino acids of DkTx and those of lipid molecules/amino acids of TRPV1 were calculated by separately analyzing two pdb files of the DkTx-TRPV1 complex—one obtained from a recently published cryo-EM structure[8] and the other from a previously published docking model[7] —by using the UCSF-CHIMERA software. In this software, the command "**split**" was entered in the command line to split the PDB structure into individual peptide chains. Subsequently, each of the four monomers of the TRPV1 channel was assigned a unique model number (0, 1, 2 or 3), the two DkTx chains were assigned model numbers 4 and 5 respectively, and each of the resiniferatoxin and lipid molecules (which were present in the cryo-EM structure but not in the docking model) were assigned unique model numbers between 6 and 25. The command "**distance #a:x@ #b:y@**" was used to obtain the distance values between the amino acid residue number "x" of the DkTx chain assigned the chain model number "a" and the amino acid residue number "y" of the TRPV1 chain assigned the chain model number "b". This command yielded the distances between every possible pairs of atoms (one each belonging to the residues "x" and "y" respectively) under analysis. For every DkTx residue, this analysis was performed with respect to every amino acid residue of each of the four monomers of the channel's pore region formed by its S5, S6 and pore helices. For determining the distance between the amino acid residues of a particular DkTx chain and a lipid molecule assigned a model number "z", the command, "**distance #a:x@ #z@"** was used. This analysis was performed for every DkTx residue with respect to all the lipid molecules in the cryo-EM structure. The distance output obtained from these analyses was saved as a **"**.txt**"** file and this data was filtered manually to select for distances within the 4.4 Å cut-off distance to yield a list of TRPV1 residues/lipid molecules proximal to each DkTx residue. The resulting interaction map is depicted in Table 2.2.

Membrane partitioning experiments on LUVs.

Fluorescence-based experiments on large unilamellar lipid vesicles (LUVs):

LUV preparation: 1-palmitoyl-2-oleoyl-*sn*-glycero-3-phosphocholine (16:0-18:1 PC from Avanti Polar Lipids Inc.) and 1-palmitoyl-2-oleoyl-*sn*-glycero-3-phospho-(1'-*rac*-glycerol) (sodium salt) (16:0-18:1 PG from Avanti Polar Lipids Inc.) were mixed at a molar ratio of 1:1 from their chloroform stock solutions, dried under a gentle nitrogen stream and kept in a vacuum desiccator for 9 h. Dried lipid films were rehydrated in HEB buffer at pH 7.0 containing HEPES (10 mM)

and EDTA (1 mM). The resulting solution was extruded through 100 nm pore-sized polycarbonate filters (Avanti Polar Lipids Inc.) to generate LUVs.

Tryptophan fluorescence spectroscopy: DkTx variants were dissolved in 2 mL of a buffer containing HEPES (10 mM) and EDTA (1 mM) at pH 7.0 to a concentration of 2 μM and the resulting solution was excited with 280 nm wavelength light by using a Horiba FluoroMax4 spectrofluorometer. Emission spectra were recorded between 300 to 450 nm both in the presence and absence of LUVs. Scattering of light from lipid vesicles was corrected following earlier reported methods[20,21] and the data was subjected to a fitting analysis by employing the following equation:

$$F/F_0(L) = 1+(F/F_0^{max}-1)Kx[L]/([W]+K_x[L])$$

where F is the fluorescence intensity at 320 nm for a given lipid concentration, F_0 is the fluorescence intensity at 320 nm in absence of lipids, F_0^{max} is fluorescence intensity at 320 nm at a concentration of lipids where partitioning saturates, [L] is molar concentration of accessible lipid (60% of total lipid, corresponding to the outer leaflet), [W] is molar concentration of water (55.3 M), and K_X is mole-fraction partition coefficient of the DkTx variants.

2.6 References

1. Overington, J. P., Al-Lazikani, B. & Hopkins, A. L. How many drug targets are there? *Nature reviews Drug discovery* **5**, 993–996 (2006).

2. Adams, R. *et al.* Binding sites in membrane proteins–diversity, druggability and prospects. *European journal of cell biology* **91**, 326–339 (2012).

3. Santos, R. *et al.* A comprehensive map of molecular drug targets. *Nature reviews Drug discovery* **16**, 19–34 (2017).

4. Long, S. B., Tao, X., Campbell, E. B. & MacKinnon, R. Atomic structure of a voltage-dependent K+ channel in a lipid membrane-like environment. *Nature* **450**, 376–382 (2007).

5. Nury, H. *et al.* X-Ray Structures of General Anaesthetics Bound to a Pentameric Ligand-Gated Ion Channel. *Biophysical Journal* **102**, 119a (2012).

6. Payandeh, J., Scheuer, T., Zheng, N. & Catterall, W. A. The crystal structure of a voltage-gated sodium channel. *Nature* **475**, 353–358 (2011).

7. Bae, C. *et al.* Structural insights into the mechanism of activation of the TRPV1 channel by a membrane-bound tarantula toxin. *Elife* **5**, e11273 (2016).

8. Julius, D., Gao, Y., Cao, E. & Cheng, Y. TRPV1 structures in nanodiscs reveal mechanisms of ligand and lipid action. (2016).

9. Autzen, H. E. *et al.* Structure of the human TRPM4 ion channel in a lipid nanodisc. *Science* **359**, 228–232 (2018).

10. Phillips, R., Ursell, T., Wiggins, P. & Sens, P. Emerging roles for lipids in shaping membrane-protein function. *Nature* **459**, 379–385 (2009).

11. Lee, A. G. Lipid–protein interactions. (2011).

12. Polley, A. *et al.* Glycosylation and Lipids Working in Concert Direct CD2 Ectodomain Orientation and Presentation. *J. Phys. Chem. Lett.* **8**, 1060–1066 (2017).

13. Miller, C. The charybdotoxin family of K+ channel-blocking peptides. *Neuron* **15**, 5–10 (1995).

14. Zhu, S., Darbon, H., Dyason, K., Verdonck, F. & Tytgat, J. Evolutionary origin of inhibitor cystine knot peptides. *FASEB j.* **17**, 1765–1767 (2003).

15. Swartz, K. J. Tarantula toxins interacting with voltage sensors in potassium channels. *Toxicon* **49**, 213–230 (2007).

16. Kalia, J. *et al.* From foe to friend: using animal toxins to investigate ion channel function. *Journal of molecular biology* **427**, 158–175 (2015).

17. Swartz, K. J. & MacKinnon, R. An inhibitor of the Kv2. 1 potassium channel isolated from the venom of a Chilean tarantula. *Neuron* **15**, 941–949 (1995).

18. Swartz, K. J. & MacKinnon, R. Hanatoxin modifies the gating of a voltage-dependent K+ channel through multiple binding sites. *Neuron* **18**, 665–673 (1997).

19. Sarkar, D., Singh, Y. & Kalia, J. Protein–Lipid Interfaces Can Drive the Functions of Membrane-Embedded Protein–Protein Complexes. *ACS Chem. Biol.* **13**, 2689–2698 (2018).

20. Ladokhin, A. S., Jayasinghe, S. & White, S. H. How to measure and analyze tryptophan fluorescence in membranes properly, and why bother? *Analytical biochemistry* **285**, 235–245 (2000).

21. Zamanian, M. *et al.* Tarantula Toxins use Common Surfaces for Interacting with Kv and ASIC Ion Channels. *Biophysical Journal* **108**, 82a (2015).

22. Milescu, M. *et al.* Tarantula toxins interact with voltage sensors within lipid membranes. *The Journal of general physiology* **130**, 497–511 (2007).

Chapter 3:

Production and functional analysis of high membrane-partitioning monovalent chimeric double-knot toxins, and characterization of tetra-knot variants of DkTx

This chapter has been published:

Singh, Y., Sarkar, D., Duari, S., Shashaank, G., Guru, P.K.I., Hrishikesh, M.V., Singh, D., Bhardwaj, S. and Kalia, J.,* 2023. "Dissecting the contributions of membrane affinity and bivalency of the spider venom protein DkTx to its sustained mode of TRPV1 activation." *Journal of Biological Chemistry* **299**, no. 7 (2023).

3.1 Introduction

The individual K1 and K2 knots of DkTx are capable of activating TRPV1, but they do so with less effectiveness and quicker wash-off rates compared to DkTx.[1,2] The slower wash-off rates of DkTx, on the other hand, can be attributed to its bivalency, which is known to enhance the binding affinity of ligand-receptor complexes.[1] In the previous chapter, it has been suggested that the high membrane affinity of DkTx is also responsible for its sustained mode of action.[3] This is because DkTx can accumulate at high concentrations in the membrane, allowing it to efficiently replace dislodged toxin molecules and establish a "toxin relay" that leads to sustained channel activation.[3] It is worth noting that this theory is further reinforced by the fact that the K1 and K2 single-knot variants, which exhibit rapid wash-off rates, also exhibit low partitioning into membranes.[1] However, since these single-knot variants are monovalent and have a weak propensity for membrane partitioning, it is unclear whether their rapid wash-off rates are due to their lack of bivalency, their low membrane affinity, or both.

In this chapter, I describe my experiments that focused on unraveling the contributions of the bivalency and the membrane affinity of DkTx to its ability to cause persistent TRPV1 channel activation. To do this, I created and characterized various DkTx variants possessing different valences and membrane affinities. These findings establish the dominant role of the high membrane affinity of DkTx in its sustained TRPV1 activation properties.

3.2 Results

Single-knots wash-off faster, and possess much lower affinity for native membranes as compared to wild-type DkTx.

Our electrophysiology experiments are consistent with previous reports,[1,2,4] showing that the single-knots wash off more quickly than DkTx, and that K2 has a higher potency for activating TRPV1 compared to K1. Specifically, when *Xenopus laevis* oocytes expressing rat TRPV1 were treated with 20 μM of K1 and K2 single-knots and then perfused with buffer, we observed a 97%

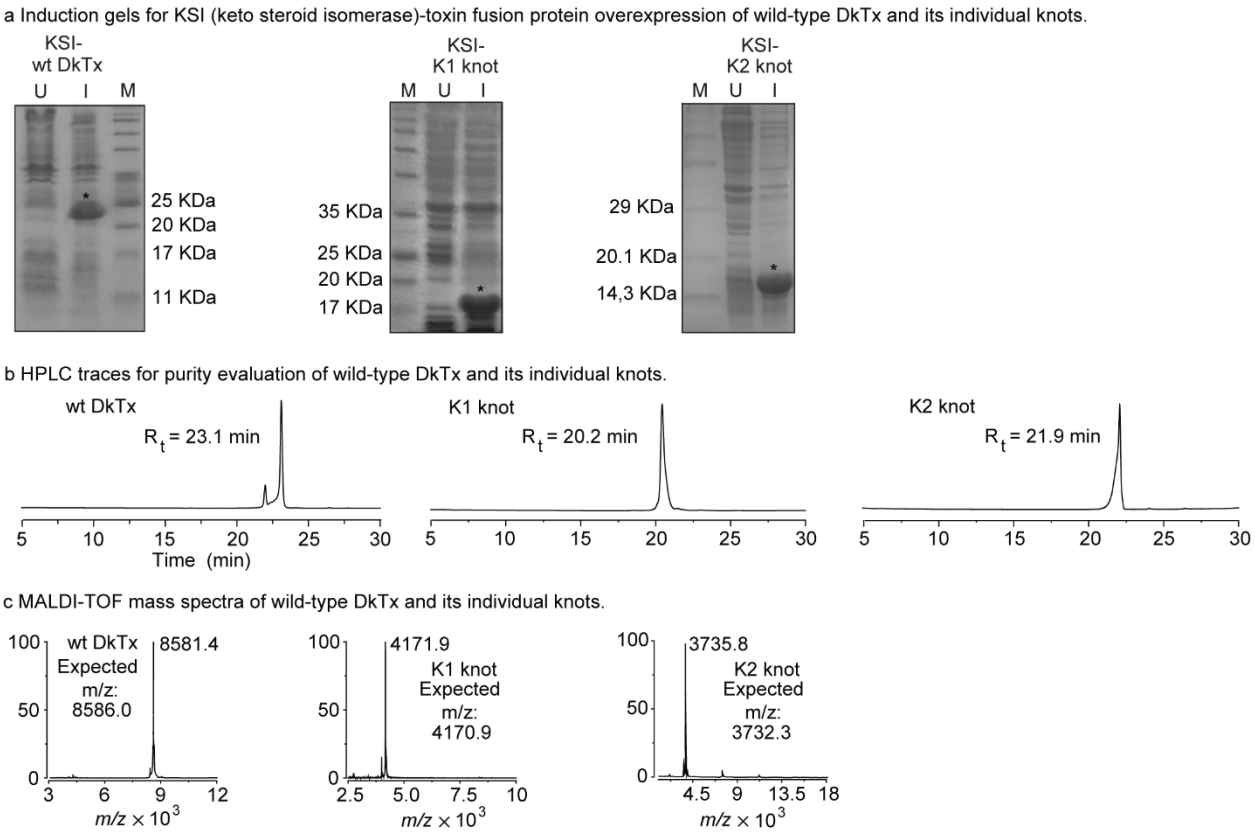

Figure 3.1: Making of wild-type DkTx and its single knots. (a) Induction gels for KSI (keto steroid isomerase)-toxin fusion wild-type DkTx and its individual knots overexpression. The bands for the overexpressed fusion proteins are marked with an asterisk on the gel image. The expected molecular weight of KSI-wt DkTx is 22.6 KDa, KSI-K1 is 18.2 KDa, KSI-K2 is 17.8 KDa. (b) HPLC traces for purity evaluation of wild-type DkTx and its individual knots. (c) MALDI-TOF mass spectra of toxins wild-type DkTx and its individual knots.

and 99% reduction in TRPV1 currents after 3 minutes of perfusion, respectively. In contrast, treatment with DkTx resulted in only a 24% decrease in TRPV1 currents shown in figure 3.2b.

Toxin depletion assays were performed on uninjected oocytes using K1 and K2 single-knots, as well as wild-type DkTx. The results showed fractional depletion values of 0.11, 0, and 0.42, respectively shown in figure 3.2d. These findings demonstrate that the single-knots have a significantly lower affinity for native membranes compared to DkTx. Moreover, the data indicates that the K1 knot has a higher membrane affinity compared to the K2 knot, which is consistent with the previous membrane partitioning data.[2]

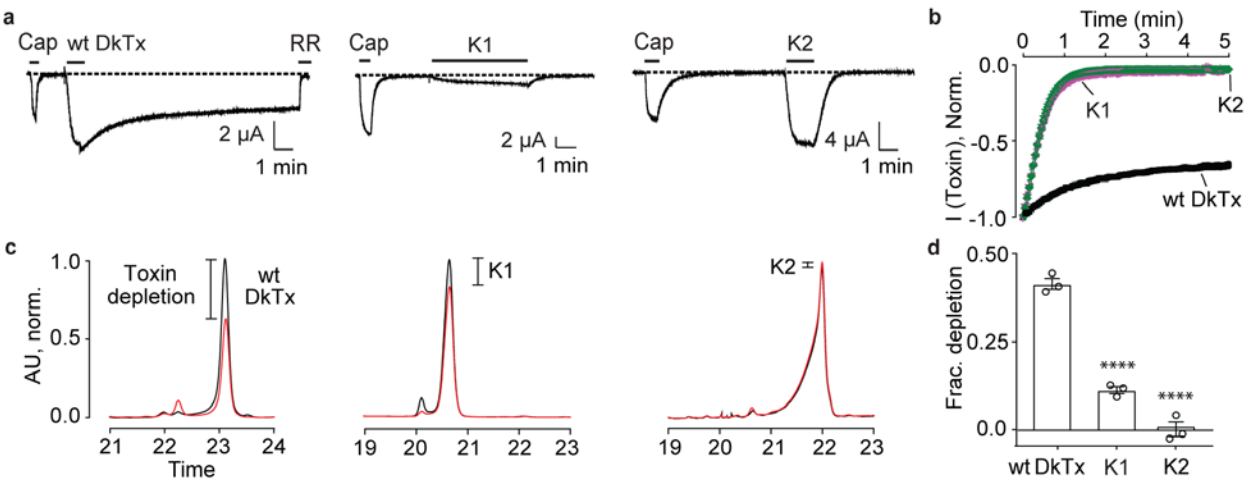

Figure 3.2: Functional and membrane affinity characterization of wild-type DkTx and its individual knots. (a) Representative electrophysiological recordings depicting TRPV1 currents obtained upon the application of the small molecule TRPV1-agonist, capsaicin (5 µM), followed by wild-type DkTx (20 µM, left), K1 knot (20 µM, center), and K2 knot (20 µM, right) to *Xenopus laevis* oocytes injected with rat TRPV1 mRNA. Wash-off was performed by starting buffer perfusion after the currents saturated in presence of the agonists. In case of wild-type DkTx, the TRPV1 blocker, ruthenium red (RR, 7 µM), was applied to completely inhibit TRPV1 currents at the end of the recording. (b) Averaged normalized wash-off current traces obtained with 20 µM wildtype DkTx (black), K1 (purple), and K2 (green); n=3 with SEM depicted in each case. (c) Representative HPLC traces depicting toxin depletion upon incubation of wild-type DkTx (left), K1 knot (center), and K2 knot (right) with uninjected *Xenopus laevis* oocytes. Traces in black correspond to the controls wherein the toxins solubilized in a buffer devoid of oocytes were subjected to HPLC analyses, and those in red were obtained from toxin solutions incubated with 100 uninjected oocytes. (d) Bar-scatter plot with SEM depicting a comparison of fractional depletion of wild-type DkTx (n=3), K1 knot (n=3), and K2 knot (n=3) into uninjected *Xenopus laevis* oocytes. Individual knots were compared with wild-type DkTx for statistical analysis. ****P = 0.0001 (ANOVA followed by a multiple comparison test). "Wild-type" has been abbreviated as "wt".

Production of high membrane-affinity monovalent chimeric double-knot toxins.

I used a unique approach to disrupt the bivalency of the toxin while maintaining its membrane affinity. This strategy involved creating chimeric toxins by replacing each knot of DkTx, one at a time, with the Kv2.1 channel-inhibitor ICK toxin, SGTx,[5–7] to generate the K1-SGTx and SGTx-K2 double-knots. This process prevented bivalent binding to TRPV1. I selected SGTx because it partitions favorably into POPC/POPG vesicles,[8] making it an ideal candidate for creating our desired monovalent, yet high membrane affinity toxins.

It was crucial to identify a method that would allow for the proper folding of SGTx as well as the K1 and K2 knots of DkTx to create the desired K1-SGTx and SGTx-K2 chimeric toxins. A

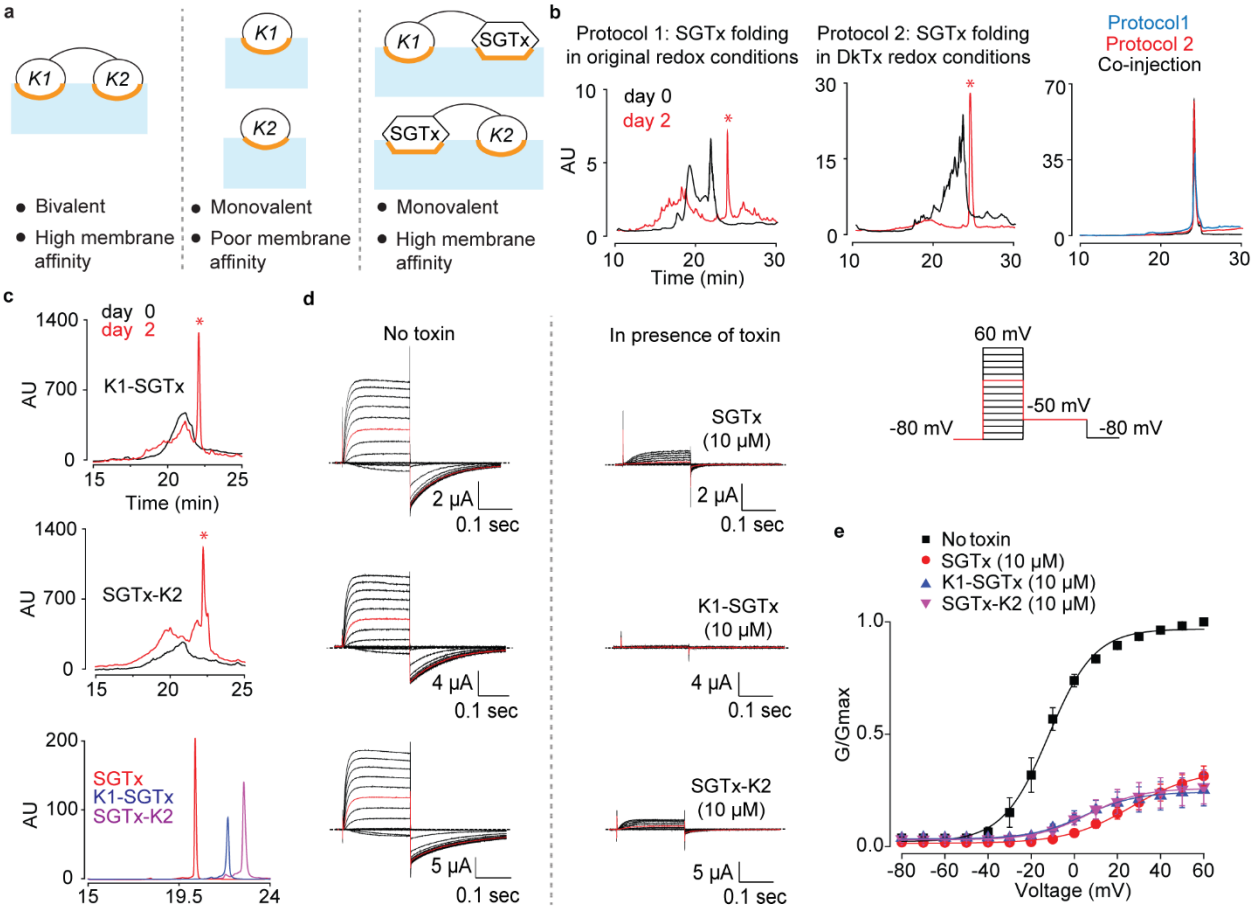

Figure 3.3: Production and Kv2.1-inhibitory properties of the chimeric double-knot toxins. (a) The TRPV1-binding valence and expected membrane interaction properties of wild-type DkTx, its single-knots, and the chimeric double-knots. (b) HPLC analyses of the time course of the folding of linear SGTx under the originally reported folding conditions (left), under DkTx-folding conditions (middle), and overlay of HPLC chromatograms obtained upon re-injection of the emergent peaks collected from both the approaches, and that obtained upon injection of a mixture of these peaks (co-injection). The emergent peaks are marked with asterisks. c) HPLC chromatograms for monitoring the folding of linear K1-SGTx (top) and linear SGTx-K2 (middle), and overlay of the chromatograms for purified folded SGTx, K1-SGTx, and SGTx-K2 (bottom). (d) Characterization of the Kv2.1-modulatory activity of the chimeric knots. Oocytes injected with the mRNA of the agitoxin2-sensitive Kv2.1Δ7 channel were held at -80 mV and subjected to depolarizations ranging from -80 mV to 60 mV in 10 mV-increments, and the voltage was then stepped down to -50 mV to elicit tail currents (voltage protocol depicted in the top right panel). Agitoxin2-subtracted current traces before and after the application of the toxins (10 µM) are depicted, with the trace for the 10 mV-depolarization sweep in red. (e) Conductance(G)-Voltage (V) relationship plots obtained from the Kv2.1Δ7 recordings. Each data point corresponds to the averaged value of 3 experiments with SEM.

comparison of previously used folding conditions for SGTx and DkTx revealed that while both employed identical ratios of oxidized and reduced glutathione, the folding of SGTx was performed in buffer containing ammonium acetate and urea,[9] whereas optimal folding of DkTx required buffer containing detergents such as Triton X-100.[4]

To determine if SGTx could fold efficiently under DkTx-folding conditions, I produced linear SGTx using our standard procedure for generating linear DkTx.[3,4] I subjected linear SGTx to both its standard folding conditions reported previously and DkTx-folding conditions, analyzing folding in both cases using HPLC analyses. A sharp peak at retention time of 24 min was observed in both the folding mixtures after two days (marked with an asterisk in Figure 3.3b, left and middle panels). A co-injection HPLC experiment yielded a single prominent peak at the same retention time as those for the two peaks injected individually (Figure 3.3b, right panel), suggesting that both the folding conditions yielded the same species.

We then tested the Kv2.1 channel-inhibitory properties of SGTx produced using the DkTx-folding protocol by performing two-electrode voltage clamp recordings on Xenopus laevis oocytes expressing Kv2.1. The resulting conductance-voltage (G-V) plot (Figure 3.3e) demonstrated a profound rightward shift (of 38.3 mV) upon toxin application (Table 3.2), as expected for SGTx,[10] demonstrating that SGTx produced recombinantly by employing the DkTx production protocol yields the properly folded, active toxin.

After successfully producing active SGTx under DkTx-folding conditions, we proceeded to produce linear KSI-N-G-K1-SGTx and KSI-N-G-SGTx-K2 fusion proteins in *E. coli* and folded them under the same conditions. The folding mixtures yielded a sharp peak for both toxins within two days (Figure 3.3c), indicating successful folding. Mass spectrometry analysis of the peaks (Figure 3.4c) confirmed that the m/z values were close to the expected values for both toxins (8684.3 obtained vs. 8687.1 expected for K1-SGTx and 8244.5 obtained vs. 8248.5 expected for SGTx-K2). When 10 μM of K1-SGTx and SGTx-K2 were applied to Kv2.1-expressing oocytes, profound inhibition was observed (Figure 3.3d), with K1-SGTx causing a 16.6 mV rightward shift

in the G-V plot and SGTx-K2 effecting an 18.5 mV rightward shift (Figure 3.3e and Table 3.2). These experiments confirmed that the SGTx knots of these chimeric toxins were folded correctly.

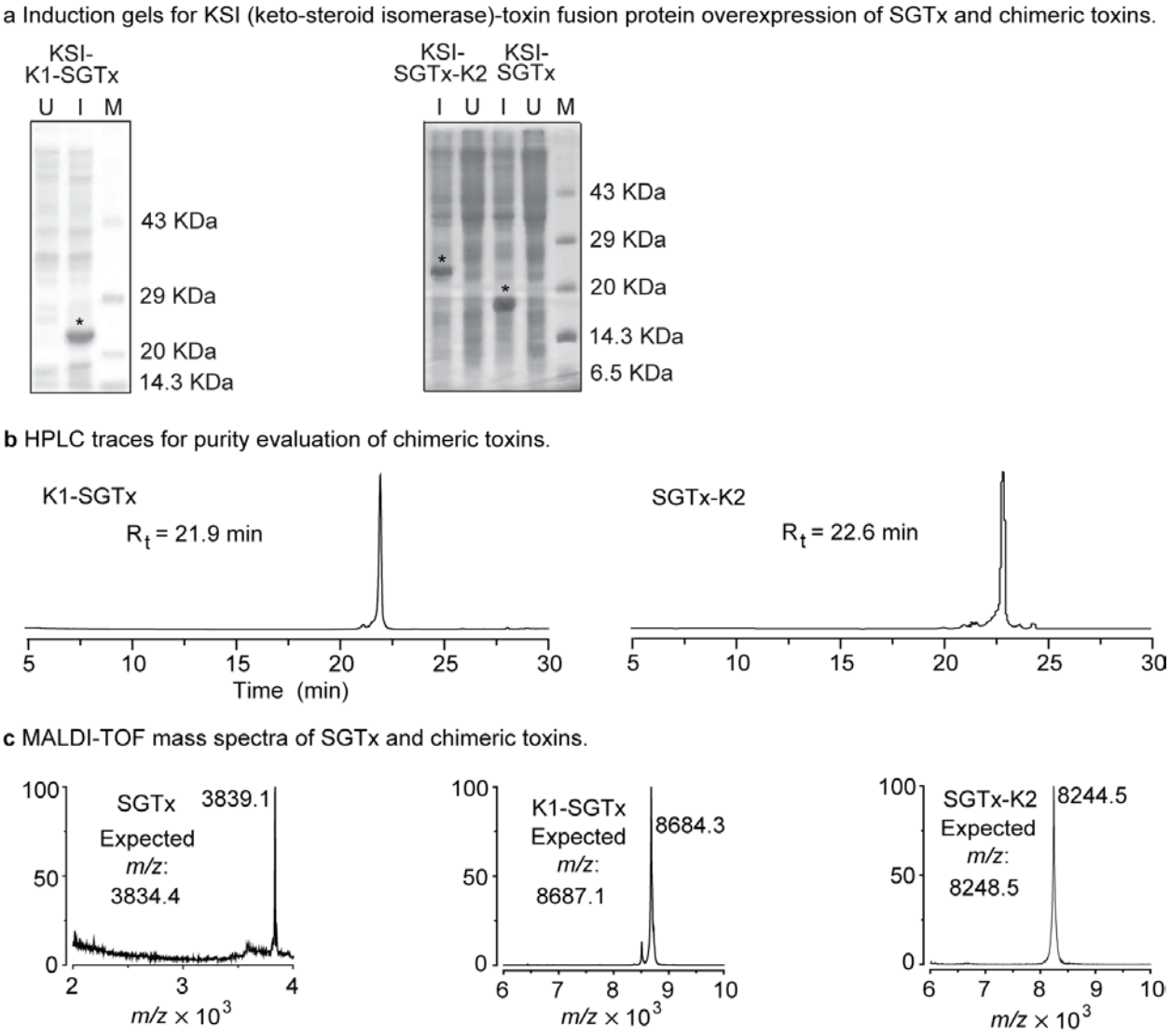

Figure 3.4: Making of SGTx and chimeric toxins. (a) Induction gels for KSI (keto-steroid isomerase)-toxin fusion overexpression of SGTx and chimeric toxins. The bands for the overexpressed fusion proteins are marked with an asterisk on the gel image. The expected molecular weight of KSI-K1-SGTx is 22.7 KDa, KSI-SGTx-K2 is 22.3 KDa, and KSI-SGTx is 17.9 KDa. (b) HPLC traces for purity evaluation of SGTx and chimeric toxins. (c) MALDI-TOF mass spectra of SGTx and chimeric toxins.

The chimeric double-knots modulate both Kv2.1 and TRPV1, and wash-off slower than the single-knots post TRPV1 activation.

Experiments involving oocyte depletion showed that K1-SGTx and SGTx-K2 had higher membrane affinity than their respective K1 and K2 single-knots, resulting in fractional depletion values of 0.28 and 0.22 compared to 0.11 and 0, respectively (Figure 3.5a, b). The ability of both chimeric toxins to activate TRPV1 indicated that their knots were folded correctly (Figure 3.5c, d). Notably, K1-SGTx and SGTx-K2 had slower wash-off rates than their single-knot counterparts (Figure 3.5e), with 67% and 70% attenuation of TRPV1 currents after 3 minutes compared to complete attenuation for the single-knots (Figure 3.5f). These findings offer important insights

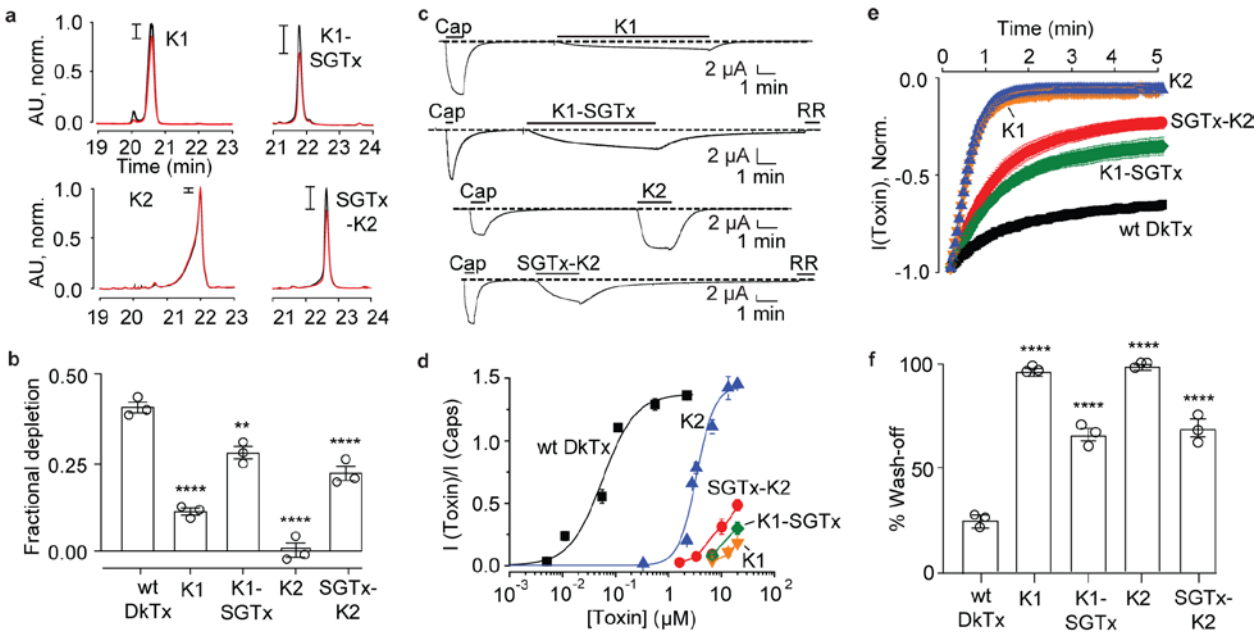

Figure 3.5: Membrane affinity and TRPV1 activation characterization of chimeric double-knot toxins. (a) Representative HPLC traces depicting toxin depletion upon incubation of K1, K2, SGTx-K2, and K1-SGTx with uninjected *Xenopus laevis* oocytes. (b) Bar-scatter plot with SEM depicting fractional depletion for wild-type DkTx (n=3), the chimeric double-knots (n=3), and the single-knots (n=3) obtained from the depletion experiments. Individual knots and chimeric double-knots were compared with wild-type DkTx for statistical analysis. ****P = 0.0001; **P = 0.01 (ANOVA followed by a multiple comparison test). (c) Representative current traces for TRPV1 activation by the single knots and chimeric double-knot toxins (20 µM each) followed by toxin wash-off by buffer perfusion. In case of chimeric double-knot toxins, the TRPV1 blocker, ruthenium red (RR, 7 µM) was applied to completely inhibit TRPV1 currents at the end of the recording. (d) Dose-response plots of the chimeric double-knots, wild-type DkTx, and the single-knots. Each data point corresponds to n=3 with SEM. (e) Averaged normalized wash-off current traces (20 µM toxin concentrations, n=3 with SEM). f) Bar-scatter plot with SEM depicting the percentage reduction in current after 3 min of buffer perfusion post toxin-mediated channel activation (n=3 for each toxin). Individual knots and chimeric double-knots were compared with wild-type DkTx for statistical analysis; ****P = 0.0001 (ANOVA followed by a multiple comparison test).

into the roles of valence and membrane partitioning in the sustained activation of TRPV1 by DkTx. The results suggest that membrane partitioning plays a crucial role in slowing the wash-off of DkTx, and that bivalency alone is not solely responsible for the slow wash-off kinetics observed.

The design and production of tetra-knot variants of the DkTx.

Recognizing the significance of membrane affinity in DkTx's ability to maintain slow wash-off rates, we hypothesized that increasing its membrane affinity would further slow-down their wash-off. To investigate this hypothesis, we designed "tetra-knot toxins," $(DkTx)_2$ and DkTx-$(SGTx)_2$, which contain four membrane partitioning knots each, twice the number found in DkTx (Figure 3.6a, e).

We anticipated that producing our proposed tetra-knots, which contained a significant number of cysteines (24 in each molecule), would be difficult due to the possibility of these cysteines forming non-native mixed disulfides during folding. Our concerns were reinforced by our recent experiments involving labeling DkTx with a fluorophore, which showed that introducing a non-

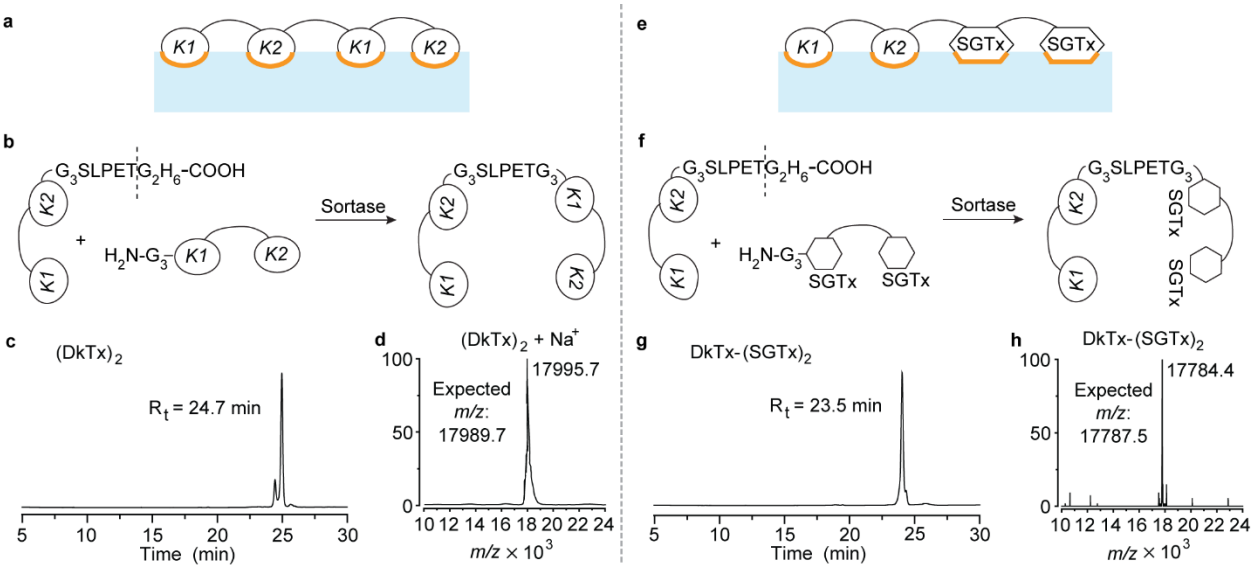

Figure 3.6: Schematic representation of making of tetra-knot toxins. (a) Schematic representation of $(DkTx)_2$ interacting with the cell membrane via its four membrane partitioning knots. (b) Schematic of the sortase A-mediated ligation reaction for producing $(DkTx)_2$. (c) HPLC traces for purity evaluation of $(DkTx)_2$. (d) MALDI-TOF mass spectra of $(DkTx)_2$. (e) Schematic representation of (DkTx)-$(SGTx)_2$ interacting with the cell membrane via its four membrane partitioning knots. (f) Schematic of the sortase A-mediated bioconjugation reaction for producing DkTx-$(SGTx)_2$. (g) HPLC traces for purity evaluation of DkTx-$(SGTx)_2$. (h) MALDI-TOF mass spectra of DkTx-$(SGTx)_2$.

native cysteine into DkTx resulted in the formation of misfolded toxin species.[11] To circumvent this issue, we decided not to use our standard protocol for producing DkTx, which involves expressing the full-length linear protein in E. coli and subjecting it to redox folding conditions. Instead, we adopted a step-wise approach that involved producing properly folded precursor double-knots and then enzymatically ligating them to create the desired tetra-knots. For the ligation process, we utilized the sortase A enzyme, which catalyzes the formation of a peptide linkage between proteins containing a C-terminal LPXTG motif (where X can be any amino acid) and those appended with an N-terminal G_3 sequence (Figure 3.6b, f).[11–14] Subhadeep Duari, a BS-MS student lab in our lab have successfully made both tetra-knot variants – $(DkTx)_2$ and DkTx-$(SGTx)_2$ by utilizing the above-mentioned strategy.

The tetra-knots possess higher membrane affinity and slower wash-off rates than DkTx.

In order to assess the activity and proper folding of the SGTx knots in both DkTx-$(SGTx)_2$ and G_3-$(SGTx)_2$ precursor double-knot, we investigated their Kv2.1-inhibitory properties using a voltage protocol depicted in the top right panel of Figure 4a. The experiments were conducted using tetra-knot concentrations of 3.3 µM or lower, as DkTx-$(SGTx)_2$ demonstrated limited solubility at higher concentrations. The application of 3.3 µM of DkTx-$(SGTx)_2$ resulted in Kv2.1 inhibition (Figure 3.7a, second panel from the top), causing a shift in the Kv2.1 G-V plot to the right by 12.9 mV (Figure 3.7b and Table 3.2). Similarly, G_3-$(SGTx)_2$ at the same concentration also inhibited Kv2.1 (Figure 3.7a, third panel from the top), causing a rightward shift of 14.2 mV in the G-V plot of the channel (Figure 3.7b). These results indicate that the SGTx knots in both DkTx-$(SGTx)_2$ and G_3-$(SGTx)_2$ were folded properly and active. The deletion experiments using oocyte membranes confirmed our hypothesis that the tetra-knots had a higher affinity for the membrane compared to DkTx. In the absence of toxin, incubating 50 uninjected oocytes resulted in a fractional depletion value of 0.21 when treated with 2.5 µM of DkTx. In contrast, $(DkTx)_2$ and DkTx-$(SGTx)_2$ showed more than a two-fold increase in membrane depletion, with fractional depletion values of 0.45 and 0.42, respectively (Figure 3.7c, d). The concentrations of the toxins used in these experiments were lower than those used for the depletion experiments on the single and double-knots described earlier, which were performed with 10 µM concentrations, due to the limited aqueous solubility of the tetra-knots.

Activation studies on the tetra-knots using TRPV1 showed that both were TRPV1 agonists and lower potency for TRPV1 activation compared to the wild-type DkTx, as seen in Figures 3.7e and 3.7f. However, despite their lower potency, both tetra-knots were observed to wash-off much slower, as seen in Figure 3.7g. For instance, while wild-type DkTx demonstrated a 45.3% attenuation of TRPV1 currents after 3 minutes of buffer perfusion post-channel activation at a concentration of 3.3 µM, identical experiments with $(DkTx)_2$ and DkTx-$(SGTx)_2$ yielded only 5.2% and 20.4% amelioration of TRPV1 currents, respectively, as seen in Figure 3.7h. Notably, the tetra-knots exhibited extremely slow wash-off rates at all concentrations tested, as seen in Figure 3.7i and 3.7j. This suggests that these toxins accumulate at high concentrations in the membrane, even when applied at low concentrations, enabling the establishment of an efficient

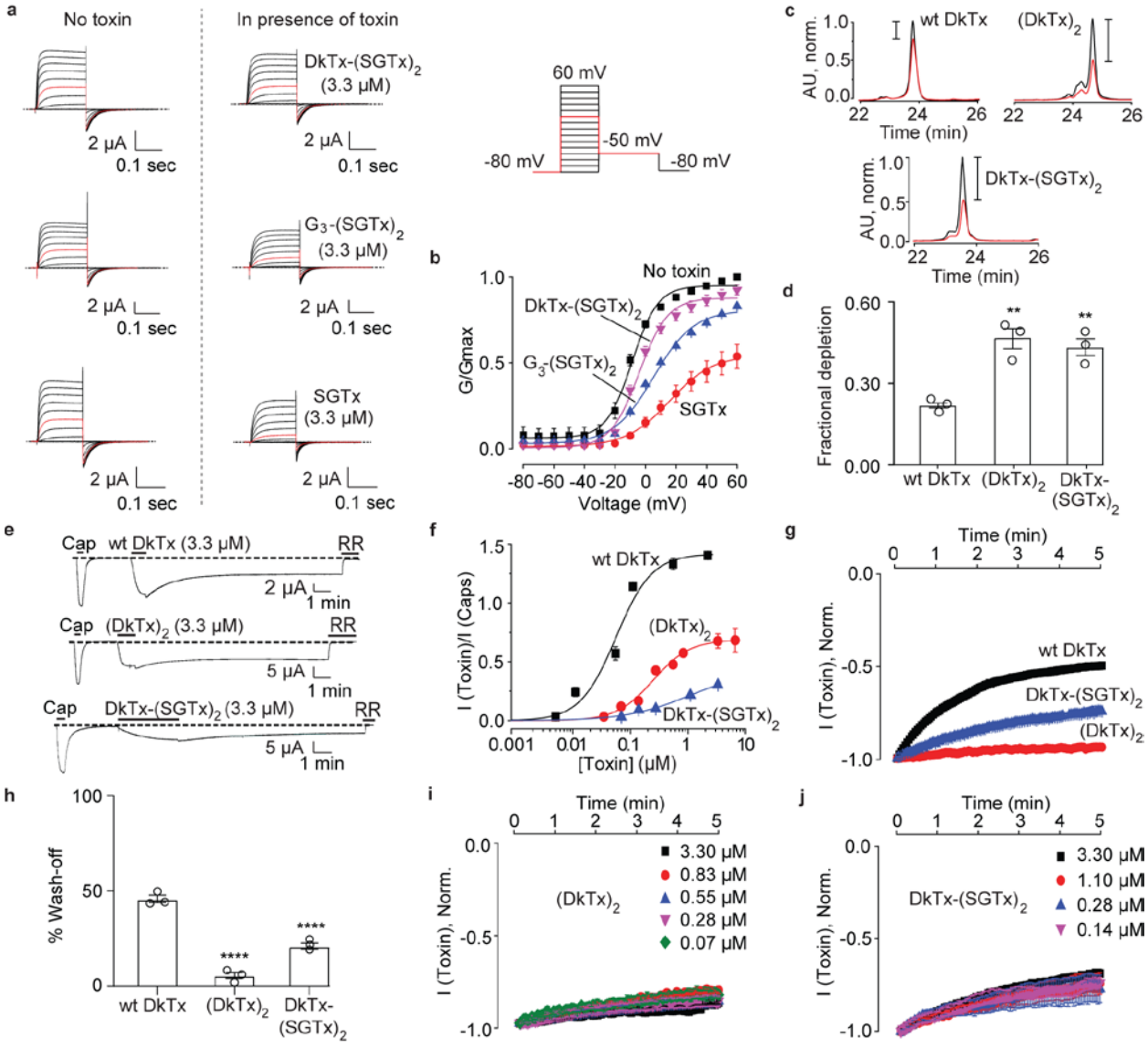

Figure 3.7: Characterization of the tetra-knot toxins and their synthetic precursors. (a) Kv2.1 channel-modulation by DkTx-$(SGTx)_2$, G_3-$(SGTx)_2$, and SGTx. Oocytes injected with the mRNA of the agitoxin2-sensitive Kv2.1Δ7 channel were held at -80 mV and subjected to depolarizations ranging from -80 mV to 60 mV in 10 mV-increments, and then hyperpolarized to -50 mV to elicit tail currents (voltage protocol on the top right). Agitoxin2-subtracted current traces before and after the toxin application (3.3 µM) are depicted, with the trace for the 10 mV-depolarization sweep in red. (b) G-V relationships for Kv2.1Δ7 in absence or presence of the toxins (3.3 µM; each data point corresponds to n=3 with SEM). (c) Representative HPLC profiles, and (d) bar-scatter plot depicting fractional depletion for wild-type DkTx and the tetra-knots (n=3 in each case) in uninjected *Xenopus laevis* oocytes. The tetra-knots were compared with wild-type DkTx for statistical analysis. **P = 0.01 (ANOVA followed by a multiple comparison test). (e) Representative current traces for TRPV1 activation by wild-type DkTx, $(DkTx)_2$ and DkTx-$(SGTx)_2$ (3.3 µM each) followed by toxin wash-off by buffer perfusion. Ruthenium red (RR, 7 µM) was applied to completely inhibit TRPV1 currents. (f) TRPV1 activation dose-response plots for wild-type DkTx, $(DkTx)_2$ and DkTx-$(SGTx)_2$. Each data point corresponds to n=3 with SEM. (g) Averaged wash-off TRPV1 current traces (n=3 with SEM) obtained with 3.3 µM toxin concentrations. (h) Bar-scatter plot with SEM depicting the percentage reduction in current after 3 min of buffer perfusion post toxin-mediated channel activation (n=3 for each toxin). The tetra-knots were compared with wild-type DkTx for statistical analysis, ****P = 0.0001 (ANOVA followed by a multiple comparison test). (i) Wash-off studies on $(DkTx)_2$ at different toxin concentrations (n=3 with SEM at each concentration). (j) Wash-off studies on DkTx-$(SGTx)_2$ at different toxin concentrations (n=3 with SEM at each concentration).

toxin relay during wash-off. Furthermore, the wash-off rates of the tetra-knots were found to be concentration-independent.

The results indicating enhanced membrane affinity of the tetra-knots and their ability to sustain TRPV1 activation represent a clear demonstration of the significant influence of membrane affinity on the characteristic activity of DkTx. These findings can be interpreted as a "gain-of-function" effect in the tetra-knots, providing compelling evidence for the crucial role played by membrane affinity in conferring sustained TRPV1 activation.

Table 3.1: Sequences of all the toxins variants

Construct	Sequence
wild-type DkTx	GDCAKEGEVCSWGKKCCDLDNFYCPMEFIPHCKKYKPYVPVTTNCAKEGEVCGWGS KCCHGLDCPLAFIPYCEKYR
K1	GDCAKEGEVCSWGKKCCDLDNFYCPMEFIPHCKKYK
K2	GNCAKEGEVCGWGSKCCHGLDCPLAFIPYCEKYR
SGTx	GTCRYLFGGCKTTADCCKHLACRSDGKYCAWDGTF
K1-SGTx	GDCAKEGEVCSWGKKCCDLDNFYCPMEFIPHCKKYKPYV PVTTTCRYLFGGCKTTADCCKHLACRSDGKYCAWDGTF
SGTx-K2	GTCRYLFGGCKTTADCCKHLACRSDGKYCAWDGTFPYVPVTTNCAK EGEVCGWGSKCCHGLDCPLAFIPYCEKYR
G_3-DkTx	GGGDCAKEGEVCSWGKKCCDLDNFYCPMEFIPHCKKYKPYVPVTTNCAKE GEVCGWGSKCCHGLDCPLAFIPYCEKYR
G_3-$(SGTx)_2$	GGGTCRYLFGGCKTTADCCKHLACRSDGKYCAWDGTFPYVPVTTTCRYLFGGCKTTA DCCKHLACRSDGKYCAWDGTF
DkTx-$G_3SLPETG_2H_6$	GDCAKEGEVCSWGKKCCDLDNFYCPMEFIPHCKKYKPYVPVTTNCAKEGEVCGWGS KCCHGLDCPLAFIPYCEKYRGGGSLP ETGGHHHHHH
$(DkTx)_2$	GDCAKEGEVCSWGKKCCDLDNFYCPMEFIPHCKKYKPYVPVTTNCAKEGEVCGWGS KCCHGLDCPLAFIPYCEKYRGGGSLPETGGGDCAKEGEVCSWGKKCCDLDNFYCPM EFIPHCKKYKPYVPVTTNCAKEGEVCGWGSKCCHGLDCPLAFIPYCEKYR
DkTx-$(SGTx)_2$	GDCAKEGEVCSWGKKCCDLDNFYCPMEFIPHCKKYKPYVPVTTNCAKEGEVCGWGS KCCHGLDCPLAFIPYCEKYRGGGSLPETGGGTCRYLFGGCKTTADCCKHLACRSDGK YCAWDGTFPYVPVTTTCRYLFGGCKTTADCCKHLACRSDGKYCAWDGTF

Table 3.2: Summary of the Kv2.1Δ7 inhibitory activity of the toxins.

		z	**$V_{1/2}$ (mV)**	**$\Delta V_{1/2}$ (mV)**
Figure 3.3e	No toxin applied	3.7 ± 0.2	-11.9 ± 0.8	-
	SGTx (10 μM)	2.6 ± 0.2	26.4 ± 1.3	38.3 ± 1.5
	K1-SGTx (10 μM)	3.2 ± 0.3	4.7 ± 1.4	16.6 ± 1.6
	SGTx-K2 (10 μM)	3.2 ± 0.3	6.6 ± 1.1	18.5 ± 1.4
Figure 3.7b	No toxin applied	3.6 ± 0.5	-8.8 ± 1.0	-
	SGTx (3.3 μM)	2.8 ± 0.2	15.9 ± 1.3	24.7 ± 1.6
	G_3-$(SGTx)_2$ (3.3 μM)	2.9 ± 0.3	5.4 ± 1.4	14.2 ± 1.7
	DkTx-$(SGTx)_2$ (3.3 μM)	3.9 ± 0.4	4.1 ± 1.1	12.9 ± 1.5

Table 3.3: TRPV1 activation and membrane affinity data summary for all toxin variants

S. No.	Toxin	Expected mass (a.m.u)	Observed mass (a.m.u) (MALDI-TOF)	HPLC retention time (min)	EC_{50} (μM)	Fold change in EC_{50}	Hill coefficient (n_H)	% wash-off after 3 min of buffer perfusion post TRPV1 activation by 20 μM of toxin (unless otherwise stated)	Mol. Fraction partition coefficient (K_x) in POPC/POPG vesicles	Fractional depletion upon incubation of 4 nmol toxin in 400 μL buffer containing 100 uninjected oocytes (unless otherwise stated)
1	wild-type DkTx	8586.0	8581.4	23.1	0.05 ± 0.01	1	1.4 ± 0.4	24.1 ± 3.2 45.3 ± 1.3 (3.3 μM toxin)	(8.2 ± 0.8)E6	0.42 ± 0.03 0.21 ± 0.05†
2	K1	4170.9	4171.9	20.2	C.N.D.	C.N.D.	C.N.D.	96.5 ± 1.9	(3.9 ± 1.1)E5*	0.11 ± 0.01
3	K2	3732.3	3735.8	21.9	3.33 ± 0.41	67	2.5 ± 0.9	98.6 ± 1.4	(2.0 ± 0.3)E4*	0.00 ± 0.03
4	SGTx	3834.4	3839.1	20.3	N.A.	N.A.	N.A.	N.A.	N.D.	N.D.
5	K1-SGTx	8687.1	8684.3	21.9	C.N.D.	C.N.D.	C.N.D.	67.3 ± 3.8	(3.7 ± 1.1)E7	0.28 ± 0.02
6	SGTx-K2	8248.5	8244.5	22.6	C.N.D.	C.N.D.	C.N.D.	70.2 ± 5.4	(4.8 ± 2.0)E7	0.22 ± 0.02
7	G_3-DkTx	8700.1	8699.7	23.3	N.D.	N.D.	N.D.	N.D.	N.D.	N.D.
8	G_3-$(SGTx)_2$	8463.7	8469.2	22.1	N.A.	N.A.	N.A.	N.A.	N.D.	N.D.
9	DkTx-$G_3SLPETG_2H_6$	10221.7	10238.12	22.5	N.D.	N.D.	N.D.	N.D.	N.D.	N.D.
10	$(DkTx)_2$	17989.7 (Na^+ adduct)	17995.7	24.7	0.25 ± 0.03	5	1.4 ± 0.2	5.2 ± 1.1 (3.3 μM toxin)	N.D.	0.45 ± 0.04†
11	DkTx-$(SGTx)_2$	17787.5	17784.4	23.5	1.05 ± 0.12	21	0.8 ± 0.1	20.4 ± 1.0 (3.3 μM toxin)	N.D.	0.42 ± 0.04†

†fractional depletion upon incubation of 1 nmol toxin variants in 400 μL buffer containing 50 uninjected oocytes, *K_x values reported by Swartz and coworkers (2), C.N.D.: could not be determined due to poor potency (only partial channel activation measurable at concentrations close to toxin solubility limit), N.A.: not applicable, N.D.: not determine

3.3 Discussion

In this study, we created various DkTx-based toxin variants and analyzed their membrane affinity and TRPV1 activation properties to investigate the contribution of the toxin's membrane affinity and valence to its sustained mode of TRPV1 activation. Our findings provide clear evidence that the toxin's high membrane affinity is crucial in giving it its persistent TRPV1 activation property. One compelling piece of evidence supporting this conclusion is the slower wash-off rates of the single-knots of DkTx when attached to the Kv2.1 channel-targeting membrane partitioning toxin, SGTx (as shown in Figure 3.5e, f). We used K1-SGTx and SGTx-K2 bifunctional chimeric double-knots to separate the effects of valence and membrane affinity. These monovalent double-knots possessed higher membrane affinities than the single-knots and served as powerful tools to analyze the importance of membrane affinity in TRPV1 activation. Furthermore, we observed that our tetra-knot variants, $(DkTx)_2$ and DkTx-$(SGTx)_2$, with hyper-membrane affinities, washed off slower than wild-type DkTx (as demonstrated in Figure 3.7g, h), further emphasizing the significance of membrane affinity in TRPV1 activation.

While our findings provide compelling evidence for the role of membrane affinity in the sustained mode of TRPV1 activation exhibited by DkTx, it is not sufficient to explain all our results. For instance, K1 and K2 demonstrate similar wash-off rates despite K1 having a higher membrane affinity. Also, both tetra-knots wash off slower than DkTx, but $(DkTx)_2$ washes off slower than DkTx-$(SGTx)_2$ despite comparable membrane affinity values. We believe that the binding affinity of the toxins for TRPV1 plays a crucial role in their wash-off rates. K1 and DkTx-$(SGTx)_2$ likely have lower binding affinities for TRPV1 than K2 and $(DkTx)_2$, respectively, which explains why K1 washes off as fast as K2 and DkTx-$(SGTx)_2$ washes off faster than $(DkTx)_2$. Previous research concluded that K1 has a lower affinity for TRPV1-binding than K2 based on experiments on the K1K1 and K2K2 homo double-knots. Furthermore, $(DkTx)_2$ would be expected to bind more tightly to TRPV1 than DkTx-$(SGTx)_2$ since it contains two TRPV1-binding units per molecule, potentially allowing for simultaneous binding to a single TRPV1 homotetramer, whereas DkTx-$(SGTx)_2$ only contains one TRPV1-binding unit per molecule. Also, the reduced potency of tetra-knot variants can be ascribed to the diminished degree of freedom for individual knots to bind to their respective binding sites on the TRPV1 channel.

An important aspect of this study is the creation of unconventional engineered toxin variants, including bifunctional chimeric double-knots and tetra-knots. While artificial double-knot toxins that target different domains of the same channel have been previously reported,[14] we believe that our K1-SGTx and SGTx-K2 variants that modulate the functions of two different channels are the first of their kind. Additionally, our $(DkTx)_2$ and DkTx-$(SGTx)_2$ toxins are the first known examples of toxins with four ICK motifs. The successful use of sortase A-mediated ligation to create these tetra-knots adds to the growing body of literature that uses this technique to engineer cysteine-rich toxins.[11,14] These protein engineering techniques could potentially be applied to study other membrane-interacting proteins, including toxins that exhibit slow wash-off rates similar to DkTx, such as hanatoxin,[15] GxTx-1E,[16] and excelsatoxin A.[17] By exploring the membrane's role in the sustained activity of these toxins, we may be able to better understand the evolutionary strategy of enhancing membrane affinity in membrane-interacting toxins to achieve sustained modulation of channel and receptor proteins.

This work not only provides insights into the mechanisms behind TRPV1 activation, but also has implications for the development of TRPV1 agonists as painkillers. TRPV1 is a crucial component of the body's pain-sensing pathway, and capsaicin and resiniferatoxin, two TRPV1 agonists, are currently used clinically for pain therapy.[18,19] While capsaicin is topically administered, resiniferatoxin is given intrathecally to treat severe pain in cancer patients at advanced stages.[20] Given the potential of TRPV1 agonists in pain therapy, it is plausible that the tetra-knot toxins we have engineered, which show highly persistent TRPV1 activation, could be developed as long-lasting analgesics. In general, our findings suggest that modifying other TRPV1 agonists to increase their membrane affinity may lead to the development of more effective long-acting painkillers.

3.4 Materials and methods

The production of single and double-knot toxin variants.

Mutagenesis and cloning: SGTx, K1-SGTx, SGTx-K2, and SGTx-PYVPVTT-SGTx (referred to as $(SGTx)_2$) DNA constructs cloned into the pUC57 vector were procured from GenScript Biotech TM, and were further subcloned downstream of the ketosteroid isomerase (KSI) gene in the pET31b vector, via restriction-free cloning.

Recombinant production of linear toxins: Toxin constructs were overexpressed in *E. coli* BL21(DE3) cells to produce linear proteins according to the workflow described previously.[3] Briefly, the toxins were overexpressed as fusion proteins with ketosteroid isomerase (KSI) to direct their expression into bacterial inclusion bodies. The toxin and KSI protein sequences were separated by the N-G (Asn-Gly) linker enabling hydroxylamine-mediated cleavage at the N-G site to produce linear toxins appended with an *N*-terminal Gly (as depicted in Table S1) after pellet processing of the bacterial cells.

Folding of linear toxins and purification of folded toxins: Lyophilized linear single and double-knot toxins were folded under conditions optimized previously[3] that involved incubating them at 4°C in redox refolding buffers containing Tris-HCl (0.4 M), EDTA (1 mM), Triton X-100 (0.5%), reduced glutathione (2.5 mM), oxidized glutathione (0.25 mM) at pH 8.0 for 2 d. Folding of SGTx was attempted by employing this standard DkTx folding protocol, as well as by using a protocol that has been previously reported for SGTx[10] that involved the slow addition of a solution of the linear toxin (2 mg/mL dissolved in an aqueous solution of 50% acetonitrile containing 0.1% TFA) into a folding buffer at pH 7.8 containing ammonium acetate (0.1 M), urea (2 M), reduced glutathione (2.5 mM), and oxidized glutathione (0.25 mM), titrated by using NH_4OH (7.7 N solution). Progress in folding was monitored by subjecting the folding mixtures to HPLC analyses on an Agilent 300SB-C18 RP-HPLC column (300 Å pore size) by employing a water-acetonitrile (0.1% TFA) linear gradient (5-65% acetonitrile over 30 min). The folded toxins were purified by HPLC, and the purity of the isolated folded toxins was also evaluated via HPLC. The folded toxins were characterized via MALDI-TOF.

Sample preparation for MALDI-TOF MS characterization of toxins.

MALDI-TOF mass spectrometry analyses were performed on 4800 Plus MALDI TOF/TOF instrument from AB Sciex at the IISER Pune MALDI facility, and on a Bruker Nano-LC MALDI TOF/TOF spectrometer at the IISER Bhopal Central Instrumentation Facility. The matrix employed was either a mixture of 2,6-dihydroxyacetophenone (65.7 mM) and diammonium hydrogen citrate (56.9 mM) in 43% ethanol in water,[21] or sinapic acid (44.6 mM) in dioxane.

Two-electrode voltage clamp (TEVC) electrophysiology and data analysis.

General: Oocytes were surgically removed from anesthetized adult female *Xenopus laevis* in accordance with a protocol approved by the Institutional Animal Ethics Committee (IAEC), IISER Bhopal, and microinjected with rat TRPV1 or Kv2.1Δ7 mRNA. Currents were recorded using an OC-725C oocyte clamp (Warner Instruments). The microelectrode (filled with 3 M KCl) resistances were between 0.1–1.2 MΩ.

TRPV1 recordings: The recordings were performed via the gap-free protocol by holding the oocytes at -60 mV, employing extracellular solutions containing NaCl (50 mM), KCl (50 mM), $MgCl_2$ (1 mM), $BaCl_2$ (0.3 mM), and HEPES (20 mM) at pH 7.4. The data was filtered at 0.5 kHz, and digitized at 2.5 kHz.

Toxin-induced currents were normalized against the currents obtained upon a prior application of 5 μM capsaicin to the same oocyte. Subsequently, these I_{Toxin}/I_{Caps} values were plotted against the concentration of the toxin and the Hill equation (below) was fit to the data using Origin 9.0.

$$y= A_{max} \{(x^n)/(k^n+x^n)\}$$

where, A_{max} is the I_{Toxin}/I_{Caps}, k is EC_{50} and n is the Hill coefficient.

To generate the normalized toxin wash-off plots, the data for 5 min of buffer perfusion post toxin-mediated channel activation was procured from the TEVC recordings in the axon test file (.atf) format using the Clampfit 10.5 software. This data was subjected to data point extraction at every 7500th point interval using the R3.4.1 package, and the current at each time point was normalized to the peak current value of the same recording (at the buffer perfusion initiation time point). The normalized data obtained from 3–5 recordings were used to obtain averaged traces for wash-off plots, and plotted to generate the figures. The SEM values at each time point were plotted as error bars.

Kv2.1Δ7 recordings: The recordings were performed by employing step-voltage protocols, and the data was filtered at 1 kHz and digitized at 10 kHz. The extracellular solutions for Kv2.1 recordings contained KCl (50 mM), NaCl (50 mM), $MgCl_2$ (1 mM), $CaCl_2$ (0.3 mM), and HEPES (20 mM) at pH 7.4. Capacitive and background currents were identified by first blocking the Kv2.1 channel with agitoxin2,[22] and then subtracting them to generate the currents shown in Figures 4d and 7a. Conductance (G)-Voltage (V) relationships depicted in Figures 3.3e and 3.7b were obtained by

measuring tail currents following depolarization to test voltages followed by fitting a single Boltzmann function to the data according to the equation,

$$G/G_{max} = [1 + \exp(-zF(V-V_{1/2})/RT)]^{-1}$$

where, z is the valence, F is the Faraday constant, R is the gas constant, and T is the temperature.

Membrane affinity experiments on uninjected Xenopus laevis oocytes.

Single and double-knots: Toxin depletion experiments depicted in Figures 3.2c, 3.5a, and 3.7c were performed as reported previously.[3] Specifically, uninjected defolliculated stage 5 or 6 oocytes (100 nos.) were incubated with 4 nmol of toxin dissolved in a 400 µL solution of HEPES (20 mM) buffer at pH 7.4 containing NaCl (50 mM), KCl (50 mM), $MgCl_2$ (1 mM), and $BaCl_2$ (0.3 mM) for 1 h at room temperature. Control experiments involved incubating the toxin under identical conditions without oocytes. Subsequently, the supernatant (200 µL) was removed and spiked with a solution of 2-nitrophenol (2.5 µL of a 2.5 mg/mL solution in water) used as an internal standard. A 100 µL aliquot of this mixture was injected into the HPLC and eluted using a water-acetonitrile (0.1% TFA) linear gradient (5-65% acetonitrile over 30 min). This experimental protocol was performed three times and the fractional depletion was calculated as follows:

$$\text{Fraction depletion} = (R_{control} - R_{oocytes})/R_{control}$$

$R_{control}$ is the averaged ratio of the area under the peak for the toxin and the area under the peak for 2-nitrophenol in the control experiments, and $R_{oocytes}$ is the ratio of the same parameters obtained from the oocyte samples (n = 3).

Tetra-knots: Uninjected defolliculated stage 5 or 6 oocytes (50 nos.) were incubated with $(DkTx)_2$ or DkTx-$(SGTx)_2$ (1 nmol) in a 400 µL solution of HEPES (20 mM) buffer at pH 7.4 containing NaCl (50 mM), KCl (50 mM), $MgCl_2$ (1 mM) and $BaCl_2$ (0.3 mM) for 1 h at room temperature. Control experiments involved incubating the toxin under identical conditions without oocytes. Subsequently, the supernatant (300 µL) was removed and spiked with a solution of 2-nitrophenol (1.25 µL of a 2.5 mg/mL solution in water) used as an internal standard. A 250 µL aliquot of this mixture was injected into the HPLC and eluted using a water-acetonitrile (0.1% TFA) linear gradient (5-65% acetonitrile over 30 min). The fractional depletion was calculated by using the same equation as depicted above.

3.5 References

1. Bohlen, C. J. *et al.* A bivalent tarantula toxin activates the capsaicin receptor, TRPV1, by targeting the outer pore domain. *Cell* **141**, 834–845 (2010).

2. Bae, C. *et al.* Structural insights into the mechanism of activation of the TRPV1 channel by a membrane-bound tarantula toxin. *Elife* **5**, e11273 (2016).

3. Sarkar, D., Singh, Y. & Kalia, J. Protein–Lipid Interfaces Can Drive the Functions of Membrane-Embedded Protein–Protein Complexes. *ACS Chem. Biol.* **13**, 2689–2698 (2018).

4. Bae, C. *et al.* High yield production and refolding of the double-knot toxin, an activator of TRPV1 channels. *PloS one* **7**, e51516 (2012).

5. Lee, S.-Y. & MacKinnon, R. A membrane-access mechanism of ion channel inhibition by voltage sensor toxins from spider venom. *Nature* **430**, 232–235 (2004).

6. Swartz, K. J. Tarantula toxins interacting with voltage sensors in potassium channels. *Toxicon* **49**, 213–230 (2007).

7. Wee, C. L., Bemporad, D., Sands, Z. A., Gavaghan, D. & Sansom, M. S. SGTx1, a Kv channel gating-modifier toxin, binds to the interfacial region of lipid bilayers. *Biophysical journal* **92**, L07–L09 (2007).

8. Jung, H. H. *et al.* Structure and orientation of a voltage-sensor toxin in lipid membranes. *Biophysical journal* **99**, 638–646 (2010).

9. Lee, C. W. *et al.* Solution Structure and Functional Characterization of SGTx1, a Modifier of Kv2.1 Channel Gating ‡. *Biochemistry* **43**, 890–897 (2004).

10. Wang, J. M. *et al.* Molecular surface of tarantula toxins interacting with voltage sensors in Kv channels. *The Journal of general physiology* **123**, 455–467 (2004).

11. Sarkar, D. *et al.* Site-Specific Fluorescent Labeling of the Cysteine-Rich Toxin, DkTx, for TRPV1 Ion Channel Imaging and Membrane Binding Studies. *Bioconjugate Chem.* **33**, 1761–1770 (2022).

12. Guimaraes, C. P. *et al.* Site-specific C-terminal and internal loop labeling of proteins using sortase-mediated reactions. *Nature protocols* **8**, 1787–1799 (2013).

13. Agwa, A. J., Blomster, L. V., Craik, D. J., King, G. F. & Schroeder, C. I. Efficient Enzymatic Ligation of Inhibitor Cystine Knot Spider Venom Peptides: Using Sortase A To Form Double-Knottins That Probe Voltage-Gated Sodium Channel Na_V 1.7. *Bioconjugate Chem.* **29**, 3309–3319 (2018).

14. Tran, H. N. T. *et al.* Enzymatic Ligation of a Pore Blocker Toxin and a Gating Modifier Toxin: Creating Double-Knotted Peptides with Improved Sodium Channel Na_V 1.7 Inhibition. *Bioconjugate Chem.* **31**, 64–73 (2020).

15. Swartz, K. J. & MacKinnon, R. Hanatoxin modifies the gating of a voltage-dependent K+ channel through multiple binding sites. *Neuron* **18**, 665–673 (1997).

16. Herrington, J. Gating modifier peptides as probes of pancreatic β-cell physiology. *Toxicon* **49**, 231–238 (2007).

17. Gilding, E. K. *et al.* Neurotoxic peptides from the venom of the giant Australian stinging tree. *Sci. Adv.* **6**, eabb8828 (2020).

18. Carnevale, V. & Rohacs, T. TRPV1: a target for rational drug design. *Pharmaceuticals* **9**, 52 (2016).

19. Maatuf, Y., Geron, M. & Priel, A. The role of toxins in the pursuit for novel analgesics. *Toxins* **11**, 131 (2019).

20. Iadarola, M. J. & Mannes, A. J. The vanilloid agonist resiniferatoxin for interventional-based pain control. *Current topics in medicinal chemistry* **11**, 2171 (2011).

21. Sandanaraj, B. S., Reddy, M. M., Bhandari, P. J., Kumar, S. & Aswal, V. K. Rational Design of Supramolecular Dynamic Protein Assemblies by Using a Micelle-Assisted Activity-Based Protein-Labeling Technology. *Chemistry A European J* **24**, 16085–16096 (2018).

22. Li-Smerin, Y. & Swartz, K. J. Gating modifier toxins reveal a conserved structural motif in voltage-gated Ca^{2+} and K^{+} channels. *Proc. Natl. Acad. Sci. U.S.A.* **95**, 8585–8589 (1998).

Chapter 4:

Study the role of TRPV1-DkTx stoichiometry on the characteristic DkTx's slow wash-off

4.1 Introduction

The cryo-EM structures of TRPV1 have revealed that its transmembrane topology and subunit organization are similar to that of voltage-gated potassium channels, where four identical subunits form a functional channel around a central ion-conducting pore in a symmetrical arrangement.[1–3]

DkTx's slow wash-off kinetics can be attributed not only to its bivalency and membrane affinity but also to its channel occupancy. The DkTx-TRPV1 complex's structure (middle panel of Figure 4.1) reveals that DkTx has a channel occupancy of two,[3] suggesting that cooperative interactions between the two channel-bound DkTx molecules stabilize the complex and slow down toxin dissociation. This hypothesis is supported by the fact that DkTx's wash-off kinetics depend on its concentration, with higher concentrations leading to progressively slower wash-off rates, which favor a channel occupancy of two.[4] A similar observation was made for hanatoxin, a Kv2.1 voltage-sensor targeting toxin, where the concentration dependence of wash-off kinetics was attributed to its multiple channel occupancy.[5]

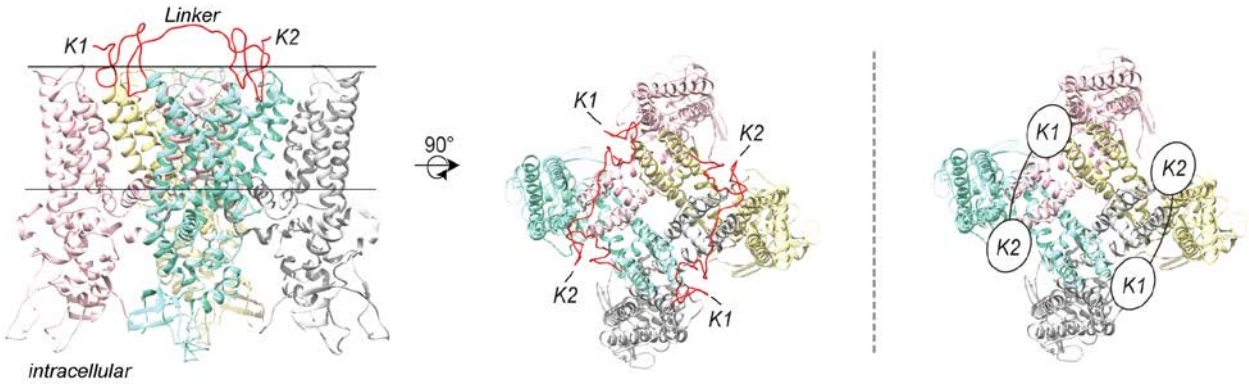

Figure 4.1: DkTx binding to TRPV1. The DkTx-TRPV1 complex (PDB: 5irx) viewed sideways from within the membrane (left panel) and the top view from the extracellular side (middle panel) along with a cartoon representation of the top view (right panel). For the sake of clarity, only one DkTx molecule is depicted in the left panel and disulfide linkages have been omitted from both the renditions. DkTx mediated TRPV1 channel activation.

In this chapter, I have studied the role of the channel occupancy of DkTx by generating a TRPV1 variant on a previously reported construct of concatemeric TRPV1,[6] where we have disrupted the binding site of one DkTx molecule and retaining the binding site of another DkTx molecule, as opposed to the wildtype channel that can bind to two DkTx molecules simultaneously (as seen in the structure of the wildtype TRPV1-DkTx complex of Figure 4.1).

4.2 Results

In order to explore how the channel occupancy of DkTx affects its wash-off kinetics, we designed a TRPV1 construct that would disrupt the binding site of one DkTx molecule while keeping the binding site of the other molecule intact. To accomplish this, we first introduced sixteen substitutions (four substitution mutations in each of the four subunits of TRPV1 channel) at the DkTx-binding site on the outer pore region of TRPV1 construct: I599A_F649A_A657P_F659A (shown in Figure 4.3c). It has been demonstrated that introducing these four substitutions into each subunit of the channel tetramer renders it insensitive to DkTx while still allowing activation by capsaicin, indicating that this channel variant disrupt the toxin's binding to the channel.[7] However, characterization of this variant of the TRPV1 channel in our lab reveals that, on the contrary, it still retains the ability to be activated by DkTx, although with a remarkable reduction in its potency and exhibiting a very fast wash-off as shown in figure 4.2. This fast wash-off ability of DkTx for

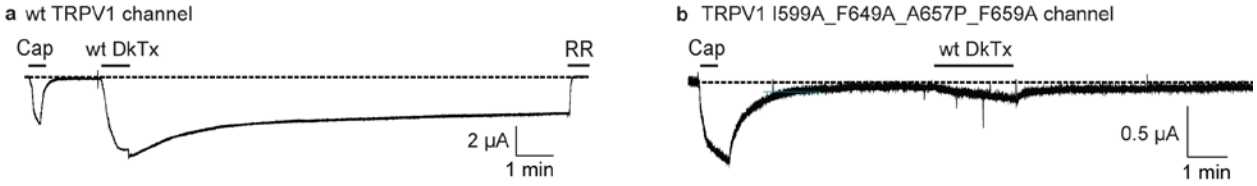

Figure 4.2: Comparison of channel activity of wt TRPV1 channel and TRPV1 I599A_F649A_A657P_F659A mutant. (a) Representative electrophysiological recordings depicting wt TRPV1 currents obtained upon the application of TRPV1-agonist, capsaicin (5 µM), followed by toxin (20 µM). Wash-off was performed by starting buffer perfusion after the currents saturated in presence of the agonists. Then, the TRPV1 blocker, ruthenium red (RR, 7 µM) was applied to completely inhibit TRPV1 currents at the end of the recording. (b) Representative electrophysiological recordings depicting TRPV1 I599A_F649A_A657P_F659A mutant currents obtained upon the application of TRPV1-agonist, capsaicin (5 µM), followed by toxin (20 µM) resulting in the complete wash-off of the toxin.

this channel variant can be attributed to the disruption in the toxin—channel interactions resulting from the channel's mutations.

In order to determine the role of the channel occupancy of DkTx in sustained activation of TRPV1, we have utilized the previously reported concatemeric wild-type (wt) TRPV1 construct,[6] which was a generous gift from Prof. Avi Priel. Concatemers have been proven a useful tool to control the number and location of a mutated subunit of a homomeric protein.[8–11] TRPV1 is assembled as a homotetrameric channel with intracellular N- and C-termini.[2,3] Using this feature as guidelines,

we have used concatemeric wt rat TRPV1 (rTRPV1) constructs[6] and generated concatemeric octamutant TRPV1 mutants to disrupt the DkTx binding sites (illustrated in Figure 4.3).

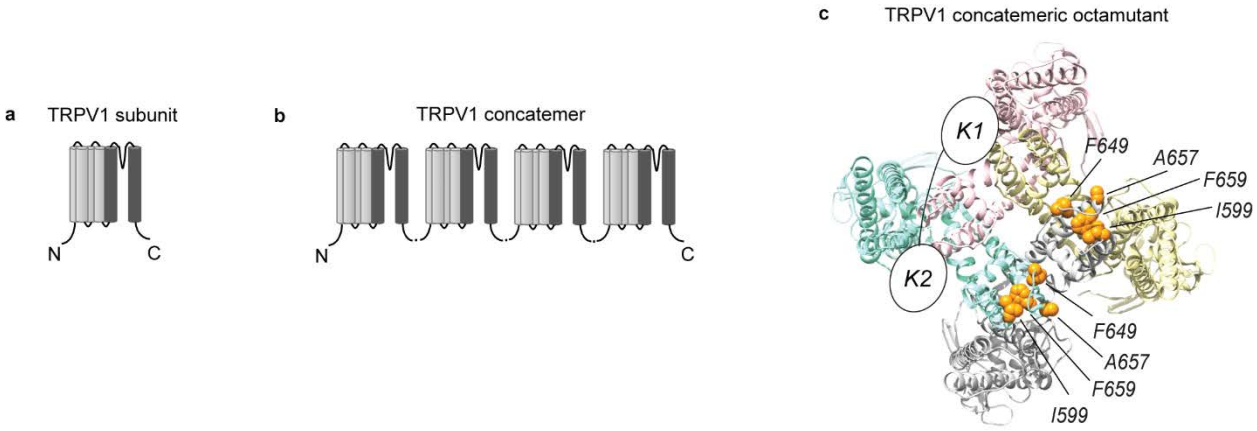

Figure 4.3: Schematic representation of TRPV1 concatemer and TRPV1 concatemeric octamutant. (a) Schematic representation of TRPV1 subunit. (b) Schematic representation of concatemeric rat TRPV1 (rTRPV1) construct with a unique restriction enzyme site at the *C*-terminal (without the stop codon) and to the N-terminal (without the start codon) of adjacent wt subunits (bottom; dotted line). (c) Top view of TRPV1 structure (PDB: 5irx) depicting toxin-binding channel residues that we substituted to generate a channel variant that has a channel occupancy of one.

Our reasoning was that introducing these four substitutions in two adjacent subunits would disrupt one DkTx molecule from binding to the channel, resulting in a channel occupancy of one, which would enable us to investigate the role of occupancy in the TRPV1-activating properties of the toxin.would enable us to investigate the role of occupancy in the TRPV1-activating properties of the toxin.

Using electrophysiological experiments, we discovered that our octamutant TRPV1 concatemer variant, still responds to activation by DkTx. This indicates that the binding of a single DkTx molecule is sufficient to activate the channel, as shown in the bottom panel of Figure 4.4a. However, the potency for DkTx activation was somewhat reduced in the octamutant concatemer compared to the wild-type concatemer, with an EC_{50} of 0.7 µM versus 0.2 µM, as seen in Figure

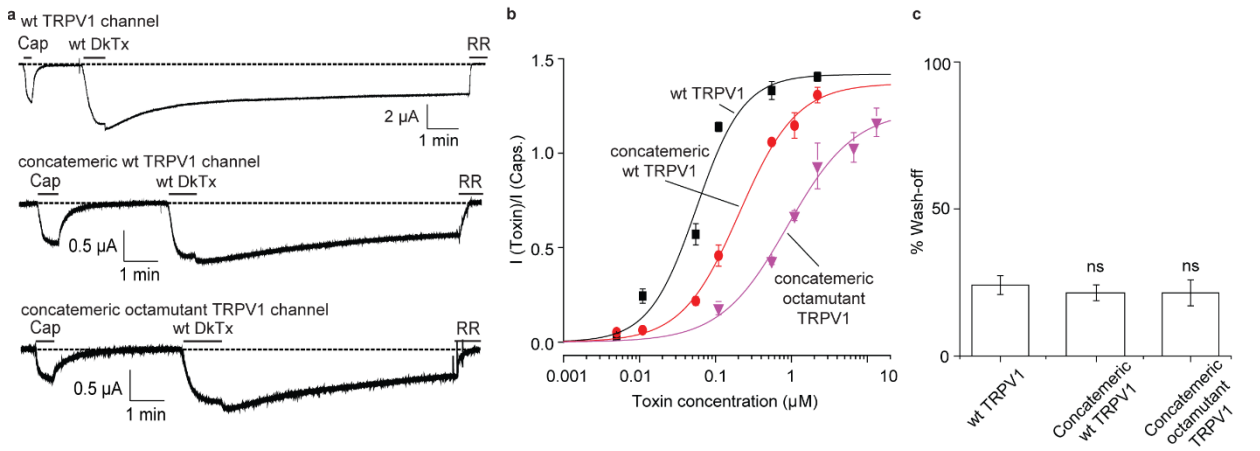

Figure 4.4: Evaluating the role of the channel occupancy of DkTx in its sustained mode of TRPV1 activation. (a) Representative current traces for the activation of wild-type TRPV1, concatemeric wild-type TRPV1, and concatemeric octamutant TRPV1, by 20 µM DkTx. (b) Dose response plots for DkTx activation of wild-type, concatemeric wild-type, and concatemeric octamutant TRPV1. (c) Bar plot with SEM depicting the percentage reduction in current after 3 min of buffer perfusion post toxin-mediated channel activation (n=3 for each toxin). The percentage wash-off were compared with wild-type TRPV1 for statistical analysis. ns = not statistically significant (ANOVA followed by a multiple comparison test).

4.4b and Table 4.1. At a DkTx concentration of 20 µM, the wash-off rates were the same for both the octamutant and the wild-type concatemer, with a 21.5% decrease in TRPV1 currents after three minutes of buffer perfusion, as depicted in Figure 4.5. Additionally, the wash-off kinetics at DkTx concentrations, 20 µM, 2.2 µM 1.1 µM, 0.55 µM and 0.11 µM, were identical for both concatemers, as shown in Figure 4.5. These findings suggest that the DkTx occupancy does not significantly contribute to the slow wash-off kinetics observed in response to this toxin.

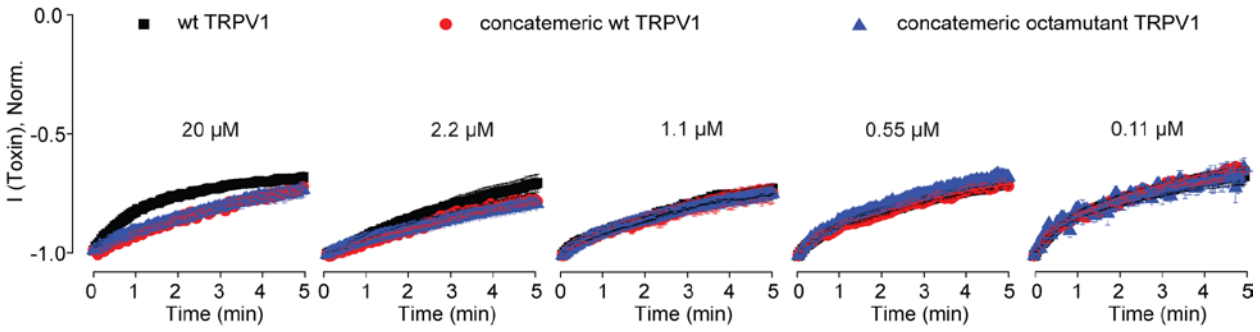

Figure 4.5: Evaluating the role of the channel occupancy of DkTx in its sustained mode of TRPV1 activation. Averaged wash-off current traces for the activation of wildtype, concatemeric wild-type, and concatemeric octamutant TRPV1 by 20 µM, 2.2 µM 1.1 µM, 0.55 µM and 0.11 µM wt DkTx. Each data point for all the plots with error bars corresponds to a mean value of 3 experiments with error bars indicating the standard error of the mean.

Table 4.1: Consolidated data summary for wild-type TRPV1, concatemeric wild-type TRPV1, and concatemeric octamutant TRPV1:

Serial no.	Ion channels	Wild-type DkTx EC_{50} (μM)	Fold change in EC_{50}	Hill coefficient (nH)	% wash-off after 3 min of buffer perfusion post channel activation by 20 μM of wt DkTx
1	Wild-type TRPV1	0.05 ± 0.01	1	1.4 ± 0.4	24.1 ± 3.2
2	Concatemeric wild-type TRPV1	0.19 ± 0.03	3.8	1.2 ± 0.1	21.5 ± 2.7
3	Concatemeric octamutant TRPV1	0.65 ± 0.11	13	1.4 ± 0.4	21.5 ± 4.4

4.3 Discussion

The crucial role as ligand-gated channels in physiology and pharmacology, the impact of ligand stoichiometry on TRP channel modulation is not yet well understood. These channels are made up of four subunits with six transmembrane segments (S1-S6),[3] and previous studies have shown that lipophilic agonists such as capsaicin,[6] resiniferatoxin, menthol (TRPM8),[10] and 4a-phorbols (TRPV4),[12] and peptide toxin such as DkTx (TRPV1)[7] bind to residues located in transmembrane domains S2-S4 and to the outer pore region of the TRPV1 channel respectively. This information suggests that a single TRP channel may interact with four ligand molecules in the case of lipophilic molecules or two in the case of DkTx. However, the exact number of ligands required to activate a TRP channel, or the energetic contribution of each individual ligand-binding event, remains unknown.

This study aimed to investigate the ligand stoichiometry of the peptide toxin DkTx with TRPV1 channels. We achieved this by analyzing the sensitivity of TRPV1 channel with a defined composition of wild-type and DkTx-insensitive subunits of TRPV1 concatemers to DkTx. Our findings demonstrate that a single DkTx molecule can bind independently to the TRPV1 channel

and activate it as shown in Figure 4.4a. Additionally, as depicted in Figure 4.5, the DkTx occupancy does not significantly contribute to sustained TRPV1 channel activation.

4.4 Materials and methods

Preparation of TRPV1 concatemer variants.

Concatemer wild-type (wt) TRPV1 construct in pCDNA vector was generously donated by Professor Avi Priel (HUJI). TRPV1 concatemer variants were generated by restriction-ligation cloning on the concatemer wild-type (wt) TRPV1 plasmid by first replacing the wt 4th subunit with tetra-mutant I599A_F649A_A657P_F659A version, then followed by replacing the wt 3rd subunit on the background of tetra-mutant TRPV1 concatemer, with tetra-mutant I599A_F649A_A657P_F659A version, thereby generating the octamutant TRPV1 concatemer.

Two-electrode voltage clamp (TEVC) electrophysiology and data analysis.

Electrophysiology experiments, and their data analysis were performed as mentioned in Chapter 3.

4.5 References

1. Cheng, Y., Julius, D., Liao, M. & Cao, E. Structure of the TRPV1 ion channel determined by electron cryo-microscopy. (2013).

2. Cao, E., Liao, M., Cheng, Y. & Julius, D. TRPV1 structures in distinct conformations reveal activation mechanisms. *Nature* **504**, 113–118 (2013).

3. Julius, D., Gao, Y., Cao, E. & Cheng, Y. TRPV1 structures in nanodiscs reveal mechanisms of ligand and lipid action. (2016).

4. Sarkar, D., Singh, Y. & Kalia, J. Protein–Lipid Interfaces Can Drive the Functions of Membrane-Embedded Protein–Protein Complexes. *ACS Chem. Biol.* **13**, 2689–2698 (2018).

5. Swartz, K. J. & MacKinnon, R. Hanatoxin modifies the gating of a voltage-dependent K+ channel through multiple binding sites. *Neuron* **18**, 665–673 (1997).

6. Hazan, A., Kumar, R., Matzner, H. & Priel, A. The pain receptor TRPV1 displays agonist-dependent activation stoichiometry. *Scientific reports* **5**, 12278 (2015).

7. Bohlen, C. J. *et al.* A bivalent tarantula toxin activates the capsaicin receptor, TRPV1, by targeting the outer pore domain. *Cell* **141**, 834–845 (2010).

8. Isacoff, E. Y., Jan, Y. N. & Jan, L. Y. Evidence for the formation of heteromultimeric potassium channels in Xenopus oocytes. *Nature* **345**, 530–534 (1990).

9. Liman, E. R., Tytgat, J. & Hess, P. Subunit stoichiometry of a mammalian K+ channel determined by construction of multimeric cDNAs. *Neuron* **9**, 861–871 (1992).

10. Janssens, A. & Voets, T. Ligand stoichiometry of the cold- and menthol-activated channel TRPM8: Ligand stoichiometry of TRPM8. *The Journal of Physiology* **589**, 4827–4835 (2011).

11. Cheng, W. *et al.* Heteromeric heat-sensitive transient receptor potential channels exhibit distinct temperature and chemical response. *Journal of Biological Chemistry* **287**, 7279–7288 (2012).

12. Inoue, R., Hu, Y., Duan, Y. & Itsuki, K. Lipid-Mediated Mechanisms Involved in the Mechanical Activation of TRPC6 and TRPV4 Channels in the Vascular Tone Regulation. in *Mechanically Gated Channels and their Regulation* (eds. Kamkin, A. & Lozinsky, I.) 281–301 (Springer Netherlands, 2012). doi:10.1007/978-94-007-5073-9_10.

Chapter: 5

Future Directions

Ligand-gated ion channels are transmembrane proteins that mediate the flow of ions across cell membranes in response to the binding of specific ligands, such as neurotransmitters, hormones, and animal toxins.[1–3] These channels are crucial for various physiological processes, including neuronal communication, muscle contraction, and sensory perception.[1,4]

The protein-lipid interface plays a significant role in ligand-gated ion channels and their function.[5–8] Lipids directly interact with specific protein regions and influence their conformational changes, which are essential for the channel's gating mechanism.[5,8] These lipids interact with specific regions of the channel protein, such as the transmembrane domains or the intracellular domains, and modulate the channel's response to ligand binding.[5,6,8] Lipids at the protein-lipid interface create a microenvironment that affects the binding of ligands to their specific binding sites on the channel protein.[6,8] This can influence the affinity and kinetics of ligand binding and subsequent channel activation.[8]

5.1 Quantitative characterization of the contributions of DkTx-TRPV1 binding and DkTx-membrane binding towards slow wash-off rates of toxin wash-off kinetics.

To quantitatively dissect the contribution of the membrane affinity of the toxin as compared to toxin-channel binding to conferring the toxin with its slow wash-off kinetics, it is imperative to develop a robust binding assay for toxin-channel binding which is currently lacking. Indeed, the comprehension of binding affinity provides valuable insights into the intricate mechanisms governing ion channel functionality. It unveils the strength of interaction between a ligand and the channel, offering clarity on how this interaction directly influences the channel's opening and closing dynamics. This knowledge is pivotal for gaining a comprehensive understanding of the crucial roles these channels play in both physiological and pharmacological contexts.[9,10] However, the task of assessing binding affinities between the ion channel and the ligand becomes notably challenging when the ligand concurrently interacts with membrane lipids while binding to the ion channel.[11,12] This complex scenario occurs in the case of DkTx binding to the TRPV1 channel. In light of these challenges, the development of a more suitable method to accurately determine the binding affinity between the TRPV1 channel and DkTx is needed.

One approach of doing this is to employ radio-ligand binding assays to study the channel-ligand binding because of minimal modification of the ligand and sensitivity of the assay.[10,13,14] However, they do come with certain limitations. Firstly, radio-ligand binding assays require the use of

radioactive materials, which can pose safety and disposal concerns, making them less attractive in terms of environmental and health considerations. Additionally, the use of radioisotopes can be expensive and subject to strict regulatory controls. Another limitation is that radio-ligand binding assays often involve homogenized or isolated cell preparations, which may not accurately represent the in vivo conditions where receptors are embedded in a complex cellular environment. This can lead to discrepancies between the binding affinities observed *in vitro* and the actual physiological responses. Therefore, in addition to radiolabeling, it will be worthwhile to develop other approaches for characterizing the binding of the TRPV1 with our DkTx variants.

Another approach that could be fruitful for characterizing the binding of TRPV1 to our DkTx variants is to employ fluorescently labeled DkTx that our laboratory has recently reported[15] for developing a Bioluminescence Resonance Energy Transfer (BRET)[16,17]or Fluorescence Resonance Energy Transfer (FRET)[18,19]-based assays.

5.2 Study the role of TRPV1-DkTx stoichiometry on the single channel conductance of TRPV1 channel

We have generated a TRPV1 concatemer octamutant variant in which only one DkTx molecule will bind to the concatemer channel variant, resulting in a channel occupancy of one. However, it remains to experimentally confirm the occupancy of one DkTx molecule on the TRPV1 concatemer octamutant channel. Then, we will proceed with single-channel experiments on this variant to determine the effects of one DkTx molecule binding to the TRPV1 channel. We will investigate its impact on single-channel conductance, open probability, and whether it leads to a different open state compared to the scenario where two DkTx molecules are bound to the TRPV1 channel.

5.3 References

1. Hille, B. Ion channels of excitable membranes (Sinauer, Sunderland, MA). (2001).

2. Nasiripourdori, A., Taly, V., Grutter, T. & Taly, A. From toxins targeting ligand gated ion channels to therapeutic molecules. *Toxins* **3**, 260–293 (2011).

3. Arias, H. R. Marine toxins targeting ion channels. *Marine Drugs* **4**, 37–69 (2006).

4. Tykocki, N. R., Boerman, E. M. & Jackson, W. F. Smooth muscle ion channels and regulation of vascular tone in resistance arteries and arterioles. *Comprehensive Physiology* **7**, 485 (2017).

5. Bergh, C., Rovsnik, U., Howard, R. J. & Lindahl, E. Discovery of lipid binding sites in a ligand-gated ion channel by integrating simulations and cryo-EM. *bioRxiv* 2023–01 (2023).

6. Dämgen, M. A. & Biggin, P. C. State-dependent protein-lipid interactions of a pentameric ligand-gated ion channel in a neuronal membrane. *PLOS Computational Biology* **17**, e1007856 (2021).

7. Jiang, Q.-X. & Gonen, T. The influence of lipids on voltage-gated ion channels. *Current opinion in structural biology* **22**, 529–536 (2012).

8. Saponaro, A. & Lolicato, M. The key role of lipids in the regulation of ion channels. *Frontiers in Physiology* **13**, 1000082 (2022).

9. McManus, O. B. HTS assays for developing the molecular pharmacology of ion channels. *Current opinion in pharmacology* **15**, 91–96 (2014).

10. Hulme, E. C. & Trevethick, M. A. Ligand binding assays at equilibrium: validation and interpretation. *British J Pharmacology* **161**, 1219–1237 (2010).

11. Julius, D., Gao, Y., Cao, E. & Cheng, Y. TRPV1 structures in nanodiscs reveal mechanisms of ligand and lipid action. (2016).

12. Efremov, R. G., Gatsogiannis, C. & Raunser, S. Lipid nanodiscs as a tool for high-resolution structure determination of membrane proteins by single-particle cryo-EM. in *Methods in enzymology* vol. 594 1–30 (Elsevier, 2017).

13. Denyer, J., Worley, J., Cox, B., Allenby, G. & Banks, M. HTS approaches to voltage-gated ion channel drug discovery. *Drug discovery today* **3**, 323–332 (1998).

14. Lefkowitz, R. J., Roth, J. & Pastan, I. Radioreceptor Assay of Adrenocorticotropic Hormone: New Approach to Assay of Polypeptide Hormones in Plasma. *Science* **170**, 633–635 (1970).

15. Sarkar, D. *et al.* Site-Specific Fluorescent Labeling of the Cysteine-Rich Toxin, DkTx, for TRPV1 Ion Channel Imaging and Membrane Binding Studies. *Bioconjugate Chem.* **33**, 1761–1770 (2022).

16. Pfleger, K. D. & Eidne, K. A. Illuminating insights into protein-protein interactions using bioluminescence resonance energy transfer (BRET). *Nature methods* **3**, 165–174 (2006).

17. Pernomian, L. *et al.* New Horizons on Molecular Pharmacology Applied to Drug Discovery: When Resonance Overcomes Radioligand Binding. *Current Radiopharmaceuticals* **10**, 16–20 (2017).

18. Jares-Erijman, E. A. & Jovin, T. M. FRET imaging. *Nature biotechnology* **21**, 1387–1395 (2003).

19. Roy, R., Hohng, S. & Ha, T. A practical guide to single-molecule FRET. *Nature methods* **5**, 507–516 (2008).

Appendix:

Functional characterization of *Arabidopsis thaliana* CNG (Cyclic Nucleotide-Gated) channel-13

The research work presented here is a part of the collaborative project with Dr. Jyothilakshmi Vadassery's lab from the National Institute of Plant Genome Research (NIPGR), New Delhi. Dr. Vadassery's lab has sent us the CNCGC13-YFP construct to investigate the expression of CNGC13 channel on the plasma membrane and determine the permeability of these channels to Ca^{2+} and K^{+} ions by performing two-electrode voltage clamp experiments on *Xenopus laevis* oocytes.

A.1 Introduction

Plant CNG (Cyclic Nucleotide-Gated) channels are a superfamily of cation channels that are permeable to divalent and monovalent cations, including Ca^{2+} and K^{+}. They are tetrameric proteins, each subunit having a cytosolic N- terminus, six transmembrane helices (S1 to S6) with a pore-forming region spanning S5 to S6, and a *C*-terminal cytosolic tail with binding domains for cyclic nucleotides (CNBD), and calmodulin (CaM) binding domains.[1]

The permeability of CNGC channels to Ca^{2+} is thought to be important for a number of reasons. First, Ca^{2+} is a critical signaling molecule in plants, playing roles in processes such as gene expression, cell division, and stress responses. Second, changes in the concentration of Ca^{2+} can trigger the opening or closing of ion channels, leading to changes in membrane potential and downstream signaling events.[2]

A.2 Results and discussion

CNGCs are a type of plant channels that allow calcium ions to pass through,[3] and while this has been demonstrated for several plant CNGCs, the permeability of CNGC13 has not been

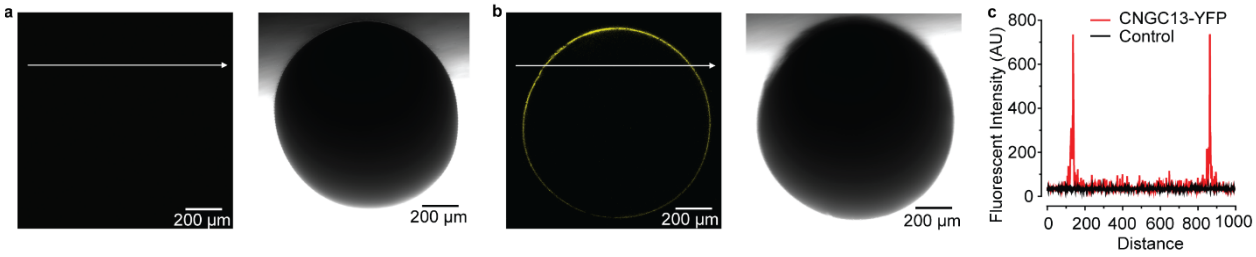

Figure A.1: Confocal imaging of CNGC13-YFP fusion protein expression in oocyte. (a) Fluorescence confocal image of an un-injected oocyte (left panel), and its bright filed image (right panel). (b) Fluorescence confocal image of an oocyte injected with CNGC13-YFP cRNA (left panel), and its bright field image (right panel). (c) Line scans of fluorescence intensities along with lines drawn in (i; left panel) and (ii; left panel). Distance (x-axis) is from the start of the arrow. Red- CNGC13-YFP injected oocyte; Black- un-injected oocyte. Scale bar: 200 µm.

characterized yet. To address this, a modified form of CNGC13 called CNGC13-YFP, which has an YFP-tag at its *C*-terminus, was expressed in *Xenopus laevis* oocytes. The oocytes that received the CNGC13-YFP cRNA injection displayed strong fluorescence at their edges, while those that were not injected did not exhibit any fluorescence. This can be seen in Figure A.1a and b. The

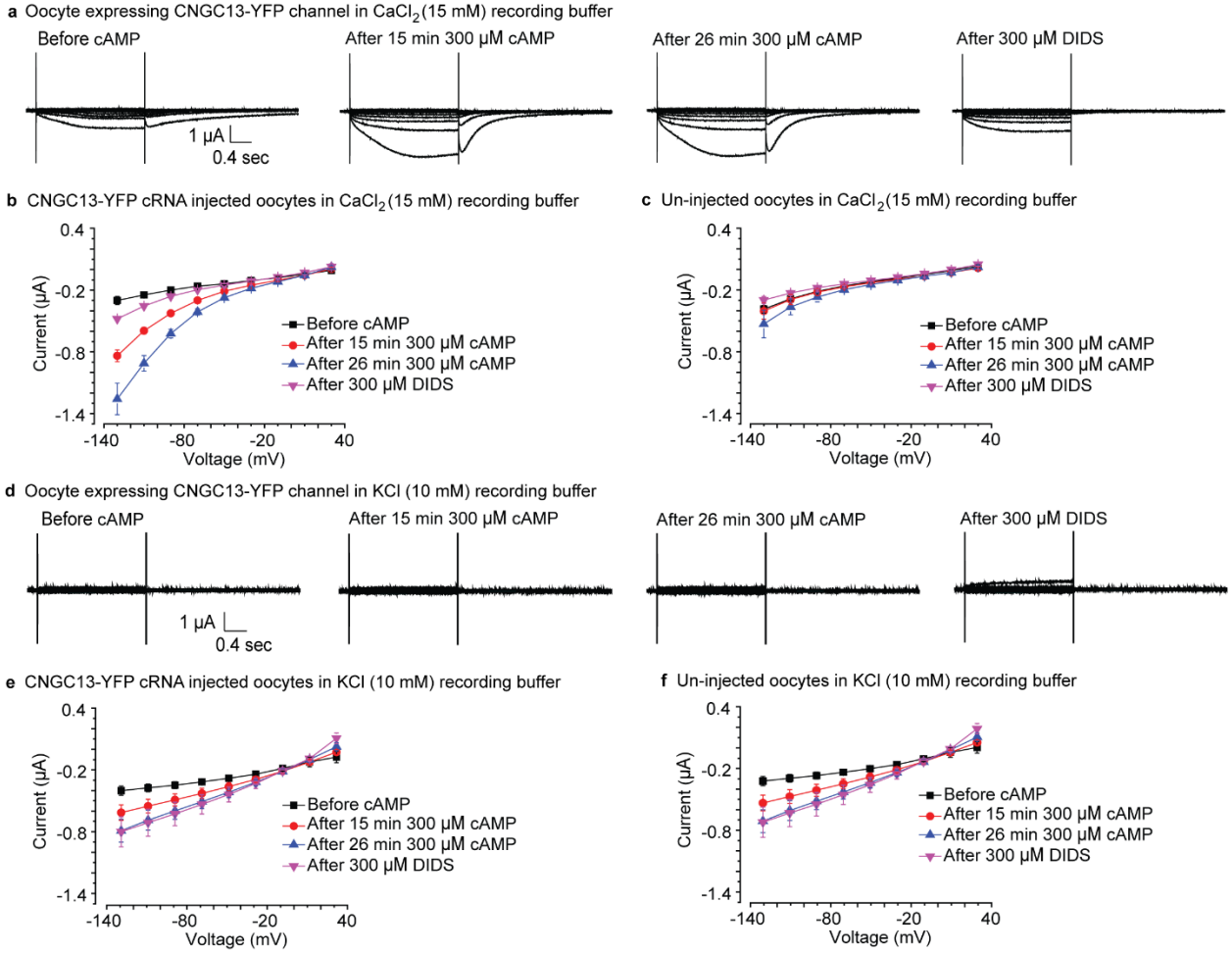

Figure A.2: TEVC recordings for CNGC13-YFP expressing oocytes in different conditions. CNGC13-YFP expressing oocytes show inward rectifying currents in $CaCl_2$ (15 mM) recording buffer. In panel (a), currents were recorded on a CNGC13 channel RNA injected oocyte before and after the addition of dibutyryl cAMP (300 µM) post 15 min and 26 min, which is followed by addition of DIDS (300 µM). All additions were done sequentially and no washout was performed for the recordings. In panel (b) and (c), plots of current values recorded from CNGC13-YFP cRNA injected oocytes and un-injected oocytes in $CaCl_2$ (15 mM) recording buffer before and after the addition of 300 µM dibutyryl cAMP (post 15 min and 26 min) followed by addition of DIDS (300 µM). Each data point is an average obtained from n=4, and the error bars correspond to standard error values. CNGC13-YFP expressing oocytes in KCl (10 mM) recording buffer. In panel (d), currents were recorded on a CNGC13 channel RNA injected oocyte before and after the addition of dibutyryl cAMP (300 µM) post 15 min and 26 min, which is followed by addition of DIDS (300 µM). All additions were done sequentially and no washout was performed for the recordings. In panel (e) and (f), plots of current values recorded from CNGC13-YFP cRNA injected oocytes and un-injected oocytes in KCl (10 mM) recording buffer before and after the addition of 300 µM dibutyryl cAMP (post 15 min and 26 min) followed by addition of DIDS (300 µM). Each data point is an average obtained from n=4, and the error bars correspond to standard error values.

fluorescence was confined to the edge of the oocyte, as shown in Figure A.1b left panel, where a

line scan indicates the fluorescence's restriction to the oocyte's boundary as shown in Figure A.1c. TEVC experiments were performed on CNGC13-YFP-expressing oocytes, subjecting them to pulses ranging from -130 mV to +30 mV. Large inward currents were observed in CNGC13-YFP–expressing oocytes upon the presence of external $CaCl_2$ (15 mM) in the recording buffer and dibutyryl cAMP (300 µM) on hyperpolarizing <-90 mV (Figures 2a, and b). No currents were seen in un-injected oocytes subject to both cAMP and Ca^{2+} (Figure 2c). *Xenopus* oocytes express Ca^{2+}–activated chloride current that is activated on elevation of $Ca^{2+}{}_{cyt}$. Treatment with the Ca^{2+}–activated chloride current inhibitor, 4, 4'-diisothiocyanatostilbene-2, 2'-disulfonic acid disodium (DIDS; 300 µM), results in reduction of the Ca^{2+}–activated inward current (Figures A.2a fouth panel from left, and b). We also tested the ion selectivity of the channel using monovalent cation K^+, and near-background currents were observed upon their addition in the presence of cAMP (Figures A.2d, e, and f). These data establish that CNGC13 is a Ca^{2+}–permeable channel.

Acknowledgement. We thank IISER Bhopal microscopy facility, and Mr. Manas, a Ph.D. student from Dr. Jeet Kalia lab for imaging the *Xenopus laevis* oocytes.

A.3 Materials and methods

Confocal Microscopy to detect expression and localization of CNGC13-YFP in Xenopus laevis oocytes.

Stage 5 and 6 oocytes from adult female *Xenopus laevis* (the African clawed frog) were surgically removed from anesthetized frogs in accordance with a protocol approved by the Institutional Animal Ethics Committee (IAEC), IISER Bhopal. Oocytes were digested with collagenase type 2 enzyme (1 mg/mL) in calcium-free OR2 buffer containing NaCl (82.5 mM), KCl (2.5 mM), $MgCl_2$ (1 mM) and HEPES (5 mM) at pH 7.6 for 1 h at 18° C on an automated rocker and then de-folliculated with cut pipettes. Capped RNA was prepared from the linearized plasmid DNA templates using the HiScribe™ T7 High Yield RNA Synthesis Kit (New England Biolabs), following the manufacturer's instructions. De-folliculated oocytes were injected with CNGC13-YFP cRNA solution (50 nL) and stored at 18° C in ND96 solution containing NaCl (96 mM), KCl (2 mM), HEPES (5 mM), $MgCl_2$ (1 mM), $CaCl_2$ (1.8 mM) and gentamycin (50 µg/mL) at pH 7.6. Un-injected and CNGC13-YFP cRNA injected oocytes (72 to 96 h post-injection) were imaged in bright field and fluorescence confocal mode. Oocytes were imaged with a 10.0X objective on a

FV3000 Confocal Microscope (Olympus). YFP was excited using the 488 nm line at 1.4% transmissivity with a PMT voltage of 640 V while the emission was recorded from 500 to 550 nm. Line scans were performed on fluorescence images of both un-injected and CNGC13-YFP cRNA injected oocytes using ImageJ software.

Activity assays of CNGC13 channels by two-electrode voltage clamp recordings.

TEVC recordings for CNGC13-YFP RNA injected oocytes were performed 72 to 96 h post-injections. The recorded data were filtered and sampled at 1 KHz and 5 KHz respectively. Recording microelectrode resistances were between at 0.1-1 MΩ when filled with 3 M KCl solution. The two separate recording buffers were prepared, the first contained $CaCl_2$ (15 mM), mannitol (200 mM) in HEPES-Tris (10 mM) at pH 7.4 and the second contained KCl (10 mM), mannitol (200 mM) in HEPES-Tris (10 mM) at pH 7.4 (Meena, Prajapati et al. 2019). Stock solution of dibutyryl c-AMP was made in mannitol (200 mM) in HEPES-Tris (10 mM) buffer at pH 7.4. The protocols for the TEVC recordings for the CNGC13-YFP channels are: CNG_IV_3.pro and CNG_pulsing2.pro.

a. CNG_IV_3.pro: Oocytes were held at -50 mV and stepped to a range of potentials from -130 mV to +30 mV with +20 mV increments.

b. CNG_pulsing2.pro: It was the pulsing protocol for oocytes, -50 mV for 100 ms, -150 mV for 2000 ms and then followed by -50 mV for 500 ms.

Injected oocytes were first clamped in the recording buffer. TEVC recordings were done by using CNG_IV_3.pro first. Then, pulsing protocol was started, and after two pulses, dibutyryl cAMP was added to the recording chamber (300 µM final concentration) while the suction was off. The pulsing protocol was used for the remainder of the TEVC recording, except after 15 and 26 minutes of dibutyryl cAMP addition, when CNG_IV_3.pro was used. TEVC recordings for the un-injected oocytes were done similarly.

A.4 References

1. Meena, M. K. *et al.* The Ca2+ channel CNGC19 regulates Arabidopsis defense against Spodoptera herbivory. *The Plant Cell* **31**, 1539–1562 (2019).

2. Seybold, H. *et al.* Ca^{2+} signalling in plant immune response: from pattern recognition receptors to Ca^{2+} decoding mechanisms. *New Phytologist* **204**, 782–790 (2014).

3. Dodd, A. N., Kudla, J. & Sanders, D. The Language of Calcium Signaling. *Annu. Rev. Plant Biol.* **61**, 593–620 (2010).

Rights and Permissions

CCC Marketplace

This is a License Agreement between Yashaswi Singh ("User") and Copyright Clearance Center, Inc. ("CCC") on behalf of the Rightsholder identified in the order details below. The license consists of the order details, the Marketplace Permissions General Terms and Conditions below, and any Rightsholder Terms and Conditions which are included below.

All payments must be made in full to CCC in accordance with the Marketplace Permissions General Terms and Conditions below.

Order Date	21-Apr-2023	Type of Use	Republish in a thesis/dissertation
Order License ID	1347430-1		
ISSN	1873-7064	Publisher	Pergamon
		Portion	Chart/graph/table/figure

LICENSED CONTENT

Publication Title	Neuropharmacology	Rightsholder	Elsevier Science & Technology Journals
Article Title	Gating modifier toxin interactions with ion channels and lipid bilayers: is the trimolecular complex real?	Publication Type	e-journal
		Start Page	32
		End Page	45
Date	01/01/1995	Volume	127
Language	English		
Country	United Kingdom of Great Britain and Northern Ireland		

REQUEST DETAILS

Portion Type	Chart/graph/table/figure	Distribution	Worldwide
Number of Charts / Graphs / Tables / Figures Requested	1	Translation	Original language of publication
		Copies for the Disabled?	No
Format (select all that apply)	Print, Electronic	Minor Editing Privileges?	No
Who Will Republish the Content?	Academic Institution	Incidental Promotional Use?	No
Duration of Use	Life of current edition	Currency	USD
Lifetime Unit Quantity	Up to 499		
Rights Requested	Main product		

NEW WORK DETAILS

Title	Dissecting the roles of toxin bivalency, membrane affinity, and stoichiometry in DkTx-activation of TRPV1	Institution Name	Indian Institute of Science Education and Research (IISER), Pune
		Expected Presentation Date	2023-05-31
Instructor Name	Dr. Jaat Kaila		

CCC Marketplace

This is a License Agreement between Yashaswi Singh ("User") and Copyright Clearance Center, Inc. ("CCC") on behalf of the Rightsholder identified in the order details below. The license consists of the order details, the Marketplace Permissions General Terms and Conditions below, and any Rightsholder Terms and Conditions which are included below.

All payments must be made in full to CCC in accordance with the Marketplace Permissions General Terms and Conditions below.

Order Date	21-Apr-2025	Type of Use	Republish in a thesis/dissertation
Order License ID	1347348-1		
ISSN	1873-7064	Publisher	Pergamon
		Portion	Chart/graph/table/figure

LICENSED CONTENT

Publication Title	Neuropharmacology	Rightsholder	Elsevier Science & Technology Journals
Article Title	Gating modifier toxin interactions with ion channels and lipid bilayers: is the trimolecular complex real?	Publication Type	e-journal
		Start Page	32
		End Page	45
Date	01/01/1995	Volume	127
Language	English		
Country	United Kingdom of Great Britain and Northern Ireland		

REQUEST DETAILS

Portion Type	Chart/graph/table/figure	Distribution	Worldwide
Number of Charts / Graphs / Tables / Figures Requested	1	Translation	Original language of publication
		Copies for the Disabled?	No
Format (select all that apply)	Print, Electronic	Minor Editing Privileges?	No
Who Will Republish the Content?	Academic Institution	Incidental Promotional Use?	No
Duration of Use	Life of current edition	Currency	USD
Lifetime Unit Quantity	Up to 499		
Rights Requested	Main product		

NEW WORK DETAILS

Title	Dissecting the roles of toxin bivalency, membrane affinity, and stoichiometry in DkTx-activation of TRPV1	Institution Name	Indian Institute of Science Education and Research (IISER), Pune
		Expected Presentation Date	2023-05-31
Instructor Name	Dr. Jaat Kaila		

CCC Marketplace

This is a License Agreement between Yashaswi Singh ("User") and Copyright Clearance Center, Inc. ("CCC") on behalf of the Rightsholder identified in the order details below. The license consists of the order details, the Marketplace Permissions General Terms and Conditions below, and any Rightsholder Terms and Conditions which are included below.

All payments must be made in full to CCC in accordance with the Marketplace Permissions General Terms and Conditions below.

Order Date	21-Apr-2025	Type of Use	Republish in a thesis/dissertation
Order License ID	1347262-1		
ISSN	1742-4658	Publisher	BLACKWELL PUBLISHING
		Portion	Chart/graph/table/figure

LICENSED CONTENT

Publication Title	FEBS Journal	Publication Type	e-Journal
Article Title	N-Terminally extended analogues of the K? channel toxin from Stichodactyla helianthus as potent and selective blockers of the voltage-gated potassium channel Kv1.3.	Start Page	2247
		End Page	2259
		Issue	12
		Volume	282
		URL	http://firstsearch.oclc.org
Author/Editor	Federation of European Biochemical Societies.		
Date	01/01/2004		
Language	English		
Country	United Kingdom of Great Britain and Northern Ireland		
Rightsholder	John Wiley & Sons - Books		

REQUEST DETAILS

Portion Type	Chart/graph/table/figure	Distribution	Worldwide
Number of Charts / Graphs / Tables / Figures Requested	1	Translation	Original language of publication
		Copies for the Disabled?	No
Format (select all that apply)	Print, Electronic	Minor Editing Privileges?	No
Who Will Republish the Content?	Academic Institution	Incidental Promotional Use?	No
Duration of Use	Life of current edition	Currency	USD
Lifetime Unit Quantity	Up to 499		
Rights Requested	Main product		

NEW WORK DETAILS